UNINTEGRATED PARTON DISTRIBUTIONS

A thesis submitted for the degree of

Doctor of Philosophy

by

M. A. Kimber

Institute for Particle Physics Phenomenology

Department of Physics

University of Durham

September 2001

UNINTEGRATED PARTON DISTRIBUTIONS

thesis submitted for the degree of Doctor of Philosophy

M. A. Kimber — September 2001

Abstract

We develop the theory of parton distributions $f_a(x, k_t^2, \mu^2)$, unintegrated with respect to transverse momentum k_t, from a phenomenological standpoint. In particular, we demonstrate a convenient approximation in which the unintegrated functions are obtained by explicitly performing the last step of parton evolution in perturbative QCD, with single-scale functions $a(x, Q^2)$ as input. Results are presented in the context of DGLAP and combined BFKL-DGLAP evolution, but with angular ordering imposed in the last step of the evolution.

We illustrate the application of these unintegrated distributions to predict cross sections for physical processes at lepton-hadron and hadron-hadron colliders. The use of partons with incoming transverse momentum, based on k_t-factorisation, is intended to replace phenomenological "smearing" in the perturbative region $k_t > k_0$ ($k_0 \simeq 1$ GeV), and enables the full kinematics of a process to be included even at leading order. We apply our framework to deep inelastic scattering and the fitting of $F_2(x, Q^2)$, to the transverse momentum spectra of prompt photons in hadroproduction and in photoproduction, and to the topical problem of $b\bar{b}$ production at HERA.

Finally, we address the issue of parton-parton recombination (shadowing) at very low values of x, building on recent work by Kovchegov and others to make predictions for the likely magnitude of shadowing effects at the LHC.

Declaration

I declare that no material in this thesis has previously been submitted for a degree at this or any other university.

Much of the research described in this thesis has been carried out in collaboration with Profs A. D. Martin, M. G. Ryskin and J. Kwieciński, together with contributions from Drs A. M. Staśto and A. Shuvaev. Chapter 1 consists mainly of a review of known results, and is not claimed to be fully original. Part of the material presented in the remaining chapters is based on work which was first published in the following articles:

[1] M. A. Kimber, A. D. Martin and M. G. Ryskin:
European Physical Journal **C12** (2000) 655

[2] M. A. Kimber, J. Kwieciński, A. D. Martin and A. M. Stasto:
Physical Review **D62** (2000) 094006

[3] M. A. Kimber, J. Kwieciński and A. D. Martin:
Physics Letters **B508** (2001) 58

[4] M. A. Kimber, A. D. Martin and M. G. Ryskin:
Physical Review **D63** (2001) 114027

I felt it informative to include other related work on prompt photon production and $b\bar{b}$ production at HERA, in Chapters 5 and 6 respectively, which is at present ongoing. Some useful results have already been obtained, although the analysis is not yet complete.

Acknowledgements

Firstly I am indebted to Professor Alan Martin for his enthusiastic supervision, great insight and resourcefulness. It was a great pleasure also to work with Professors Misha Ryskin and Jan Kwieciński, who provided interesting research problems and were very helpful in guiding my efforts to solve them.

I much enjoyed occasional collaboration with Drs Anna Staśto and Andrei Shuvaev, and also benefited greatly from the expertise of my colleagues in the Durham particle physics group. It was a great place to work and I have had a really good three years. Thanks to Maria and Jeppe especially. I am grateful to PPARC for funding my PhD studentship, including some travel and transferable skills opportunities.

Finally I should like to thank all my family for their encouragement and support, and in particular my wife Catherine. My father Rod first inspired my interest in fundamental physics, but Catherine has had to put up with the consequences.

Martin Kimber
Durham, 2001

Contents

Chapter 1

Introduction

Particle physics is the area of modern science dedicated to uncovering the fundamental structure of matter. In the course of history, scientists have successfully described physical objects and substances as consisting of progressively smaller entities. Thus we understand the properties of macroscopic materials in terms of the interactions of their constituent molecules and atoms; the behaviour of atoms is concisely explained by the fact that each atom consists of a tiny, dense, positively charged nucleus surrounded by a cloud of electrons; and the characteristics of any atomic nucleus derive from its composition as a certain number of protons and a certain number of neutrons bound tightly together. When each of these layers of matter had been experimentally discovered, it subsequently became possible to isolate the new constituent units and perform experiments on them to determine whether they, in turn, had further substructure.

The last thirty years have been different in one important respect. Bombarding protons and neutrons with high energy electron beams in the late 1960s revealed another layer of matter: the hadrons[1] are themselves composite, behaving as strongly bound

[1] "Hadron" refers to particles which interact via the strong (nuclear) force: the fermionic hadrons

collections of "partons". By 1974 physicists were convinced that these partons could be identified as spin-$\frac{1}{2}$ particles named *quarks*, which come in various different "flavours", and spin-1 particles named *gluons*. However, the attractive force between quarks and gluons becomes increasingly enormous at distances greater than 10^{-15} m (the approximate radius of a hadron). In fact, the pionic exchange force between "colourless" nucleons, itself very large, can be regarded as a residual spilling over of the even stronger "colour" force between these "coloured" partons, akin to Van der Waal's force binding together "neutral" atoms into molecules.

This enormous attraction between quarks and gluons means that it is quite impossible to isolate these supposedly fundamental particles from the hadrons in which they live. At the current research frontier, therefore, the properties of quarks and gluons can not be measured directly, because we are not able to prepare a beam of quarks; instead we have to infer the behaviour of the constituent partons indirectly from the detailed results of collisions involving hadrons. A good example is the machine currently being constructed at CERN in Geneva, the Large Hadron Collider (LHC), which will collide beams of protons at very high energies.

It follows that we need accurate descriptions of how the quarks and gluons behave inside the protons and neutrons that are available for experimentation. Fortunately, another property of quantum chromodynamics (QCD), which is the part of the "Standard Model" of particle physics pertaining to the colour force, means that this force between quarks and gluons becomes very weak — and asymptotically, goes to 0 — at short distances $d \ll 10^{-15}$ m. Experiments at high energies examine the physics of what happens on short timescales, and we can factorise off the probability of finding, inside

("baryons") include the proton and the neutron, and the bosonic hadrons ("mesons") include pions, for example.

an incoming proton, a quark or a gluon moving in a certain way, which is then involved in a high energy interaction, *independently* of the details of the high energy interaction. Therefore, since the 1970s probability density functions, called "parton distribution functions", have been measured and fitted from experimental data. Although some of the information contained in sets of parton distribution functions comes at present from "ignorant" parametrisation and measurement[2], the theory of parton evolution in QCD means that we can compute the parton distributions at higher energies with confidence, using the lower energy information. This, combined with the universality of parton distributions so that the data from electron-proton collisions[3] may be used to predict the results of proton-proton collisions, makes knowledge of parton distributions essential for modern particle physics. In addition, much recent research has focused on the theory of parton evolution itself, which is of theoretical as well as practical interest.

1.1 The QCD lagrangian

Quantum chromodynamics is a gauge field theory based on an exact $SU(3)$ symmetry of colour charges. There is no connection with the approximate $SU(3)$ flavour symmetry resulting from the existence of three nearly massless quarks, "up", "down" and "strange". Instead colour is a different property of quarks and gluons, which bind together to form colour singlet ("colourless") combinations which make hadrons.

It is informative to examine very briefly the earlier theory of quantum electrodynamics (QED), which is the quantum theory of electromagnetism, based on a $U(1)$ gauge

[2]Ultimately, "lattice QCD" may give us important information about the low-energy contents of hadrons.

[3]The *ep* collider HERA at DESY in Hamburg has been a fertile source of data on the structure of the proton since 1992.

symmetry of electrical charge.

Consider first the interaction between an electron with charge $-e$ and mass m, and a photon. A classical lagrangian (density) $\mathcal{L}$, varied with respect to the electron spinor field $\psi(x)$ and the photon vector field $A^\mu(x)$, yields as Euler-Lagrange equations the Dirac equation for the electron and Maxwell's equation for the photon, in the vacuum:

$$\mathcal{L} = \bar{\psi}\left(i\gamma^\mu \partial_\mu - m\right)\psi - \frac{1}{4}F_{\mu\nu}F^{\mu\nu}. \tag{1.1}$$

The electromagnetic field tensor is defined in terms of the vector potential as $F_{\mu\nu} \equiv \partial_\mu A_\nu - \partial_\nu A_\mu$. We generally adopt the notation $\not{\partial} \equiv \gamma^\mu \partial_\mu$ and similarly for any other vector. The spinor ψ is a column four-vector in spin space and each gamma matrix γ^μ is four by four in spin space; they satisfy the anticommutation relation $\{\gamma_\mu, \gamma_\nu\} = 2g_{\mu\nu}$.

With the lagrangian (1.1), we are free to redefine our electron field by a *global* phase transformation, $\psi \to e^{i\alpha}\psi$, which has no physical effect. The opposite phase rotation is made to the positron (antiparticle) field, and the bilinear product terms in the lagrangian remain unchanged overall.

However, suppose we wish to change our phase conventions in a way which arbitrarily depends on the spacetime coordinates x^μ. This is a *local* phase rotation which we can write as

$$\psi(x) \to e^{i\alpha(x)}\psi(x). \tag{1.2}$$

We can also vary the definition of the vector potential A_μ in a local fashion, exploiting the gauge freedom of classical electrodynamics because the electric and magnetic fields, contained as components of $F_{\mu\nu}$, remain invariant under the transformation

$$A_\mu(x) \to A_\mu(x) - \frac{1}{e}\partial_\mu \alpha(x). \tag{1.3}$$

Taken together the redefinitions (1.2) and (1.3) are known as a local $U(1)$ gauge transformation. It is called $U(1)$ because the rotating "matrix" $R = e^{i\alpha}$ is one-dimensional (just a complex number), and, of course, unitary ($R^\dagger R = I$).

To write a lagrangian which is invariant under this gauge transformation, we have to make a change to the electron-photon interaction term, to use the covariant derivative

$$D_\mu \equiv \partial_\mu + ieA_\mu(x), \tag{1.4}$$

thereby linking the otherwise separate transformations (1.2) and (1.3), in the $U(1)$ invariant QED lagrangian

$$\mathcal{L}_{QED} = \bar{\psi}\left(i\not{D} - m\right)\psi - \frac{1}{4}\left(F_{\mu\nu}\right)^2. \tag{1.5}$$

For the purposes of quantum field theory we now wish to use this lagrangian to extract perturbative Feynman rules, and calculate approximations for quantum amplitudes in terms of expressions corresponding to individual particle interaction vertices and particle propagators, multiplied together. Although results of such calculations should not be gauge-dependent, we need to make a definite gauge choice to perform the calculations. To incorporate a choice of gauge into the Feynman rules, it is convenient to add a gauge-fixing term to the lagrangian, such as for example for a "covariant gauge",

$$\mathcal{L}_{gauge} = -\frac{1}{2\xi}\left(\partial_\mu A^\mu\right)^2 , \tag{1.6}$$

where ξ is an arbitrary parameter, for instance $\xi = 1$ for the Feynman gauge. With this addition, the QED quantum lagrangian is complete.

Now we move on to QCD. The presence of the colour property, which is another fundamental physical attribute of an elementary particle field like its spin, complicates matters. In the preceding discussion I have already suppressed the spin indices which we could write on the spinors ψ and the Dirac gamma matrices γ_μ; these are distinct from the Greek spacetime indices μ. The $SU(3)$ group is the group of three-dimensional unitary matrices with determinant 1, and the fundamental representation is a triplet of three quark fields, "red", "green" and "blue":

$$\psi = \begin{pmatrix} \psi_R \\ \psi_G \\ \psi_B \end{pmatrix} . \tag{1.7}$$

Thus the colour structure of a pure red quark would be $\psi_R =$ spin-$\frac{1}{2}$ fermion field just like an electron (a Dirac 4-spinor each of whose components depend on the spacetime coordinates x^μ), $\psi_G = \psi_B = 0$. We can refer to an individual *colour* component of (ψ_R, ψ_G, ψ_B) by ψ_i, where i runs from 1 to 3.

However the key physical input is that the definition of the basis red, green, and blue is of no physical significance — like the phase of ψ in the QED case. For local colour gauge invariance, we must be able to premultiply ψ of (1.7) by a 3×3 position-dependent matrix which mixes up the original definitions R, G, B as we please. For conservation of probability we want a unitary transformation, so we can write a general rotating matrix as

$$U(x) = e^{i\alpha^a(x)t^a}. \tag{1.8}$$

Notice that we now have yet another index a, with the sum over 1 to 8 implied in (1.8). This is because the generators of $SU(N)$, in the adjoint representation, are of dimension N^2-1. We have eight different arbitrary functions $\alpha^a(x)$ to parametrise the transformation, and eight Gell-Mann colour matrices t^a, which obey the commutation relation $[t^a, t^b] = if^{abc}t^c$ with f^{abc} the known structure constants of $SU(3)$. It is the non-abelian nature of the group that makes the structure so complicated (and in the early days it was important to distinguish QCD experimentally from a simpler possible theory with separate commuting $U(1)$ transformations for each of the three colours).

What about the gluon field? To have local gauge invariance in the QCD lagrangian, similar to the QED gauge invariance, we need to have eight different gluon fields $A^a_\mu(x)$. Whereas a photon does not carry electrical charge, a gluon can have one of eight different colours. We label members of the octet as $R\bar{G}$, $R\bar{B}$, $B\bar{G}$, $B\bar{R}$, $G\bar{R}$, $G\bar{B}$, $(R\bar{R}-G\bar{G})/\sqrt{2}$ and $(R\bar{R}+G\bar{G}-2B\bar{B})/\sqrt{6}$ — there is in addition a colourless singlet $(R\bar{R}+B\bar{B}+G\bar{G})/\sqrt{3}$, which does not mix with any of the other states under the operation of $U(x)$, and which does not have physical significance. This assignation of colours can be helpful in understanding the amplitudes for different processes involving gluons, see Fig. 1.1.

In terms of the overall coupling g of QCD, we write the field transformations of quarks and gluons, analogous to (1.2) and (1.3) in QED, as

$$\begin{aligned} \psi_i(x) &\rightarrow e^{i\alpha^a(x)t^a_{ij}}\,\psi_j(x) \\ A^a_\mu(x) &\rightarrow A^a_\mu(x) + \frac{1}{g}\partial_\mu\alpha^a(x) + f^{abc}A^b_\mu(x)\alpha^c(x), \end{aligned} \tag{1.9}$$

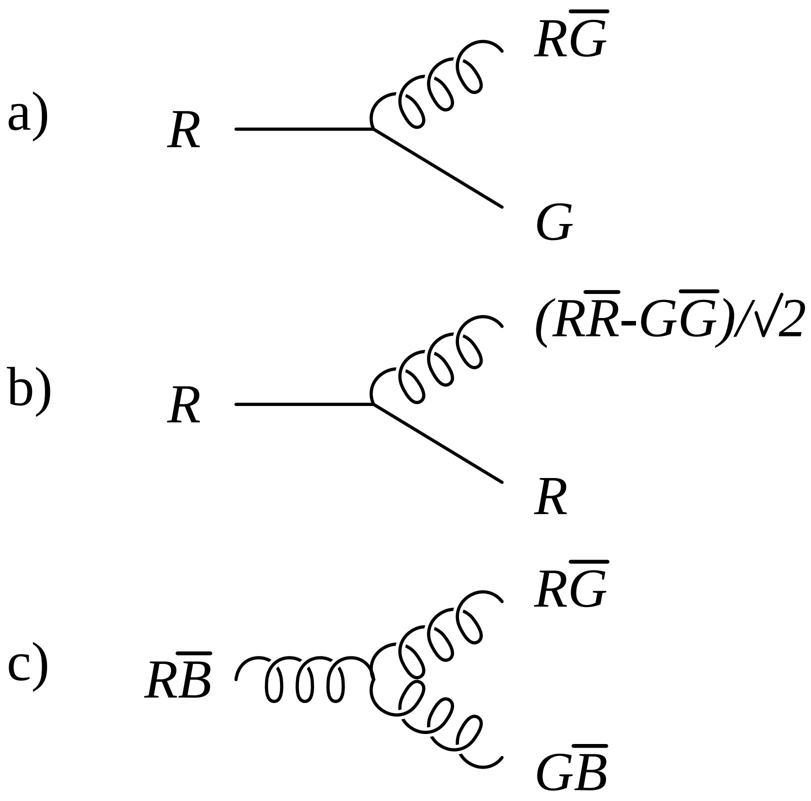

Figure 1.1: Examples of colour flow (diagrams read left to right). a) A red quark emits a gluon, turning green in the process. b) A red quark emits a gluon without changing colour. c) A gluon splits into two gluons.

where all colour indices are shown explicitly. The classical lagrangian invariant under such a local gauge transformation is

$$\mathcal{L}_{classical} = \bar{\psi}_i \left(i\not{D}_{ij} - m\delta_{ij} \right) \psi_j - \frac{1}{4} F^{a\,\mu\nu} F^a_{\mu\nu} \tag{1.10}$$

with revised definitions

$$F^a_{\mu\nu} \equiv \partial_\mu A^a_\nu - \partial_\nu A^a_\mu + g f^{abc} A^b_\mu A^c_\nu \tag{1.11}$$

and

$$D_{\mu\, ij} \equiv \delta_{ij} \partial_\mu - ig A^a_\mu(x) t^a_{ij} \ ; \tag{1.12}$$

note that $[D_\mu, D_\nu] = -ig F^a_{\mu\nu} t^a$. The more complicated field tensor F leads to self-interaction of gluons (triple and quadruple gluon vertices), whereas photons never scatter directly off one another.

Again for Feynman diagram computation we wish to fix a specific gauge. We could use the equivalent of (1.6), making sure the square includes summation over the eight different gauge fields. An alternative is the axial class of gauge, for which the appropriate lagrangian term is

$$\mathcal{L}_{gauge} = -\frac{1}{2\lambda} \left(n^\mu A^a_\mu \right)^2 , \tag{1.13}$$

such as for example the light-cone gauge with $\lambda = 0$, $n^2 = 0$.

There is one final problem in going from the classical lagrangian to a quantum one. It is sometimes necessary to add unphysical "ghost" terms, $\mathcal{L}_{ghost}$, to the lagrangian, to ensure that only the physical, transverse polarisations of external gluons contribute to the amplitudes for physical processes. (The simpler abelian structure of QED means that the other components always cancel without any need for ghost terms.) However, the choice of an axial gauge as in (1.13) avoids the need for such ghost fields, because only physical gluons propagate anyway.

1.2 Asymptotic freedom and perturbative series

An important feature of quantum field theories is the possibility of loop diagrams. A propagating photon, for example, can fluctuate briefly into a fermion-antifermion pair, which then recombine to a photon. This short-lived vacuum polarisation effect has great physical significance. Suppose the photon in question is mediating an interaction between two electrons: then we have to consider the "bubble" diagram (b) of Fig. 1.2 as an amplitude that can interfere with the simple tree diagram (a), so the strength of the repulsion between the two electrons is affected.

Each QED vertex in the diagrams shown is accompanied by a factor of the electromagnetic coupling e (the electrical charge) in the matrix element, leading to a factor[4] $\alpha_{em} \equiv e^2/4\pi$ in the cross section. This coupling comes directly from the coefficient of the electron-electron-photon ($\bar{\psi}\gamma_\mu A^\mu \psi$) term in the lagrangian (1.5) — hidden in the covariant derivative (1.4). The field theory dictates that we should draw every possible diagram with the same incoming and outgoing particles, including many possible internal vertices for virtual corrections, and the total quantum amplitude is the sum of the expressions associated with each Feynman diagram. However, it is known that the coupling e is numerically small, and this motivates an expansion in the small parameter α_{em}, whereby the diagrams with fewest vertices come first in the perturbative series. Higher order diagrams, all other things being equal, are suppressed by extra factors of

[4] We always use natural units, in which $\hbar = c = 1$.

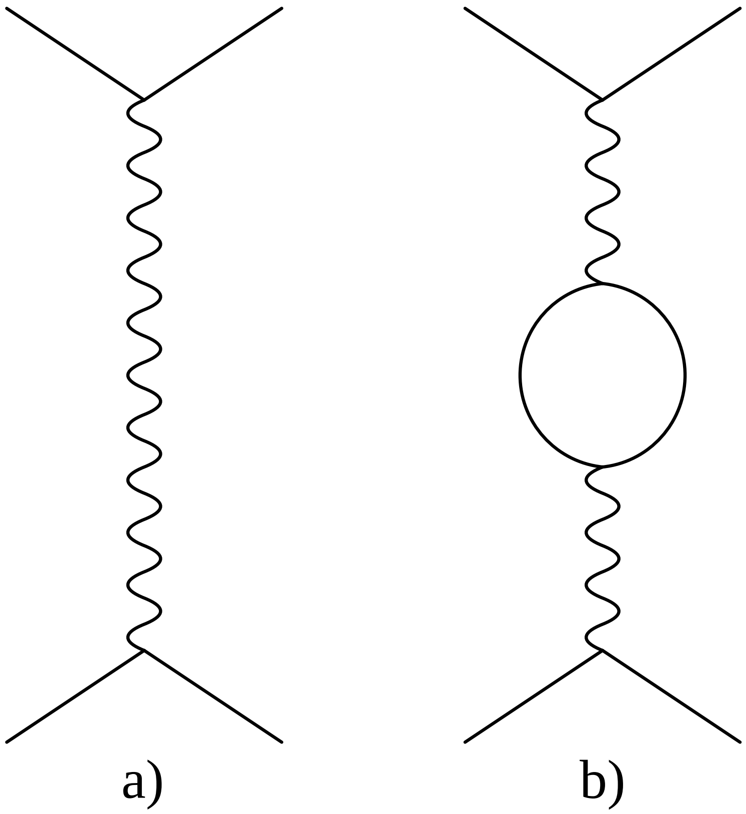

Figure 1.2: Two possible Feynman diagrams for the electromagnetic interaction between two electrons. a) The lowest order tree diagram (photon exchange). b) A bubble diagram (virtual correction).

α_{em}, so we hope to obtain a good approximation to the true cross section by truncating the series after a few terms[5].

The problem with the loop diagram shown in (b) of Fig. 1.2 is that the momentum of the electron in the bubble can take any value, as it is an internal particle (in Uncertainty Principle language we might talk about the electron-positron pair "borrowing" the energy from the vacuum for a very short time interval, and giving it back on annihilation). Computation of diagram (b) involves not only an extra power of α_{em} but also an integration over the possible values of the loop momentum k, $\int d^4k$. We can introduce an arbitrary ultraviolet (UV) cutoff λ, but the bubble contribution is proportional to $\ln(\lambda^2/Q^2)$, where two propagator denominators like k^2 make the divergence only logarithmic, and the other momentum scale, Q, comes from the virtuality of the spacelike exchanged photon, $q^2 \equiv q^\mu q_\mu = -Q^2$.

To achieve physically meaningful answers from calculating such diagrams, we have to turn to the process called renormalisation. For this example in QED the physical justification is particularly clear. We know the repulsion between two electrons at large distances, so when $Q^2 \sim 0$, $\alpha_{em} \approx 1/137$. If we compute the scattering cross section in terms of an *effective* coupling $\alpha_{em}^{eff.}(Q^2)$ dependent on the scale Q, and call the original parameter α_{em} (equivalently the charge e in the lagrangian) the *bare* value, which is not directly observed, we deduce the relationship between $\alpha_{em}^{eff.}$ and α_{em}^{bare}. There are many virtual diagrams which can contribute, but if we make the one-loop approximation so

[5]In fact the perturbation series produced are *asymptotic*, which means that they eventually diverge because of the growing coefficients of the later terms, but nevertheless for up to a certain, hopefully large, number of terms at the beginning of the series, we obtain improving approximations to the true result by going to successively higher orders.

that all we consider are possible successive bubbles along the propagator, we have

$$\begin{aligned}
\alpha_{em}^{eff.}(Q^2) &= \alpha_{em}^{bare}\left(1+\alpha_{em}^{bare}B(Q^2)+\left(\alpha_{em}^{bare}B(Q^2)\right)^2+\cdots\right) \\
&= \frac{\alpha_{em}^{bare}}{1-\alpha_{em}^{bare}B(Q^2)} \\
\Rightarrow \frac{1}{\alpha_{em}^{eff.}(Q^2)} &= \frac{1}{\alpha_{em}^{bare}} - B(Q^2)
\end{aligned}$$

where $B(Q^2)$ is the bubble contribution to the photon propagator. The dangerous piece of $B(Q^2)$ when $\lambda \to \infty$ is like $\ln(\lambda^2/Q^2)$. However, we can rewrite everything in terms of the observed value $\alpha_{em}^{eff.}(Q^2=\mu^2)$ at a known reference scale μ, which for QED can be taken as $\mu = 0$, or a small energy like $\mu = m_e$, and we get

$$\frac{1}{\alpha_{em}^{eff.}(Q^2)} = \frac{1}{\alpha_{em}^{eff.}(\mu^2)} - \left(B(Q^2)-B(\mu^2)\right).$$

Now everything is finite, because $(B(Q^2)-B(\mu^2)) \sim \ln(\mu^2/Q^2)$. The actual lowest order result for the QED running coupling is [27]

$$\alpha_{em}(Q^2) = \frac{\alpha_{em}(\mu^2)}{1+b^{QED}\alpha_{em}(\mu^2)\ln(Q^2/\mu^2)}, \tag{1.14}$$

with $b^{QED} = -1/3\pi$; there is no need to write "effective" any more because the bare, unphysical charge has been banished by this renormalisation procedure.

The key point is the sign of the function b, which for QED is negative. This means that the coupling becomes stronger than $1/137$ as the typical scale of an interaction increases to higher Q^2. (At $Q \sim M_Z$, the mass of the Z^0 boson, $\alpha_{em} \sim 1/129$.) There is a neat physical picture to describe this in terms of the probing photon Q^2. The nature of these bubble diagrams means that the vacuum is polarised in such a way as to screen or shield the charge of an electron from a low-Q^2, coarse-precision probe. There are electron-positron pairs spontaneously being created around a charge source which make the charge look less than it actually is; but as we probe shorter distances with a higher virtuality photon, we are sensitive only to a smaller spatial area and the screening is less, so α_{em} is greater.

Now apply the same approach to QCD. From the lagrangian point of view, the only difference is that there are more types of loop that can be inserted into a gluon propagator. We therefore proceed as before and eliminate the bare strong coupling α_s^{bare} in favour of some measured value at a reference scale μ:

$$\alpha_s(Q^2) = \frac{\alpha_s(\mu^2)}{1 + b^{QCD}\alpha_s(\mu^2)\ln(Q^2/\mu^2)}. \tag{1.15}$$

However, the value of b is different [27]:

$$b^{QCD} = \frac{-(\frac{2}{3}n_f + 5 - 16)}{4\pi}, \tag{1.16}$$

where n_f is the number of quark flavours available for loops ($u\bar{u}$, $d\bar{d}$, $s\bar{s}$, $\ldots$ count separately). The n_f part is very similar to the QED case (NB colour factors), and the $+5$ corresponds to the propagation of transversely polarised gluons in the loop, but there is in addition a negative term for gluons with other polarisation, which are allowed as internal (virtual) particles. This negative term means that for values of $n_f \leq 16$ the sign of b^{QCD} is in fact positive, $b = (33 - 2n_f)/12\pi$. In physical terms, the gluon-gluon coupling is allowing colour charge to "leak" out into the surrounding spatial area and hence we see *less* of it if we probe more energetically.

This has vital consequences for the domain in which we can hope to apply perturbative QCD successfully. Unlike QED, as the typical energy scale increases, quarks and gluons couple more and more *weakly* and behave more like free particles. From (1.15) we conclude that as $Q^2 \to \infty$, $\alpha_s(Q^2) \to 0$, which is called asymptotic freedom. A suitable scale μ for a measured reference value is no longer a small energy but something larger: $\mu^2 = M_Z^2$ is a favourite choice, for example. As Q drops below 1 GeV the value of α_s grows fast and perturbation theory becomes rapidly unreliable (and therefore we cannot trust (1.15) at small values of Q^2).

Another convenient expression for α_s is

$$\alpha_s(Q^2) = \frac{12\pi}{(33 - 2n_f)\ln(Q^2/\Lambda_{QCD}^2)}, \tag{1.17}$$

in terms of a fundamental low energy scale $\Lambda_{QCD} \sim 300$ MeV, but in this case we effectively determine the value of Λ_{QCD} from experiment, as an alternative to working from a measured reference value $\alpha_s(M_Z^2)$.

In some senses the phenomenon of "confinement" is the converse of asymptotic freedom. The fact that our expression for the strong coupling increases rapidly as $Q \to \Lambda_{QCD}$ seems consistent with the experimental observation that quarks and gluons are trapped within hadrons of radius $\sim 1/\Lambda_{QCD}$, or forcibly hadronise after propagating away from another coloured object for a time $\sim 1/\Lambda_{QCD}$. However, if restricted to the methods of perturbative QCD, we cannot address the $Q \lesssim \Lambda_{QCD}$ region at all, so we have not proved confinement[6]. Nevertheless, while the smallness of the QCD coupling gives us hope that we may apply perturbative methods and calculate simple Feynman diagrams for high-energy processes, the rapid increase of α_s as the energy decreases to the order of the mass of the proton (1 GeV) warns us that quarks and gluons are difficult to

[6]Lattice QCD studies approach the phenomenon from the same lagrangian, but using non-perturbative methods.

disentangle from the behaviour of composite particles.

1.3 Quarks in collider experiments

e^+e^- experiments, where electrons and positrons collide head-on, are a particularly clean form of high energy physics, because electrons and positrons seem to be fundamental units of matter. In such experiments there are no coloured particles in the initial state. Nevertheless, QCD is still involved in possible final states of the reaction: for example, the colliders LEP at CERN and SLAC in California have provided much experimental data in favour of quantum chromodynamics, as well as the other components of the Standard Model. What happens is that the initial lepton-antilepton state annihilates to give an s-channel[7] boson (photon or Z^0, if the CM energy is sufficient) which decays to a new fermion-antifermion pair (for example; or something more exotic, like the charged boson pair W^+W^-).

If only a quark and antiquark are produced, which is often the case because there are many available flavours and colours of quark for the boson to decay into, we seem to have a conundrum. The value of $\alpha_s(Q^2)$ is fairly small, for the typically high centre of mass energy reached at these machines, such as $Q \sim M_Z \approx 91$ GeV, so in the first instance we do not expect the quark and antiquark to interact with each other, once created. The coloured quark and (oppositely-) coloured antiquark spring into existence travelling at high speed in opposite directions in the detector. How does this fit with the property of confinement of coloured objects? The answer is that after the particles have travelled a distance of about $1/\Lambda_{QCD}$, which is about 10^{-15} m, corresponding to a time

[7] A virtual particle propagating in the s-channel is timelike, having an excess of energy over momentum.

of order 10^{-23} s at nearly the speed of light, non-perturbative physics must step in. Much lower energy gluons, or, more properly, some kind of colour flux can be established with that kind of wavelength, and create more coloured particles and antiparticles out of the vacuum with some of the stored energy, binding them into colourless hadrons following the directions of the original quark and antiquark. Experimentally, "jets" composed of many hadrons are seen in the detectors, but well collimated with the original back-to-back directions of the original $q\bar{q}$ pair. The interesting point is that the hadronisation process only happens a comparatively long time after the high energy interaction, and causality arguments mean this subsequent rearrangement does not interfere with the high energy QCD part. In particular, the total rate of $e^+e^- \to q\bar{q}$ is unaffected by the low energy behaviour, because the hadronisation happens with probability 1, once a real $q\bar{q}$ state has been formed. The ratio of the rate of $e^+e^- \to \mathit{hadrons}$ and the similar non-QCD rate $e^+e^- \to \mu^+\mu^-$ is a famous and very well-measured quantity, which shows different quark flavours becoming available as the centre of mass energy is increased, and provides good evidence for a colour factor of 3.

In experiments involving hadrons, we do not have the luxury of a simple initial state with no composite particles. Nevertheless, protons are readily available and their much greater mass than electrons makes them suitable for accelerating in a ring (like the Tevatron at Fermilab, IL) to very high energies indeed, without extensive loss of energy through synchrotron radiation. It is also of theoretical interest to perform experiments on protons, to probe their structure as bound states of quarks.

There are therefore essentially three different types of collider experiment in the premier league of large high energy physics machines:

1. lepton-lepton scattering;

2. lepton-hadron scattering;

3. hadron-hadron scattering.

The first class is generally e^+e^- annihilation as discussed, in both linear and circular accelerators, but $\mu^+\mu^-$ is an interesting future possibility (as muons are 200 times more massive than electrons). The second class includes an enormous range of experiments, such as the scattering of neutrinos off stationary nuclei, but a leading machine of particular interest is the high energy electron- (or positron-) proton collider, the HERA ring at DESY. The third class offers the highest energies (although also includes older, fixed target experiments, such as the bombardment of beryllium by protons). The Tevatron collides protons and antiprotons at a centre of mass energy $\sqrt{s} \sim 2$ TeV, and the planned LHC will collide protons on protons at CM energies of order 14 TeV.

Parton distribution functions are designed to describe initial states involving hadrons, separating information about the densities of the various quarks and gluons inside a high energy proton, say, from the details of high energy interactions that a constituent quark or gluon might be involved in. The remainder of this thesis will therefore focus on reactions involving protons, in the second and third classes above. I start with an introduction to electron-proton scattering.

1.4 Deep inelastic scattering

The fact that protons have substructure (partons) was first revealed in experiments at SLAC, where stationary protons were bombarded by electrons from the linear accelerator. At SLAC energies, the only interaction is electromagnetic, so effectively the electron is being used to generate a virtual photon of 4-momentum q^μ, which is absorbed by the

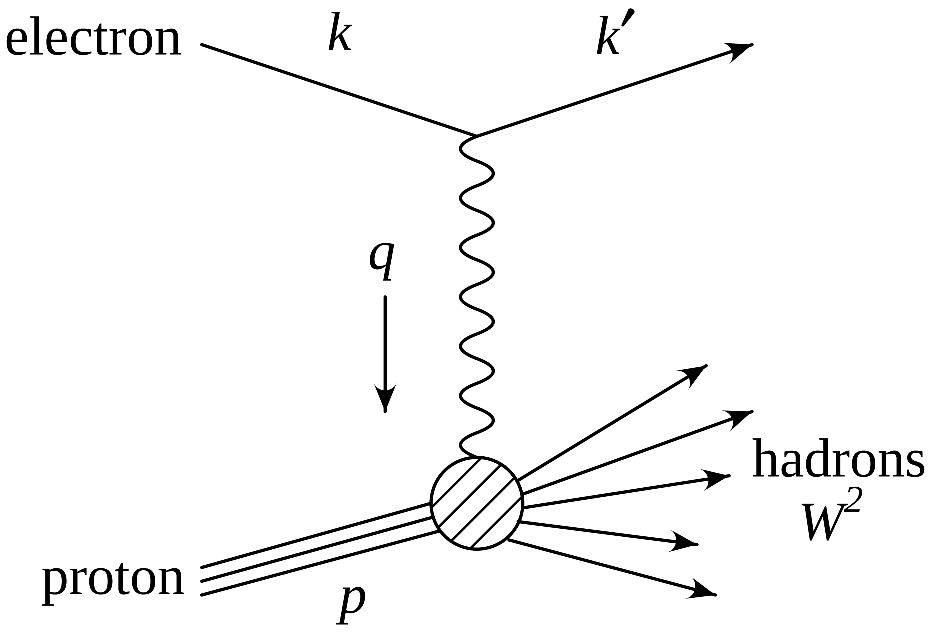

Figure 1.3: Probing the proton with a virtual photon. If the collision is inelastic, we end up with a hadronic final state X of invariant mass squared $W^2 > M_p^2$.

proton, see Fig. 1.3. This is a t-channel process with a spacelike virtual photon γ^*, so $q^2 < 0$ and we define $Q^2 \equiv -q^2$.

We can deduce Q^2 by measuring the electron after the collision and evaluating $q = k - k'$. If Q^2 is small, an elastic collision is most probable, and the proton is deflected but remains intact (invariant mass squared of X is $W^2 = M_p^2$). A low energy photon is only sensitive to the overall, large-distance structure, which is a single positive charge. However high-Q^2 collisions probe smaller spatial regions, and the extra energy transferred breaks up the proton into a complicated hadronic final state, whose invariant mass is greater than the proton mass M_p. An elastic collision corresponds to $Q^2 = 2p \cdot q$, but we need an extra variable to describe inelastic collisions, in addition to Q^2. The standard choice is another Lorentz invariant, "Bjorken" x,

$$x \equiv \frac{Q^2}{2p \cdot q} = \frac{Q^2}{W^2 - M_p^2 + Q^2}, \tag{1.18}$$

which ranges between 0, when $W^2/Q^2 \to \infty$, and 1 in the elastic limit. For completeness we also define a variable y which is commonly used as it represents the fraction of energy transferred from the electron in the fixed target frame:

$$y \equiv \frac{p \cdot q}{p \cdot k} = \frac{Q^2}{xs}, \tag{1.19}$$

where the CM energy squared, $s \equiv (p+k)^2$, is calculated neglecting the masses of the proton and electron. y also ranges between 0 and 1. It is the situation where $\sqrt{s}$ is large and we can achieve large Q^2 values that we call *deep inelastic scattering.*

Let us consider the differential cross section for the two spin-$\frac{1}{2}$ particles A and B (here the electron and proton) interacting to give a final state consisting of particle 1 (the scattered electron) and some other particles $2 \ldots N$ making up the hadronic final state X, see for example [26]. Assuming an unpolarised situation, we write

$$d\sigma = \frac{\left(\frac{1}{2}\right)^2 \sum\limits_{spins\ A,B} \sum\limits_{spins\ 1..N} |\mathcal{M}|^2}{4\sqrt{(p_A \cdot p_B)^2 - m_A^2 m_B^2}} (2\pi)^4 \delta^4 \left(p_A + p_B - \sum_{i=1}^{N} p_i\right) \prod_{i=1}^{N} \frac{d^3 p_i}{(2\pi)^3\, 2E_i}. \tag{1.20}$$

If we neglect the electron and proton masses we can write this as a differential cross section with respect to just the electron's final state,

$$d\sigma = \frac{1}{p \cdot k} \left(\frac{\alpha_{em}}{q^2}\right)^2 L^{\mu\nu} W_{\mu\nu} \frac{d^3 k'}{2E'} \tag{1.21}$$

where we have taken the coupling constant α_{em} and the propagator $1/q^2$ out of the matrix element, and expressed the remaining part of $\overline{|\mathcal{M}|^2}$ as a product of a tensor for the lepton part, $L^{\mu\nu}$, and a tensor for the hadronic part, $W^{\mu\nu}$. The index μ refers to the photon, and ν enters when we square $\mathcal{M}$.

The lepton tensor is[8]

$$L^{\mu\nu} = \frac{1}{2}\mathrm{Tr}\left(\not{k}\gamma^{\mu}\not{k}'\gamma^{\nu}\right) = 2\left(k'^{\mu}k^{\nu} + k^{\mu}k'^{\nu}\right) + q^2\, g^{\mu\nu}. \tag{1.22}$$

We know little about the vertex between the virtual photon and the proton, because the proton is composite. However, we can parametrise $W^{\mu\nu}$ in terms of the available vectors as

$$\begin{aligned} W_{\mu\nu}(p,q) &= \left(\frac{p_\mu q_\nu + q_\mu p_\nu}{p\cdot q} - g_{\mu\nu} - \frac{p_\mu p_\nu\, q^2}{(p\cdot q)^2}\right)\frac{F_T\left(x,Q^2\right)}{x} \\ &+ \left(\frac{p_\mu q_\nu + q_\mu p_\nu}{p\cdot q} - \frac{q_\mu q_\nu}{q^2} - \frac{p_\mu p_\nu\, q^2}{(p\cdot q)^2}\right)\frac{F_L\left(x,Q^2\right)}{x}, \end{aligned} \tag{1.23}$$

where F_T and F_L are invariant functions corresponding to interaction with transversely and longitudinally polarised photons respectively. This simple form of the hadronic tensor, in terms of just two unknown functions, comes from

1. the Lorentz structure, given that for an unpolarised proton beam p^μ and q^μ are the only 4-vectors relevant to this vertex, and so $p \cdot q$ and q^2 are the only available Lorentz invariants (assuming we neglect the proton's mass, so $p^2 = 0$);

2. the requirement that $W_{\mu\nu}$ be symmetric under $\mu \leftrightarrow \nu$, coming from the conservation of parity for the electromagnetic interaction (if we include parity-violating interactions, such as Z^0 exchange, the hadronic tensor can contain the antisymmetric $\epsilon_{\mu\nu\rho\sigma}$);

3. the requirement $q^\mu W_{\mu\nu} = 0$, which follows from current conservation.

[8] Some other examples of application of the Feynman rules to compute cross sections are given in Appendix B.

$W^{\mu\nu}$ is sometimes written in terms of $F_1 \equiv F_T/2x$ and $F_2 \equiv F_T + F_L$. These F functions are all referred to as *structure functions*, because they are measurable quantities containing information about the structure of the proton.

We often work with the cross section differential with respect to the two independent DIS variables, Q^2 and x. From (1.21) we have

$$\frac{d^2\sigma}{dx\,dQ^2} = \frac{4\pi\alpha_{em}^2}{Q^4}\,L^{\mu\nu}W_{\mu\nu}\,\frac{E'}{2p\cdot k}\,\frac{\partial(E',\cos\theta')}{\partial(x,Q^2)}, \tag{1.24}$$

with the Jacobian, evaluated in whichever frame in which E' is the final electron energy (the *ep* CM frame is convenient), giving the frame-independent expression

$$\frac{d^2\sigma}{dx\,dQ^2} = \frac{4\pi\alpha_{em}^2}{Q^4}\,L^{\mu\nu}W_{\mu\nu}\,\frac{y}{2xs}. \tag{1.25}$$

If we substitute (1.22) and (1.23) into (1.25), we obtain the familiar result (compare, for example, with [28])

$$\frac{d^2\sigma}{dx\,dQ^2} = \frac{4\pi\alpha_{em}^2}{Q^4}\left[\frac{(1+(1-y)^2)}{2x}\,F_T + \frac{(1-y)}{x}\,F_L\right]. \tag{1.26}$$

1.5 Parton densities and factorisation

Let us now consider the "naive" parton model in which we propose that the proton consists of various spin-$\frac{1}{2}$ particles of negligible mass: quarks. We hope to describe the collision of Fig. 1.3 as an *elastic* scattering between the electron and one such quark, while the rest of the proton continues unscathed. We also make the assumption that we can represent the interaction in terms of a probability density, $q(\xi)$, to hit a particular quark q, moving in the same direction as the proton but carrying a fraction ξ of its momentum ($0 < \xi < 1$). Then the cross section for the proton can be expressed as the sum of weighted cross sections for the individual partons.

The fact that we propose to add *probabilities* to strike different constituent partons, rather than working at the quantum amplitude level, is important. The assumption is that the typical timescale of the "hard" interaction, $1/\sqrt{Q^2}$, is much shorter than that of the likely "soft" parton-parton interactions which hold the proton together, $1/\Lambda_{QCD}$. The parton model assumes we can treat the quarks as essentially free, therefore, and the results rely on an incoherent sum of probabilities for different types of quark.

If all these conditions are appropriate, we can construct a hadronic tensor based on the leptonic tensor of (1.22), with the quark having an initial 4-momentum ξp, and of course a final 4-momentum $\xi p + q$ after deflection. If the rest of the proton is not involved in the interaction, multiplying by a parton density function will correct for the fact that we do not have a known quark with a fixed momentum in the initial state, but some distribution of quarks.

$$W^{\mu\nu} = \sum_q e_q^2 \int_0^1 d\xi \; \left((\xi p + q)^\mu \xi p^\nu + \xi p^\mu (\xi p + q)^\nu - \xi p \cdot q \, g^{\mu\nu} \right) \, q(\xi) \, / Q^2 \tag{1.27}$$

Note that we have introduced a factor of e_q^2 into the cross section, where e_q is the fractional charge of a quark (such as $-1/3$), and we sum over all possible types of quark q (and antiquarks if need be). We also need to integrate over possible values of ξ. The assumption at this stage is that $\sum_q \int_0^1 q(\xi) \, d\xi = \mathcal{N}$, where $\mathcal{N}$ is the total number of quarks within one proton. Finally we have a factor of $1/Q^2$ inserted for dimensional reasons (compare with (1.23) — we can check the normalisation by computing the $2 \to 2$ electron-quark scattering from first principles).

Using (1.22) and (1.27) we find, remembering that $k \cdot q = q^2/2$ from $k'^2 = k^2$ $(= 0)$,

$$L^{\mu\nu} W_{\mu\nu} = \sum_q e_q^2 \, \frac{2s}{y} \int_0^1 d\xi \, \left(\frac{\xi^2 (1-y)}{x} + \frac{\xi y^2}{2} \right) q(\xi). \tag{1.28}$$

However, we have not considered the outgoing quark's mass-shell condition. The assumption of elastic scattering means that $(\xi p + q)^2 = (\xi p)^2$ $(= 0)$, and it follows that

$$2\xi \, p \cdot q - Q^2 = 0 \quad \Rightarrow \; \xi = x. \tag{1.29}$$

Our momentum fraction ξ must correspond to the Bjorken variable x describing the collision, if the kinematics are to match up. Therefore we can insert the requirement $\delta(\xi - x)$ into (1.27) and (1.28) — only a quark carrying the right fractional momentum will be available to scatter elastically in an electron-proton DIS interaction characterised by x, Q^2. This leaves

$$L^{\mu\nu} W_{\mu\nu} = \sum_q e_q^2 \, \frac{2xs}{y} \left(1 - y + \frac{y^2}{2} \right) q(x). \tag{1.30}$$

Therefore from (1.25),

$$\frac{d^2\sigma}{dx \, dQ^2} = \frac{4\pi\alpha_{em}^2}{Q^4} \left(\frac{1 + (1-y)^2}{2x} \right) \sum_q e_q^2 \, xq(x). \tag{1.31}$$

We conclude that the naive parton model gives structure functions

$$\begin{aligned} F_T \left(x, Q^2 \right) &= \sum_q e_q^2 \, xq(x) \\ F_L \left(x, Q^2 \right) &= 0. \end{aligned} \tag{1.32}$$

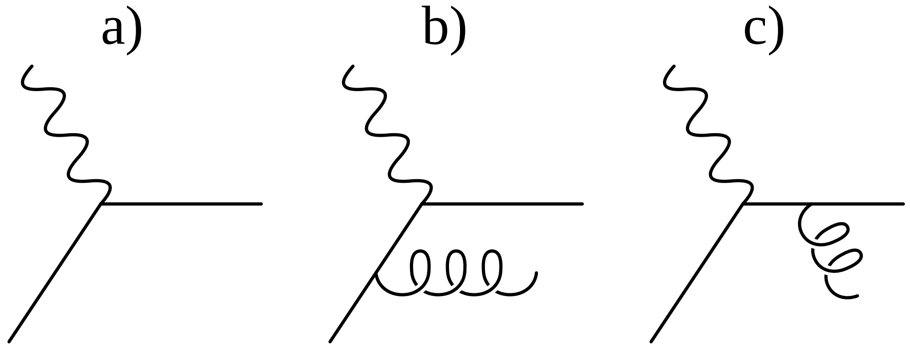

Figure 1.4: Explaining the structure function of the proton in terms of single quarks interacting with the virtual photon in DIS. a) Naive parton model (other "spectator" quarks in proton not shown). b) A possible radiative correction in which a gluon is emitted from the quark. c) Another diagram for gluon emission; in a physical (axial) gauge only transverse gluon polarisations need to be considered and we do not have to include diagrams like (c).

It is striking that, with the simplest approximations, the structure functions only depend on x, and not on the probing virtuality Q^2. This is the well-known property of *scaling*.

We now examine how we can improve the naive parton model in the light of QCD, which leads to scaling violations, introducing some dependence of $F_{T,L}$ on Q^2, the form of which has been extensively confirmed in experiments.[9]

The QCD corrections to the cross section come, firstly, from the possibility of high-energy, perturbative gluon emission from the quark involved in the interaction with the virtual photon. See the illustration in Fig. 1.4. (Note that I do not discuss so-called "higher-twist" corrections, in which more than one of the original partons in the proton are involved in the hard interaction; these are suppressed by powers of Λ^2_{QCD}/Q^2.) We consider diagram (b) of Fig. 1.4, in which the incoming quark radiates away a gluon before being struck by the photon. In an axial gauge, this is the key diagram.

[9]First the scaling behaviour was observed, and subsequently the gentle dependence on Q^2 was measured in slightly different kinematical regions — it happens that around $x \sim 0.1$ curves of F_2 against Q^2 are very flat anyway.

The effect of introducing this real gluon emission can be shown [26] to be to multiply the probability of interaction by a factor

$$\frac{\alpha_s}{2\pi}\frac{1}{k_t^2}P_{qq}\left(\frac{x}{\xi}\right)\,dk_t^2\,d\left(\frac{x}{\xi}\right), \tag{1.33}$$

where now ξ is the momentum fraction of the quark *before* the gluon is radiated. Rather than $\xi = x$, we have some part of the longitudinal momentum going to the emitted gluon, therefore $\xi > x$, and the splitting fraction $z \equiv x/\xi$ plays an important role. The leading order (LO) splitting function turns out to be

$$P_{qq}(z) = C_F\,\frac{1+z^2}{1-z} \tag{1.34}$$

($C_F \equiv (N_C^2-1)/2N_C$ from $SU(N_C)$, with $N_C = 3$ colours giving a colour factor $C_F = 4/3$). In addition a transverse momentum k_t is gained by this branching, and we have to integrate over possible values of k_t^2 and z which could contribute to the DIS cross section at our given x and Q^2.

Thus QCD gives an $O(\alpha_s)$ correction to the structure functions (and deep inelastic cross section) such that the following form replaces (1.32):

$$F_2\left(x,Q^2\right) = x\sum_q e_q^2\int_x^1\frac{d\xi}{\xi}\,q\left(\xi\right)\left\{\delta\left(1-\frac{x}{\xi}\right)+\frac{\alpha_s}{2\pi}\left[P_{qq}\left(\frac{x}{\xi}\right)\ln\frac{Q^2}{\delta^2}+R\left(\frac{x}{\xi}\right)\right]\right\}. \tag{1.35}$$

$R(z)$ represents finite corrections at order α_s. However the most important term is $\ln Q^2/\delta^2$. This comes from integrating in (1.33) over possible transverse momenta dk_t^2/k_t^2 up to Q^2 (which provides a natural scale beyond which we do not expect to resolve the transversely small spatial detail associated with an emission at high k_t). The problem comes from the lower limit in this $d\ln k_t^2$ integration. We can not set this to 0, but have to invent some small unphysical limiting scale δ, which protects (1.35) from the *collinear* singularity. Implicit in (1.33) is the fact that in quantum field theory, the emission of particles at small angles is unremittingly favoured. We see this in the (Mandelstam variable) $t \to 0$ singularity in the $2 \to 2$ matrix element for diagram (b) of Fig. 1.4; it comes from the propagator for massless particles.

The crucial point is that our problems as $\delta \to 0$ are associated with long-distance physics. We have already realised (from confinement, and from the increase of $\alpha_s(\mu^2)$ at low energy scales μ) that we can not apply perturbative QCD methods to describe anything that happens over a long time or across a large spatial region. Therefore we will not really be able to address $k_t \to 0$. However, δ is an unphysical cutoff and we wish to remove it from our equation for the observable F_2. The important step to achieve this is very similar to the renormalisation of α_s in Section 1.2. We define a renormalised, or *factorised*, parton density function

$$q\left(x, Q^2\right) = q\left(x\right) + \frac{\alpha_s}{2\pi} \int_x^1 \frac{d\xi}{\xi} \, q\left(\xi\right) P_{qq}\left(\frac{x}{\xi}\right) \ln \frac{Q^2}{\delta^2}. \tag{1.36}$$

The idea is that this factorisation absorbs the infrared sensitivity into a parton distribution function $q(x, Q^2)$ which now depends on our chosen scale Q^2. Eq. (1.36) contains the unphysical cutoff δ, but also our original parton function $q(x)$, which we claim is unphysical too — its role is like that of the bare charge for α_{em}. We can now rewrite (1.35) in terms of the new parton distribution to $O(\alpha_s)$:

$$F_2\left(x, Q^2\right) = x \sum_q e_q^2 \int_x^1 \frac{d\xi}{\xi} \, q\left(\xi, Q^2\right) \left[\delta\left(1 - \frac{x}{\xi}\right) + \frac{\alpha_s}{2\pi} R\left(\frac{x}{\xi}\right)\right]. \tag{1.37}$$

Because F_2 is an observable, finite quantity, we conclude that our new parton functions

$q(x,Q^2)$ which appear in (1.37) — an equation now without singularities — must be finite also.

1.6 Evolution equations

We have introduced the traditional parton distribution function $q(x,Q^2)$ in (1.36), but we now need to examine how we can calculate or measure this quantity. Eq. (1.36) is not directly helpful, because the right-hand side contains unphysical infinities, even though the left-hand side must be finite. Also, our understanding of how low energy scales relate to long-distance physics suggest that there must be some scales $Q \lesssim \Lambda_{QCD}$ at which we will not be able to calculate $q(x,Q^2)$ under perturbative QCD.

Nevertheless, perturbative QCD does give us powerful information in our treatment of parton distribution functions. If we differentiate (1.36) with respect to $\ln Q^2$, we remove dependence on the two pieces which are unphysical: $q(x)$ and $\ln \delta^2$. The result is

$$\frac{\partial q\left(x,Q^2\right)}{\partial \ln Q^2} = \frac{\alpha_s}{2\pi} \int_x^1 \frac{d\xi}{\xi}\, q\left(\xi, Q^2\right)\, P_{qq}\left(\frac{x}{\xi}\right). \qquad (1.38)$$

We are happy that we can use this parton *evolution* equation for sufficiently large, perturbative values of Q^2. The equation tells us how the parton function $q(x,Q^2)$ varies with Q^2. However, we need to pick some reference energy scale k_0 ($k_0 \gg \Lambda_{QCD}$, although nowadays people go as low as 1 GeV which might be only about three times Λ_{QCD}) and measure the value of $q(x,k_0^2)$ for all accessible values of x at this scale. Having input this experimental information, the evolution equation then predicts the behaviour of q at all higher values of Q^2. Notice that we only need to use the values of the function at *higher* values $\xi > x$.

Now is an appropriate point to introduce the remaining pieces of the evolution framework. We can write an analogous equation for a parton distribution function describing the gluon density, $g(x, Q^2)$, which works in a similar fashion and is justified by the same reasoning. We also need to include cross-terms which account for different types of splitting from that pictured in Fig. 1.4, such as a gluon turning into a quark-antiquark pair. The parton evolution equations are known as DGLAP equations, after Dokshitzer, Gribov, Lipatov, Altarelli and Parisi. An early reference by Altarelli and Parisi is [5].

The complete equation for quark evolution is

$$\frac{\partial q\left(x, Q^2\right)}{\partial \ln Q^2} = \frac{\alpha_s}{2\pi} \int_x^1 \frac{dz}{z} \left[P_{qq}(z)\, q\left(\frac{x}{z}, Q^2\right) \;+\; P_{qg}(z)\, g\left(\frac{x}{z}, Q^2\right)\right], \tag{1.39}$$

where I prefer to integrate directly over the splitting fraction z, $x < z < 1$. The gluon, meanwhile, evolves in a similar way,

$$\frac{\partial g\left(x, Q^2\right)}{\partial \ln Q^2} = \frac{\alpha_s}{2\pi} \int_x^1 \frac{dz}{z} \left[P_{gg}(z)\, g\left(\frac{x}{z}, Q^2\right) \;+\; P_{gq}(z) \sum_q q\left(\frac{x}{z}, Q^2\right)\right]. \tag{1.40}$$

Here we have to sum over all different types (i.e., flavours) of quark that can turn into a quark (radiated away with fraction $x(1/z - 1)$ of the proton's momentum) plus the gluon of interest, involved in some interaction with a momentum fraction x. We had better include antiquarks in the sum too, and therefore (1.39) applies to antiquarks (i.e., $\bar{q}(x, Q^2)$) as well. A common distribution for consideration is the *non-singlet* quark distribution, defined as $q^{NS} \equiv q^i - q^j$, the difference between two different flavours i, j of quark, or for example $q - \bar{q}$, such as $u - \bar{u}$, up "valence". The merit of working with q^{NS} is that in its evolution the effect of the P_{qg} term cancels out, because the gluon distribution feeds equally into different types of quark or antiquark[10]. So this is the only distribution satisfying (1.38).

For completeness, the leading order splitting functions are:

$$
\begin{aligned}
P_{gg}(z) &= 2C_A \left(z(1-z) + \frac{1-z}{z} + \frac{z}{1-z} \right) && (1.41)\\
P_{gq}(z) &= C_F \, \frac{(\,1 + (1-z)^2\,)}{z} && (1.42)\\
P_{qg}(z) &= \frac{z^2 + (1-z)^2}{2} && (1.43)\\
P_{qq}(z) &= C_F \, \frac{(\,1 + z^2\,)}{1 - z}, && (1.44)
\end{aligned}
$$

where C_A is another colour factor, equal to the number of colours $N_C = 3$. Note that I have not yet addressed what happens when $z \to 1$. I found this to be particularly important in the context of our research, so I discuss it in the next chapter. We can see there are difficulties in the use of the P functions as written in (1.41) and (1.44) when $z = 1$, and also when $z = 0$ for P_{gg}.

It is worth mentioning here one point about the momentum fraction ξ, which we matched up in (1.29) with the Bjorken DIS variable $x \equiv Q^2/2p \cdot q$. We can only understand a parton having a fraction ξ of the proton's 4-momentum if we can work in a frame where the masses are negligible compared to the proton's momentum. Light quarks have small masses (of order MeV) but the proton has a mass of about 1 GeV and therefore the parton model is often spoken of as applying in the "infinite momentum frame" where the proton is boosted by a relativistic γ factor tending to infinity. (Time dilation thus slows down the rate of parton-parton interactions, encouraging us that we can ignore them.) However in fact we apply these calculations in various frames, simply

[10] I have only discussed massless quarks, of course.

exploiting the fact that the high momenta involved in modern collider experiments mean that finite-mass corrections are often small. An example is the Breit frame, in which the proton and the virtual photon have equal and opposite momenta. This momentum is likely to be much greater than the mass of the proton.

Chapter 2

Transverse momentum in parton evolution

Firstly, I address how we can define and compute *unintegrated* parton distribution functions as in [1, 4]. The basic suggestion is to work in terms of functions

$$f_a\left(x, k_t^2, \mu^2\right) \tag{2.1}$$

which are analogous to the usual parton densities $a(x, \mu^2)$, but give us information about the probability to find a parton a ($= q$, $\bar{q}$ or g) at a scale μ, not only with plus momentum[1] fraction x but with a specified transverse momentum k_t.

We start by constructing expressions for these functions in terms of a scheme based on conventional DGLAP evolution. Later I discuss equivalent approaches with modified evolution schemes which may be more appropriate for lower values of x [2, 4].

[1]In terms of light-cone variables, $k^+ \equiv k^0 + k^3$ is the plus momentum of an object with 4-momentum k^μ, $\mu = 0, 1, 2, 3$. See Section A.2.

2.1 Modifying DGLAP evolution

Consider the master equation [5] for evolution with parton virtuality of (for example) the non-singlet quark distribution, with $t \equiv \ln Q^2/Q_0^2$:

$$\frac{d}{dt}\, q^{NS}(x,t) = \frac{\alpha_s(t)}{2\pi} \int_x^1 \frac{dz}{z}\, q^{NS}\left(\frac{x}{z}, t\right)\, P_{qq}(z). \tag{2.2}$$

This describes all possible splittings from a parent parton with (plus) momentum fraction x/z, resolved at scale t, to a daughter parton with $x < x/z$, resolved at scale $t + dt$. The higher-x distribution of a few partons holding most of the momentum, such as the crude valence *uud* quark content of the proton, feeds into more partons with lower x as we probe more deeply.

However, the LO splitting function $\hat{P}_{qq}(z) = C_F\,(1+z^2)/(1-z)$, written as P_{qq} in (1.44), gives a famous *soft* singularity as $z \to 1$. We need to consider more carefully the role of $q^{NS}(x,t)$ in the evolution: this contributes virtual processes where a parent quark subsequently reabsorbs its own radiated gluon. Loop calculations, or imposing conservation of quark number, give the complete LO result

$$P_{qq}(z) = C_F \left(\frac{1+z^2}{(1-z)_+} \;+\; \frac{3}{2}\,\delta\,(1-z) \right) \tag{2.3}$$

where both terms lead to separately finite integrals, because the *plus prescription*

$$\int_0^1 \frac{f(z)}{(1-z)_+}\, dz \equiv \int_0^1 \frac{f(z) - f(1)}{1-z}\, dz$$

encapsulates the cancellation of the soft ($z \to 1$) real emission singularity with the corresponding infrared limit of virtual emission and reabsorption, which is physically indistinguishable.

A more convenient form of (2.2) can be derived as follows. In

$$\frac{dq^{NS}}{dt} \Bigg/ \frac{C_F\,\alpha_s(t)}{2\pi} = \int_x^1 \frac{dz}{z} \left(\frac{1+z^2}{(1-z)_+} + \frac{3}{2}\,\delta\,(1-z) \right) q^{NS}\left(\frac{x}{z}, t\right),$$

we extend the lower limit of the integral down to 0, on the understanding that $q^{NS} \to 0$ as $x/z \to 1$ and that we can define $q^{NS}(x/z, Q^2) = 0$ for $x/z > 1$. Then

$$\begin{aligned} \frac{dq^{NS}}{dt} \Bigg/ \frac{C_F\,\alpha_s(t)}{2\pi} &= \frac{3}{2}\,q^{NS}(x,t) + \int_0^1 \frac{dz}{1-z} \left(\frac{1+z^2}{z}\,q^{NS}\left(\frac{x}{z}, t\right) - 2q^{NS}(x,t) \right) \\ &= \int_x^1 \frac{dz}{z}\,\frac{1+z^2}{1-z}\,q^{NS}\left(\frac{x}{z}, t\right) - q^{NS}(x,t) \int_0^1 \frac{1+z^2}{1-z}\,dz, \end{aligned} \qquad (2.4)$$

since $\int_0^1 (1+z)dz = 3/2$. As (2.4) stands, the two separate pieces each contain a singularity at $z = 1$.

For computation, we can introduce a small cut-off Δ without affecting the result much, then we have

$$\frac{dq^{NS}}{dt}(x,t) = \frac{\alpha_s(t)}{2\pi} \int_x^{1-\Delta} \frac{dz}{z}\,\hat{P}_{qq}(z)\,q^{NS}\left(\frac{x}{z}, t\right) - \frac{\alpha_s(t)}{2\pi} q^{NS}(x,t) \int_0^{1-\Delta} dz\,\hat{P}_{qq}(z). \qquad (2.5)$$

The first term ("real") describes the growth of q^{NS} at x from x/z parents splitting to x, the second term ("virtual") accounts for x partons themselves disappearing by splitting to zx.

For general partons, therefore, the DGLAP evolution is described by[2]:

$$\frac{\partial a}{\partial \ln \lambda^2} = \frac{\alpha_s}{2\pi} \left[\int_x^{1-\Delta} P_{aa'}(z)\, a'\left(\frac{x}{z}, \lambda^2\right) dz \;-\; a(x,\lambda^2) \sum_{a'} \int_0^{1-\Delta} P_{a'a}(z')\, dz' \right], \qquad (2.6)$$

where λ is the scale, and $a\left(x, \lambda^2\right)$ denotes $xg\left(x, \lambda^2\right)$ or $xq\left(x, \lambda^2\right)$. We understand a sum over possible a' in the first term as well as the second. From now on I use $P_{aa'}$ to refer to the real parts of the splitting functions (which I wrote as $\hat{P}$ in (2.5)), in other words just the splitting functions listed in (1.41), (1.42), (1.43), and (1.44), because virtual ($z = 1$) effects are now taken into account in the second integral.

Let us summarise the logic so far. In Sections 1.5 and 1.6 I explained how consideration of radiative corrections to the process of deep inelastic scattering leads us to update the "naive" parton model densities $q(x)$, $g(x)$ to scale-dependent functions $q(x, \mu^2)$, $g(x, \mu^2)$, where for DIS a suitable scale is $\mu = Q$. We found that perturbative QCD makes definite predictions as to how the parton distribution functions depend on the scale. Eq. (2.6) describes this dependence in terms of the different splitting functions $P_{a'a}$. Fig. 2.1 shows the different vertices associated with the various splitting functions. In fact this diagram can be interpreted as a Feynman diagram, which contributes to the DIS cross section. (The virtual corrections are not shown, however, and we should also note that numerically, the gluon tends to dominate in the evolution at low x.)

The purpose of factorisation is to include situations like that pictured in Fig. 2.1, when we calculate cross sections for scattering processes with a hadron in the initial state. All of the diagram up to and including the P_{qq} splitting, plus also virtual corrections, can be incorporated in the probability $q(x, Q^2)$ to find a quark with 4-momentum $k \simeq$

[2]For the P_{gg} splitting this equation needs an extra factor of z' in the final integral, accounting for the identity of the gluons produced... this takes care of the $z' \to 0$ singularity in this symmetric splitting function.

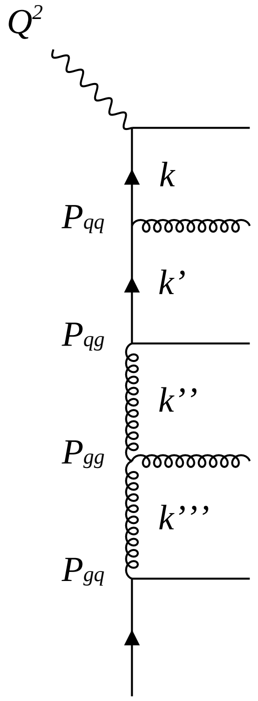

Figure 2.1: Parton splittings in evolution to scale Q^2.

$(xp, 0, k_t, xp)$. We would then convolute this probability with the simple cross section for the subprocess involving this quark, here just the absorption of the virtual photon coming from the electron in DIS.

Then the ladder diagram[3] represents the evolution of the partons to a high spacelike virtuality μ. At the bottom of the diagram, a parton emerges nearly on-shell from some non-perturbative regime (according to the long-distance structure of the proton) which we can only parametrise, obtaining values of $g(\xi, k_0^2)$ and $q(\xi, k_0^2)$ from experimental data. Then the parton undergoes various real radiations and virtual corrections in the evolution, governed by (2.6), taking it up to the virtuality scale μ. In an axial gauge the ladder-type diagrams such as Fig. 2.1 dominate. At each splitting a fraction of the

[3]Often the diagram shown is drawn squared, with the vertical lines duplicated and the horizontal lines as "rungs", suggesting use of the optical theorem.

longitudinal momentum (strictly, "plus" momentum $k^+ = k^0 + k^3$) is lost and so

$$x < x' < x'' < x'' < \cdots < \xi. \tag{2.7}$$

Now for the diagram shown to be a significant contribution to the cross section, there must be some compensating factor to counteract the α_s introduced at each QCD vertex in the ladder. For the DGLAP equation, the appropriate condition is so-called strong ordering of transverse momenta: that is, the numerically favoured configurations of momenta in Fig. 2.1 are those in which

$$k_t \gg k_t' \gg k_t'' \gg \cdots \tag{2.8}$$

In a similar way, we also require that μ, the factorisation scale such as $\mu = Q$, is much greater than the transverse momentum k_t at the top of the ladder. Effectively we are integrating over a nested sequence of splitting factors as given in (1.33), and if the strong ordering holds, can write

$$\int^{\mu^2} \frac{dk_t^2}{k_t^2} \int^{k_t^2} \frac{dk_t'^2}{k_t'^2} \int^{k_t'^2} \frac{dk_t''^2}{k_t''^2} \cdots$$

picking out a large transverse logarithm to compensate for each α_s factor of the n vertices (the contribution of the integration shown is like $\alpha_s^n (\ln \mu^2/\delta^2)^n/n!$). Note however that this is purely a numerical requirement to resum what we think are the dominant contributions from the collinear-enhanced behaviour in the evolution.

An alternative form of large logarithm could come from small $z_n \equiv x_n/x_{n+1}$, if we have strong ordering in *longitudinal* momentum, $x \ll x' \ll x'' \ll \cdots \ll \xi$. However it is clear that such effects can only feature for small values of x (the parton at the beginning of the ladder must of course have $\xi < 1$) and this possibility is ignored in traditional DGLAP evolution. I shall discuss it later.

Therefore, in the framework of collinear factorisation, the parton entering the subprocess has fairly small transverse momentum $k_t \ll \mu$, at leading order. However we are interested in going beyond the leading order and investigating the numerical effect of non-negligible k_t. In particular we wish to work with k_t factorisation [7] (also called high energy factorisation) whereby we attempt to incorporate information about some non-zero k_t in the parton distribution functions. The legitimate alternative is always to include Next-to-Leading-Order (NLO) effects in the coefficient function for the subprocess, but clearly it would be valuable if we could characterise a parton initial state with full kinematics from the starting order.

We see that the conventional parton distribution functions $a(x, \mu^2)$ describe transverse momentum $k_t \ll \mu$; in the construction of the DGLAP framework, the transverse momentum degree of freedom has been integrated out. For this reason we refer to the traditional functions xg and xq as *integrated* partons. However we might well want to introduce "unintegrated" functions f_a which display dependence on k_t as well, representing the probability of finding a parton a with plus momentum fraction x, transverse momentum k_t, at a (factorisation) scale μ. When we perform a calculation for an *inclusive* observable in which transverse momentum does not play a particularly important role, such as F_2, then we expect to integrate over possible transverse momenta k_t and recover the original integrated partons. In the case of a more *exclusive* observable, however, where we look at the differential cross section for some outcoming particle with high transverse momentum, or some cross section in which transverse momentum is particularly significant for experimental cuts, the k_t-dependent functions may be especially useful.

Since the unintegrated functions $f_a(x, k_t^2, \mu^2)$ depend on two scales, the evolution equations for such functions could potentially be rather more complicated [8] than (2.6). An example is the equation for the unintegrated gluon developed by Ciafaloni, Catani, Fiorani and Marchesini (CCFM) [9]. At present it has only been practical to use the CCFM equation in the context of Monte Carlo generators [10], which simulate the emissions of Fig. 2.1 in a parton shower for the initial state. Although Monte Carlo generators are of great importance to both theoretical and experimental particle physicists, it is interesting to investigate what we can learn from an analytic approach.

I have discussed the strong ordering of transverse momenta which is applied to the parton ladder in DGLAP evolution. This is only an approximate ordering, selecting the leading phase space region which contributes. There is also the limitation that for small enough values of x, logarithms $\ln 1/x$ are expected to dominate and this leads in the Balitskiĭ-Fadin-Kuraev-Lipatov (BFKL) framework [11] to contributions with strong longitudinal (x) ordering but *diffusion* in transverse momenta along the chain, quite contrary to strong k_t ordering.

However, there is a general ordering constraint which is better motivated for physics reasons. Colour coherence [6, 12] leads to an ordering of the *angles* at which gluons are emitted along the chain. For coherent radiation of these gluons, their angles of emission

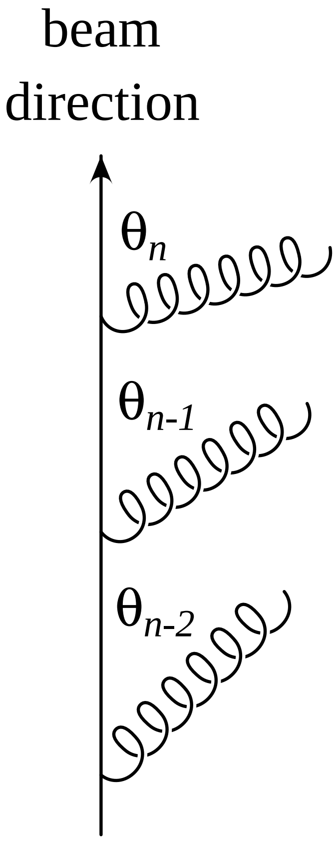

Figure 2.2: Angular ordering enforces increasing angles from the beam axis for the radiated gluons, as the spacelike (initial state) parton cascade develops (t-channel partons attaining successively greater negative virtualities).

must increase as we go up the ladder towards the hard subprocess[4],

$$\cdots\ \theta_n > \theta_{n-1} > \theta_{n-2}\ \cdots \tag{2.9}$$

see Fig. 2.2.

In fact this physical constraint embodies both of the situations already discussed. At large values of x, where we would expect the DGLAP framework to be appropriate, angular ordering corresponds to successively increasing k_t at each splitting. In a

[4]In timelike *final state* parton showers the converse applies: as the parton shower decreases in virtuality from the hard process to a multi-parton final state, the angles of emission become successively smaller [12].

BFKL-type situation, alternatively, the angle ($\theta \simeq k_t/k_l$) grows due to the decreasing longitudinal momentum k_l as we proceed along the emission chain from the proton.

Essentially this single quantity, the angle of emission, controls the evolution process. For this reason we would expect to obtain the unintegrated distributions $f_a(x, k_t^2, \mu^2)$ from evolution equations involving only a single scale. However, we have to examine the role of μ carefully. We can argue that μ, specified by the hard subprocess into which our parton enters from the top of the evolution chain, provides a limit on the maximum angle for the final radiation in the parton ladder. In other words μ restricts the allowed range of the transverse momentum k_t (see Appendix A.1), so that a typical angle characterising the high-virtuality subprocess is greater than the angle of the last emission prior to the parton entering the subprocess.

Our key observation is therefore that the μ dependence of $f_a(x, k_t^2, \mu^2)$ only enters at the final step of the evolution. For this reason, because the angle in the angular ordering is the governing variable[5], we can divide the evolution process into two parts. The first piece encompasses the bulk of the evolution, and this is performed in terms of a single scale. Then we separate the final step (the last rung of the ladder) and explicitly perform the last part of the evolution in such a way as to introduce the scale μ separately from the other scale of interest, k_t.

2.2 Unintegrated DGLAP partons

To construct our unintegrated parton densities, we unpick the final step of the evolution. Ignoring, for the moment, possible BFKL effects, we first establish a simple way of

[5]For example in Appendix A.1 and in Section 2.5 we write the "rescaled" transverse momentum, which is closely related to the angle, as the evolution variable.

generating a probability to measure a parton with transverse momentum k_t, in the context of the DGLAP framework described so far. It is convenient to work with the DGLAP equation as written in (2.6),

$$\frac{\partial a}{\partial \ln \lambda^2} = \frac{\alpha_s}{2\pi} \left[\int_x^{1-\Delta} P_{aa'}(z)\, a'\left(\frac{x}{z}, \lambda^2\right)\, dz \;-\; a(x,\lambda^2) \sum_{a'} \int_0^{1-\Delta} P_{a'a}(z')\, dz' \right].$$

We start off by using this equation to evolve $a(x,\lambda^2)$ (i.e. the gluon density function $xg(x,\lambda^2)$ and all the various quark and antiquark functions $xq(x,\lambda^2)$) from a starting parametrisation up to the scale $\lambda = k_t$. This provides values of $a'(x/z, k_t^2)$, representing the number density (times x/z) of parton type a' resolved at that single scale, carrying a fraction x/z of the proton's plus momentum.

Now let us require that parton a' undergoes a real emission characterised by splitting fraction z. From the first term in (2.6), we write the number density of parton type a emerging from such a splitting as

$$f_a(x,\ldots) \sim \frac{\alpha_s(k_t^2)}{2\pi} \int_x^{1-\Delta} P_{aa'}(z)\, a'\left(\frac{x}{z}, k_t^2\right)\, dz. \tag{2.10}$$

(λ is the usual choice of scale for α_s in (2.6). To choose something other than k_t would make only a subleading difference. There is often scale dependence of various kinds in perturbative QCD.)

The parton emerging from (2.10) has gained a transverse momentum $\sim k_t$ from the splitting at scale $\lambda = k_t$. This is because in the normal framework the parton virtuality is dominated by its transverse momentum, see Appendix A.

The distributions we seek are sampled at another momentum scale μ. Having gained

k_t from the final emission, the parton must continue evolving to scale μ but *without emitting any more real radiation*; if further splittings were to occur, the transverse momentum would be changed. If we consider now the second, remaining term of (2.6),

$$\frac{\partial a\left(x,\lambda^2\right)}{\partial \ln \lambda^2} = \ldots - a(x,\lambda^2)\,\frac{\alpha_s\left(\lambda^2\right)}{2\pi}\sum_{a'}\int_0^{1-\Delta} P_{a'a}(z')\,dz'$$

we effectively resum the possible further splittings to give a "survival probability" for the parton to evolve from $\lambda = k_t$ to $\lambda = \mu$ without further emission, to give a negative exponential suppression factor[6] similar to the Sudakov factor [6]:

$$T_a(k_t,\mu) = \exp\left(-\int_{k_t^2}^{\mu^2}\frac{\alpha_s(p_t^2)}{2\pi}\,\frac{dp_t^2}{p_t^2}\sum_{a'}\int_0^{1-\Delta} P_{a'a}(z')\,dz'\right). \qquad (2.11)$$

Here p_t is a possible intermediate scale between k_t and μ. If $k_t > \mu$, we set $T_a(k_t,\mu) = 1$ — there is no enhancement.

It follows from (2.10) and (2.11) that we can compute the number density of partons a with x, transverse momentum k_t, resolved at scale μ as [1, 2, 4]:

$$f_a(x,k_t^2,\mu^2) = T_a(k_t,\mu)\,\left(\frac{\alpha_s(k_t^2)}{2\pi}\int_x^{1-\Delta} P_{aa'}(z)\,a'\left(\frac{x}{z},k_t^2\right)\,dz\right). \qquad (2.12)$$

The only part of this equation we have not yet specified is how to treat Δ in (2.12) (and in (2.11), the definition of T_a). There is no longer a neat cancellation between real and virtual terms as in (2.6), so we need to consider carefully suitable values for Δ.

[6] Again note that the P_{gg} term in (2.11) should be accompanied by an extra factor of z'.

2.3 Δ is a physical cutoff

In the DGLAP equation (2.6) we can let $\Delta \to 0$. However here we must impose a physical cutoff in z, because evaluation of (2.12) will be dependent on the form of Δ. With non-negligible k_t emitted, we expect some energy loss ($\Rightarrow z < 1$). In [1] we imposed $\Delta = k_t/\mu$, which has a k_t-ordering effect. However, as discussed in Section 2.1, k_t ordering is too harsh if we are interested in going beyond the leading behaviour.

Angular ordering provides the appropriate constraint, see Section A.1 of Appendix A:

$$\Delta = \frac{k_t}{k_t + \mu}. \tag{2.13}$$

The same functional form of Δ must be used in the suppression factor T_a (so here $\Delta = p_t/(p_t + \mu)$) and in the last splitting at $\lambda = k_t$.

We make T_g and T_q more explicit for computational purposes. Writing $z_{max} \equiv 1 - \Delta(p_t, \mu) = \mu/(\mu + p_t)$, and substituting for the splitting functions (1.41) and (1.43) in (2.11), the gluon suppression factor is

$$\begin{aligned} T_g(k_t,\mu) &= \exp\left(-\int_{k_t^2}^{\mu^2} \frac{dp_t^2}{p_t^2}\,\frac{\alpha_s\left(p_t^2\right)}{2\pi}\int_0^{\mu/(\mu+p_t)} dz'\,\left(z'\,P_{gg}\left(z'\right) + n_F\,P_{qg}\left(z'\right)\right)\right) \\ &= \exp\left(-\int_{k_t^2}^{\mu^2} \frac{dp_t^2}{p_t^2}\,\frac{\alpha_s\left(p_t^2\right)}{2\pi}\left\{2N_C\left(\frac{z_{max}^3}{3} - \frac{z_{max}^4}{4} - z_{max}^2 - \ln\left(1 - z_{max}\right)\right)\right.\right. \\ &\qquad \left.\left. + \frac{n_F}{6}\left(3z_{max} - 3z_{max}^2 + 2z_{max}^3\right)\right\}\right) \end{aligned} \tag{2.14}$$

where n_F is the number of light flavours of $q\bar{q}$ pair available for the gluon to branch to (e.g. $n_F = 3$). Again we stress $T_a\left(k_t > \mu, \mu\right)$ is defined to be 1. The quark suppression factor is even simpler, as there is only one type of splitting that can be originated by a quark, so

$$
\begin{aligned}
T_q(k_t,\mu) &= \exp\left(-\int_{k_t^2}^{\mu^2}\frac{dp_t^2}{p_t^2}\,\frac{\alpha_s\left(p_t^2\right)}{2\pi}\int_0^{\mu/(\mu+p_t)} dz'\,P_{qq}(z')\right)\\
&= \exp\left(-\int_{k_t^2}^{\mu^2}\frac{dp_t^2}{p_t^2}\,\frac{\alpha_s\left(p_t^2\right)}{2\pi}\,C_F\left(-z_{max}-\frac{z_{max}^2}{2}-2\ln\left(1-z_{max}\right)\right)\right). \quad (2.15)
\end{aligned}
$$

2.4 Different limits

In the BFKL limit, when $\alpha_s \ln 1/x$ dominates, the $1/z$ term in the splitting function P_{gg} becomes most important. We neglect the virtual correction part of (2.6) and the suppression factor $T \to 1$ (we also do not have any ordering in k_t in this limit). In that case,

$$
f_g(x,k_t^2,\mu^2) \to h_g(x,k_t^2) \equiv \left.\frac{\partial\left(xg(x,\lambda^2)\right)}{\partial\ln\lambda^2}\right|_{\lambda=k_t}. \quad (2.16)
$$

The function $h_g(x,k_t^2)$ is the original type of "unintegrated" parton, which satisfies the BFKL equation [11]. Note that this is a single-scale function, because the leading logarithmic part does not depend on the other scale μ.

An alternative limit, often of interest, is the double leading logarithm approximation (DLLA). This applies for moderate Q^2 and moderate x values, such that $\alpha_s \ln Q^2 \ll 1$ (therefore not DGLAP), $\alpha_s \ln 1/x \ll 1$ (therefore not BFKL), but the combination $\alpha_s \ln Q^2 \ln 1/x \sim 1$. Effectively we have to have strong ordering both in k_t and in $1/x$ to pick out this region. In this situation, only the singular part $1/(1-z')$ of the diagonal splitting functions P_{aa} contributes. The suppression factor becomes

$$
T_a^{\mathrm{DLLA}}(\lambda,\mu) = \exp\left(-\int_{\lambda^2}^{\mu^2}\frac{\alpha_s(p_t^2)}{2\pi}\,\frac{dp_t^2}{p_t^2}\int_0^{1-\Delta}\frac{dz'}{1-z'}\,2C_a\right), \quad (2.17)
$$

where C_a denotes C_F for the quark factor or C_A for the gluon. Because we have restored strong k_t ordering, Δ will be numerically small, and we can choose the same Δ in the DGLAP equation (2.6); so we can also express f in this limit as a derivative:

$$f_a^{\rm DLLA}(x, k_t^2, \mu^2) = \frac{\partial}{\partial \ln \lambda^2} \Big[a(x, \lambda^2)\, T_a(\lambda, \mu) \Big] \Big|_{\lambda = k_t} . \tag{2.18}$$

This exploits the fact that we can express the second term of (2.6) in this limit as $-a(x, \lambda^2)\, \partial \ln T_a / \partial \ln \lambda^2$.

2.5 A unified BFKL/DGLAP approach

We wish to generalise the method described in Section 2.2 to incorporate the leading $\ln 1/x$ contributions in our framework. This necessitates adding BFKL-type terms to both the single-scale and final step parts of our evolution scheme. Clearly there can be different ways of doing this, leading to slightly different forms of "unified" evolution equations, where the ambiguity occurs at a subleading level. Our aim is to find a good physically-motivated prescription which is not too complicated, but which can account for all the relevant kinematic effects just at LO level. So we seek an equation which sums up the major part of the subleading corrections in a LO framework.

The BFKL equation has an enormous literature, see for example [29]. The description of the involvement of gluons in processes of moderate Q^2 (in general, moderate t channel momenta) but large centre of mass energy squared s, which probe the low x region, requires a framework in terms of effective ladder diagrams with "reggeised" gluons exchanged in the t channel. This is collective behaviour which picks out the dominant $\ln s$ contributions to high energy cross sections. For our purposes it is suf-

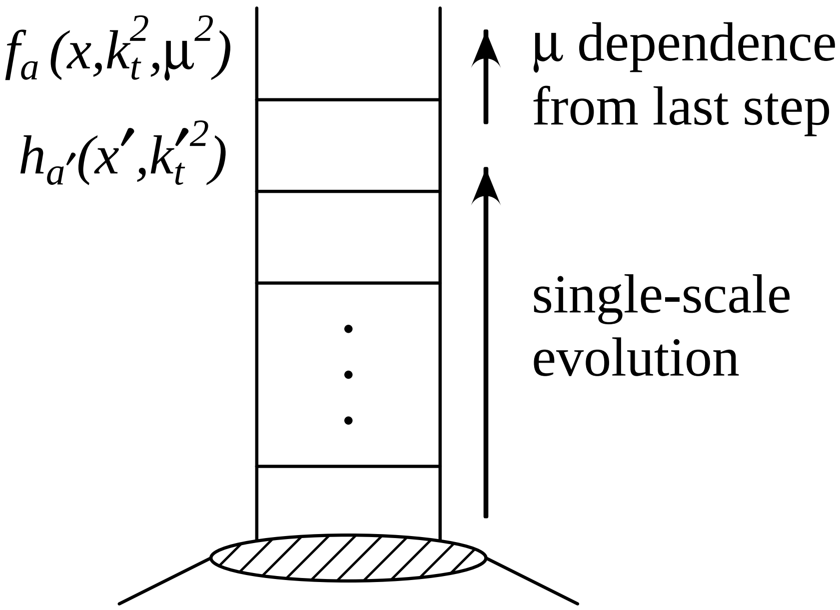

Figure 2.3: An illustration of our procedure, in which the evolution of a single-scale unintegrated parton is followed by a final step of the ladder which introduces dependence on the second hard scale, μ.

ficient to modify the $1/z$ part of the DGLAP splitting function, to incorporate the BFKL kernel which accounts for evolution of such reggeised gluons. We of course have to work in terms of the basic low-x distribution, the single-scale unintegrated gluon $h_g(x, k_t^2) \equiv \partial xg(x, k_t^2)/\partial \ln k_t^2$ discussed in Section 2.4. Therefore our procedure of single-scale evolution followed by an explicit final step has to be recast in terms of unintegrated single-scale functions [2, 4]. We preserve the remaining DGLAP structure for those parts of the equations which are not dominant at low x, in a manner inspired by the unified BFKL/DGLAP equation of [19]; in such a way we include BFKL effects at finite x. The essence of the procedure is unchanged. Fig. 2.3 is a reminder of the relationship between the auxiliary functions h and the two-scale unintegrated partons we seek, f.

The unified equation for h_g, which closely follows that presented in [19], takes the form

$$
\begin{aligned}
h_g(x,k_t^2) = h_g^0(x,k_0^2) \;+\; & \frac{\alpha_s(k_t^2)}{2\pi} \int_0^1 dz \int_{k_0^2}^{k_t^2} \frac{dk_t'^2}{k_t'^2} \qquad\qquad (2.19) \\
& \left[\Theta(z-x)\bar{P}(z)\, h_g\left(\frac{x}{z}, k_t'^2\right) - zP_{gg}(z) h_g(x,k_t'^2) \right. \\
& \qquad \left. + \Theta(z-x) P_{gq}(z) \sum h_q \left(\frac{x}{z}, k_t'^2\right) - n_F P_{qg}(z)\, h_g(x,k_t'^2) \right] \\
+ \frac{\alpha_s(k_t^2)}{2\pi} 2N_C \int_x^1 \frac{dz}{z} & \int \frac{d^2q}{\pi q^2}\, \Theta(k_t'^2 - k_0^2) \left[\Theta(k_t^2 - zq^2)\, \frac{k_t^2}{k_t'^2}\, h_g\left(\frac{x}{z}, k_t'^2\right) \right. \\
& \qquad \left. - \Theta(k_t^2 - q^2)\, h_g\left(\frac{x}{z}, k_t^2\right) \right].
\end{aligned}
$$

Here k_t' is the transverse momentum of the parent parton, and q is the rescaled transverse momentum of the radiated gluon, such that $\boldsymbol{k_t'} = \boldsymbol{k_t} + (1-z)\boldsymbol{q}$. The splitting function $\bar{P}(z) = P_{gg} - 2N_C/z$ is constructed to account for the parts of the gluon-gluon splitting which are subleading in $1/z$.

The final part of (2.19) (with the integration over q) contains the BFKL evolution, treating the $2N_C/z$ piece of the splitting function differently. $\Theta(k_t^2 - zq^2)$ comes from the consistency constraint imposed for the low x evolution, see Section A.3. I have not written any cutoff Δ on the z integrals, because the cancellation should take place within the square-bracketed terms.

Notice that I have symmetrically introduced a single-scale unintegrated function for quarks, $h_q(x,k_t^2) \equiv \partial xq(x,k_t^2)/\partial \ln k_t^2$. I use h_q for different flavours q to refer to any individual quark or antiquark distribution. In (2.19) we sum over all $2n_F$ active flavours q of quarks or antiquarks with mass $m_q < k_t$.

We also need to supply a driving term, $h_g^0(x,k_0^2)$, for the right-hand side of the evolution equation (2.19), which contains the starting distributions $a(x', k_0^2)$:

$$h_g^0(x,k_0^2) = \frac{\alpha_s(k_t^2)}{2\pi} \int_0^1 dz \left\{ \Theta(z-x) \left[P_{gg}(z)\,\frac{x}{z} g\left(\frac{x}{z}, k_0^2\right) + P_{gq}(z) \sum \frac{x}{z} q\left(\frac{x}{z}, k_0^2\right) \right] - zP_{gg}(z)\, xg(x,k_0^2) - n_F P_{qg}(z) xg(x,k_0^2) \right\}. \quad (2.20)$$

The equation we use for the quark evolution is simply DGLAP evolution, written in terms of our h functions with explicit integration over the transverse momentum. (This is unlike the Kwieciński-Martin-Staśto (KMS) equation [19] in which a more complicated structure is needed to generate *physical* a_q sea quark distributions to compare directly with F_2 data. Here h_q is an auxiliary function, but we will introduce a subtler framework for predicting F_2 in terms of our f_a functions, in Chapter 3.) So the single-scale evolution for a particular quark or antiquark flavour q is

$$h_q(x,k_t^2) = h_q^0(x,k_0^2) + \frac{\alpha_s(k_t^2)}{2\pi} \int_0^1 dz \int_{k_0^2}^{k_t^2} \frac{dk_t'^2}{k_t'^2} \left\{ \Theta(z-x) \left[P_{qg}(z)\, h_g\left(\frac{x}{z}, k_t'^2\right) + P_{qq}(z)\, h_q\left(\frac{x}{z}, k_t'^2\right) \right] - P_{qq}(z)\, h_q(x,k_t'^2) \right\}, \quad (2.21)$$

with a driving term h_q^0 like (2.20).

Finally, we write equations based on (2.19) and (2.21), to describe the last-step evolution, but in the folded form with suppression factors and the explicit, physically motivated z cutoff from Section 2.3. Thus x times the number of gluons produced at the last step with transverse momentum k_t which initiate a hard subprocess with factorisation scale μ is

$$f_g\left(x, k_t^2, \mu^2\right) = T_g\left(k_t, \mu\right)\, \frac{\alpha_s\left(k_t^2\right)}{2\pi} \times \left\{ \int_x^{\mu/(\mu+k_t)} dz \int_0^{k_t^2} \frac{dk_t'^2}{k_t'^2} \left[\bar{P}(z)\, h_g\left(\frac{x}{z}, k_t'^2\right) + P_{gq}(z) \sum_q h_q\left(\frac{x}{z}, k_t'^2\right) \right] \right.$$

$$+ 2N_C \int_x^{\mu/(\mu+k_t)} \frac{dz}{z} \int \frac{d^2q}{\pi q^2} \left[\frac{k_t^2}{k_t'^2} h_g\left(\frac{x}{z}, k_t'^2\right) - \Theta\left(k_t^2 - q^2\right) h_g\left(\frac{x}{z}, k_t^2\right)\right]\Bigg\} . \quad (2.22)$$

Note that angular ordering in the last step has superseded the consistency constraint and we do not need $\Theta(k_t^2 - zq^2)$. We integrate in principle over all of the phase space of q. The suppression factor T_g is calculated as before in (2.14). For quarks we do not write a BFKL part, so the analogous last-step equation is

$$f_q\left(x, k_t^2, \mu^2\right) = T_q\left(k_t, \mu\right) \frac{\alpha_s\left(k_t^2\right)}{2\pi} \times$$
$$\int_x^{\mu/(\mu+k_t)} dz \int_0^{k_t^2} \frac{dk_t'^2}{k_t'^2} \left[P_{qq}(z)\, h_q\left(\frac{x}{z}, k_t'^2\right) + P_{qg}(z)\, h_g\left(\frac{x}{z}, k_t'^2\right)\right] . \quad (2.23)$$

The quark version is nearly ready to compute as it stands, but there is an angular integral in the gluon equation (2.22) which can be performed analytically. We rewrite the $\Theta(k_t^2 - q^2)$ function as $1 - \Theta(q^2 - k_t^2)$. With this simple trick, this integral becomes

$$\int \frac{d^2q}{\pi q^2} \left[\frac{k_t^2}{k_t'^2} h_g\left(\frac{x}{z}, k_t'^2\right) - h_g\left(\frac{x}{z}, k_t^2\right)\right] + \int_{k_t^2}^{\infty} \frac{dq^2}{q^2} h_g\left(\frac{x}{z}, k_t^2\right) . \quad (2.24)$$

We then change integration variable from q to k_t', that is

$$\frac{d^2q}{\pi q^2} \rightarrow \frac{d^2k_t'}{\pi k_t'^2} \frac{k_t'^2}{k_t'^2 + k_t^2 - 2k_t' k_t \cos\phi} , \quad (2.25)$$

giving

$$\int_0^{k_{max}^2} \frac{k_t^2\, h_g\left(x/z, k_t'^2\right) - k_t'^2\, h_g\left(x/z, k_t^2\right)}{|k_t'^2 - k_t^2|} \frac{dk_t'^2}{k_t'^2} + h_g\left(\frac{x}{z}, k_t^2\right) \ln\left(\frac{k_{max}^2}{(1-z)^2 k_t^2}\right) . \quad (2.26)$$

An arbitrary maximum for k_t' has been introduced, k_{max}. Typically $k_{max} = 10k_t$ would be sufficient. In the logarithm term we have approximated q_{max} to $k_{max}/(1-z)$, which is well justified as we take the limit $(1-z)q \gg k_t$ of the exact relation

$$(1-z)^2 q^2 = k_t'^2 + k_t^2 - 2k_t' k_t \cos\phi. \tag{2.27}$$

2.6 Plots of the unintegrated partons

I have now presented two alternative frameworks for computing two-scale unintegrated parton distribution functions $f_a(x, k_t^2, \mu^2)$. The first, from Sections 2.2 and 2.3, involves the single-scale DGLAP evolution of integrated partons $a(x, k^2)$ up to a scale k_t, followed by an explicit last step integration based on the DGLAP equation (2.6). In the final step we employ a cutoff Δ on the z integrals in accordance with the requirement of angular ordering. The second approach (Section 2.5) attempts to include BFKL effects which are likely to be prominent at low values of x. With a "unified" BFKL/DGLAP equation (2.19) for the single-scale unintegrated gluon $h_g(x, k^2)$, based on that in [19], and a DGLAP equation for the single-scale unintegrated quark functions $h_q(x, k^2)$ (2.21), we perform evolution up to scale k_t. Then again an angular-ordered last step is explicitly computed to yield $f_g(x, k_t^2, \mu^2)$ and $f_q(x, k_t^2, \mu^2)$, where our equation for f_g incorporates the BFKL kernel also.

The role of the single-scale functions in either approach is as auxiliary functions; they are input to our last-step procedure. Ideally, we should treat the unintegrated partons $f_a(x, k_t^2, \mu^2)$ as the fundamental objects and perform a new global fit, using these quantities to predict physical observables, in a new formalism.

$$
\begin{array}{lll}
a(x, k_0^2) & \text{parametrised} & \\
\quad\downarrow & & \\
a(x, k^2) & \text{DGLAP} \quad \text{or} \quad h_a(x, k^2) & \text{BFKL/DGLAP} \\
\quad\downarrow & & \\
f_a(x, k_t^2, \mu^2) & \text{DGLAP} \quad \text{or} \quad \text{BFKL/DGLAP} & \\
\quad\downarrow & & \\
\text{observables} & \text{e.g. } F_2, \text{ prompt photon cross section} &
\end{array}
$$

However a proper parton fit is a sophisticated and time-consuming business, mostly carried out nowadays by established experts. It is beyond the scope of my current research and this thesis to do justice to such a fit, although I discuss by way of illustration in Section 3.4 a crude attempt I have made.

We can nevertheless obtain workable unintegrated partons from our formalism *without* undergoing the fitting process, if we are prepared to use existing parton distributions as input to our last-step procedure, as in [4]. That is, rather than generating our own auxiliary functions $a(x, k^2)$ for instance, we might hope to obtain similar results by using an existing set of integrated parton distribution functions in their place. For the DGLAP framework, it is appropriate to use the Martin-Roberts-Stirling-Thorne (MRST99) [32] set of integrated partons. These have been fitted to data via the conventional, collinear formalism, but we expect the effect of the last evolution step to be mostly a redistribution in k_t-space, so for a first investigation of our unintegrated partons, we shall take these as the single-scale functions $a(x, k^2)$. (I am grateful to Jeppe Andersen for developing efficient C++ code which provides values of the MRST99 parton distributions, see [32].)

Alternatively, for our unified BFKL/DGLAP approach, we need functions h_g and h_q to feed into the final evolution step. In this case the most appropriate available distributions come from the KMS paper [19]. In fact the evolution in that paper is slightly different in form from that we propose in (2.19) and especially (2.21), but it incorporates essentially maximal BFKL effects. The functions provided have been fitted, via their own formalism, to data, and with caveats, we may also adopt them as suitable auxiliary functions for our last step evolution in (2.22) and (2.23). (I am also grateful to Anna Staśto for her C code which provides values of the distributions from [19].)

There is one final point about the calculation of our new unintegrated partons in the unified BFKL/DGLAP approach. We need to divide the calculation of (2.22) and (2.23) into perturbative ($k_t' > k_0$) and non-perturbative ($k_t' < k_0$) contributions. The argument of the input functions must not drop below k_0, so we add new terms to account (approximately) for the low k_t' region. The total gluon result is

$$
\begin{aligned}
f_g\left(x,k_t^2,\mu^2\right) = T_g\left(k_t,\mu\right)\ \frac{\alpha_s\left(k_t^2\right)}{2\pi}\ \Bigg\{ \int_x^{\mu/(\mu+k_t)} dz \qquad\qquad (2.28)\\
\left[P_{gq}(z)\sum_q a_q\left(\frac{x}{z},k_t^2\right) + \bar{P}(z)\,a_g\left(\frac{x}{z},k_0^2\right) + \int_{k_0^2}^{k_t^2}\frac{dk_t'^2}{k_t'^2}\,\bar{P}(z)\,h_g\left(\frac{x}{z},k_t'^2\right)\right]\\
+\,2N_C\int_x^{\mu/(\mu+k_t)}\frac{dz}{z}\,\left[\int_{k_0^2}^{k_{max}^2}\frac{k_t^2\,h_g\left(x/z,k_t'^2\right) - k_t'^2\,h_g\left(x/z,k_t^2\right)}{|k_t'^2-k_t^2|}\,\frac{dk_t'^2}{k_t'^2}\right.\\
\left. +\,h_g\left(\frac{x}{z},k_t^2\right)\ln\left(\frac{k_{max}^2}{(1-z)^2k_t^2}\right) + a_g\left(\frac{x}{z},k_0^2\right) - \frac{k_0^2}{k_t^2}\,h_g\left(\frac{x}{z},k_t^2\right)\right]\Bigg\}.
\end{aligned}
$$

Note that k_0, the minimum parton set scale, is set to 1 GeV as used in the KMS fit [19]. Staśto's code provides $h_g(x,k^2)$ (which can be negative) and the *integrated* single-scale quark functions $a_q(x,k^2) \equiv \int^{k^2} h_q(x,k'^2)\,dk'^2/k'^2$, and the initial function $a_g(x,k_0^2) = 1.57\,(1-x)^{2.5}$. In the same way the actual unintegrated quarks generated with the functions from [19] are

$$f_q\left(x,k_t^2,\mu^2\right) = T_q\left(k_t,\mu\right)\ \frac{\alpha_s\left(k_t^2\right)}{2\pi}\ \times \tag{2.29}$$
$$\int_x^{\mu/(\mu+k_t)} dz\ \left[P_{qq}(z)\ a_q\left(\frac{x}{z},k_t^2\right)\ +\ P_{qg}(z)\ a_g\left(\frac{x}{z},k_0^2\right)\ +\ \int_{k_0^2}^{k_t^2}\frac{dk_t'^2}{k_t'^2}\,P_{qg}(z)\ h_g\left(\frac{x}{z},k_t'^2\right)\right].$$

Therefore we compare the results of computing the unintegrated gluon $f_g(x,k_t^2,\mu^2)$ in several different ways, as in [4]. Comparison of the gluon computed using the KMS functions as input, which therefore incorporates BFKL effects, see (2.28), with the simpler alternative form of (2.12) using as a convenient input the MRST integrated partons [32], gives some idea of the importance of the BFKL effects in the evolution.

Fig. 2.4 shows the k_t dependence of three types of unintegrated gluon $f_g(x,k_t^2,\mu^2)$. None of these are the result of new fits to data, but they are illustrative of the typical results of using the last-step procedure, with input from existing parton functions. The continuous curves show our unified BFKL/DGLAP version, with the input from the KMS functions h_g and a_q as written in (2.28). The scale μ has been chosen as 10 GeV and we plot[7] $f_g(x,k_t^2,\mu^2)$ for various fixed values of x, for a range of k_t^2 including the region $k_t > \mu$. The shape of the distribution changes significantly as we go to lower values of x, developing, as expected, more of a tail for high k_t.

However it appears that this small-x behaviour is not specifically because of the BFKL terms, at the range of x shown in Fig. 2.4. The dotted curves show our "DGLAP" version of the unintegrated gluon as written in (2.12), computed with the MRST99 integrated partons a as input. The key point is that the cutoff in the last evolution step, motivated by angular ordering, allows the unintegrated partons to develop a tail

[7]Note that some authors define the quantity f_g/k_t^2 as the unintegrated gluon, but our choice shows the high-k_t detail particularly clearly.

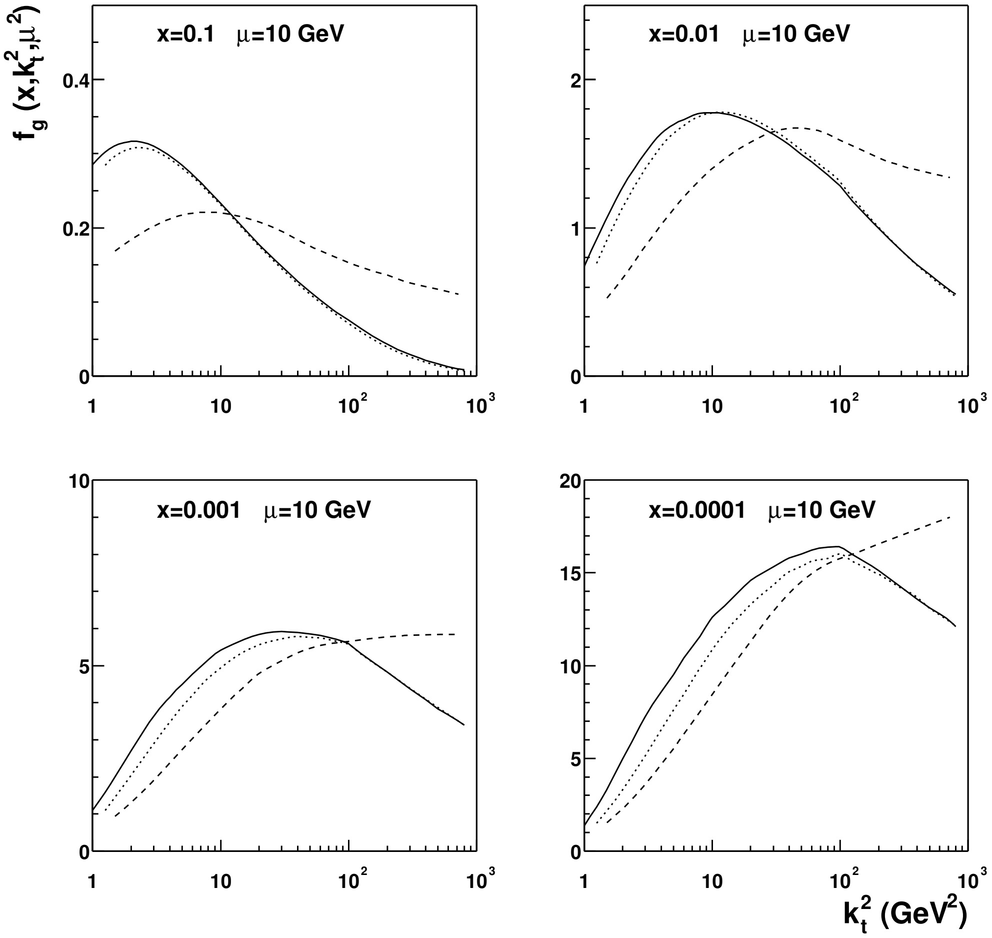

Figure 2.4: Plots of the k_t dependence of the unintegrated gluon $f_g(x, k_t^2, \mu^2)$ for various values of x, at $\mu = 10$ GeV. The continuous curves are our unified BFKL/DGLAP version of f_g, computed from (2.28), taking input functions from [19]; for comparison we show with dashed lines the unintegrated gluon from [2] (as in [2], the dashed lines have been smoothed in the transition region $k_t \sim \mu$). Also we plot our "DGLAP" unintegrated gluon with dotted lines, computed from (2.12) with input integrated MRST partons. With the correct angular ordering cutoff in the last step the DGLAP version is very close to our unified BFKL/DGLAP gluon, especially at high x.

at high k_t when the kinematics allow (that is, at lower x values). Although the input functions to the unified BFKL/DGLAP approach of Section 2.5 are quite different from the integrated partons fed into the angular-ordered DGLAP approach of Section 2.2, we find that because they have both separately been fitted in appropriate frameworks to inclusive F_2 data, the two-scale unintegrated gluons we compute from them are very similar. Our conclusion is that the role of angular ordering in the last step of evolution is particularly important, even more so than BFKL effects in the HERA domain.

We also compare in Fig. 2.4 with another definition of the unintegrated gluon, coming from [2]: the dashed curves. In [2] we wrote an equation in a somewhat similar unified BFKL/DGLAP framework, but without the full (correct) angular ordering in the last step[8]. We prefer the new version (that of [4]), although we stress the need to perform a new global fitting analysis to constrain the unintegrated partons f_a by comparison to data within the context of the new framework.

In Fig. 2.5 we show similar k_t plots for the unified BFKL/DGLAP gluon of Section 2.5, compared to the angular-ordered DGLAP gluon of Section 2.2, but at a lower scale $\mu = 5$ GeV. Again the two approaches yield similar results. The angular ordering cutoff on the z (and z') integrations, $\Delta = k_t/(k_t + \mu)$, is very significant. In Fig. 2.6 the dotted curves are still those computed from (2.12) with $\Delta = k_t/(k_t + \mu)$, but for comparison I also show an unintegrated gluon generated from the same equation (and same MRST input integrated partons $a'(x/z, k_t^2)$) but with the k_t-ordering cutoff $\Delta = k_t/\mu$. This is in fact the form of unintegrated parton we proposed in [1]. At this low scale μ, the effect of the different cutoffs is especially striking.

Figs. 2.7 and 2.8 are equivalent to Figs. 2.5 and 2.6, but at the scale $\mu = 25$ GeV.

[8] The choices of scale in [2] are also slightly different, which increases the computation time.

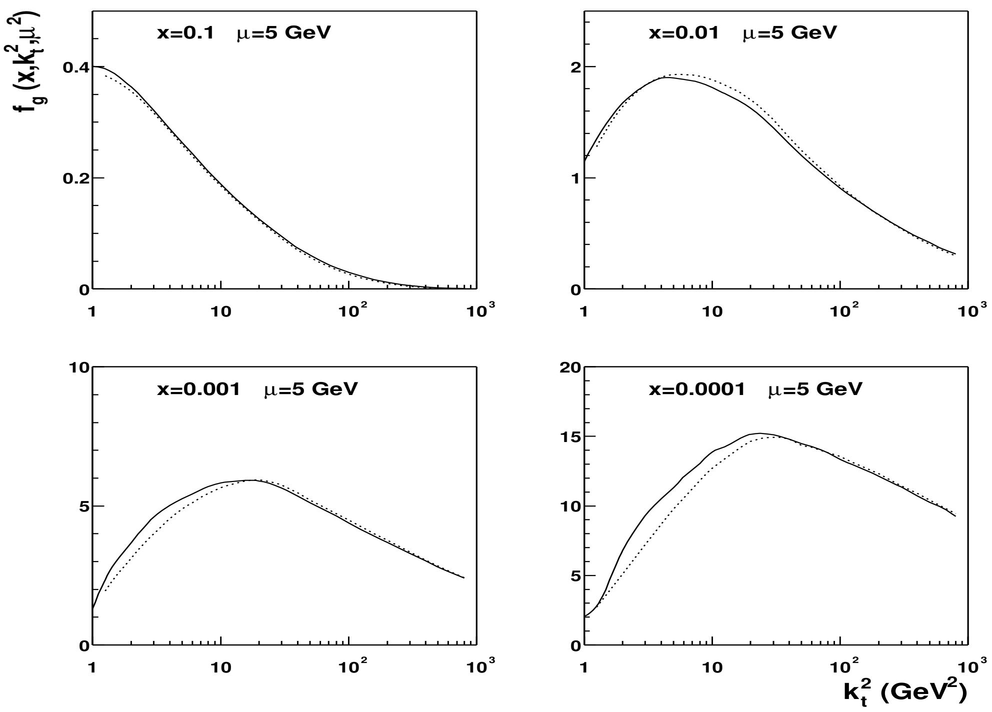

Figure 2.5: Similar to Fig. 2.4, but at $\mu = 5$ GeV. The continuous curves are our unified BFKL/DGLAP version of f_g; the dotted curves are our "DGLAP" unintegrated gluon.

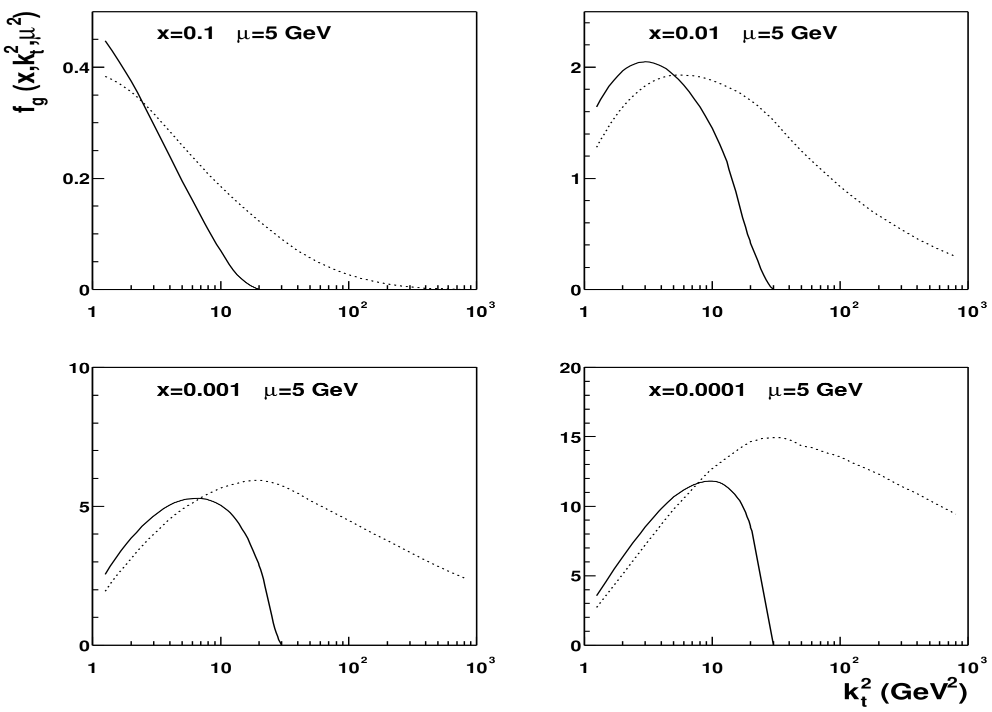

Figure 2.6: The dotted curves are as in Fig. 2.5, but here we plot continuous curves from the prescription of [1], using the same (2.12) but with the cutoff $\Delta = k_t/\mu$.

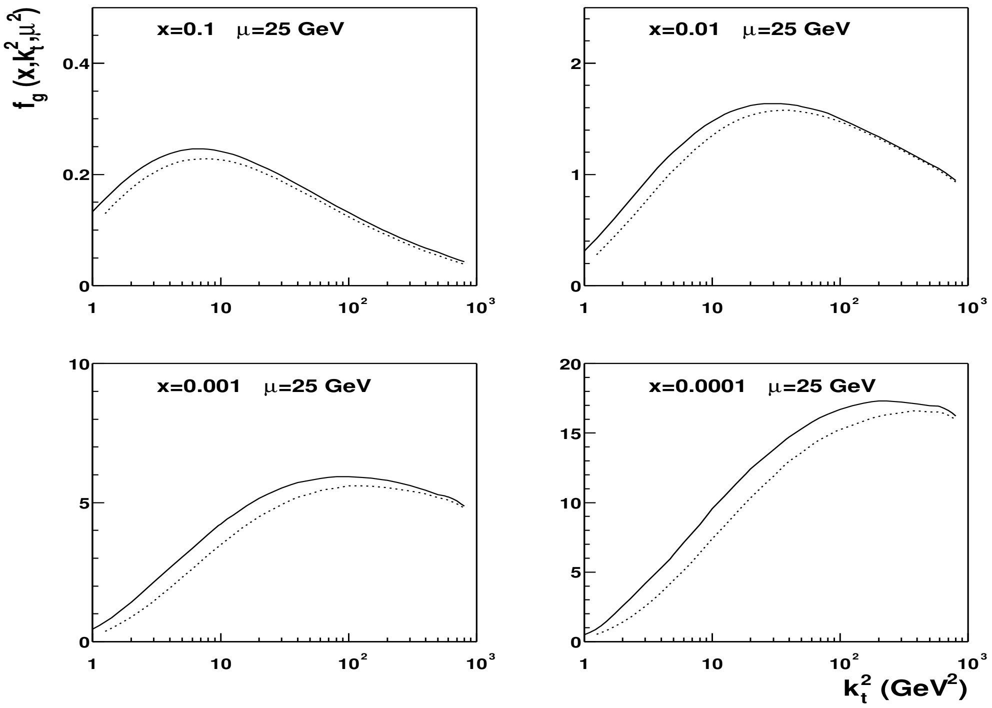

Figure 2.7: Similar to Fig. 2.5, but at $\mu = 25$ GeV. The continuous curves are our unified BFKL/DGLAP version of f_g; the dotted curves are our "DGLAP" unintegrated gluon.

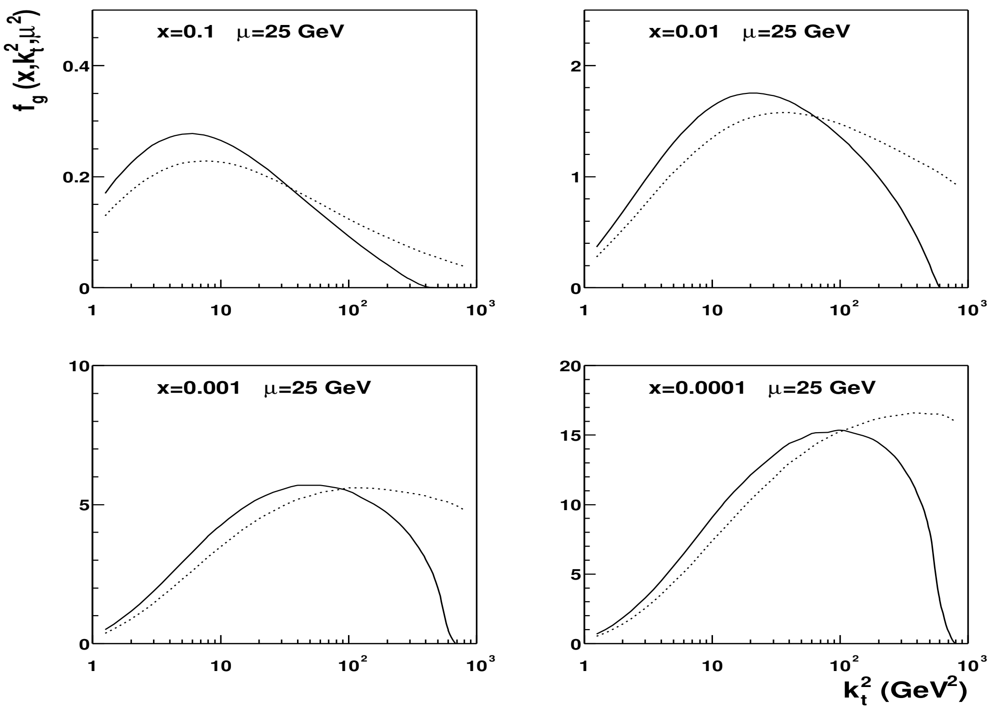

Figure 2.8: The dotted curves are as in Fig. 2.7, but here we plot continuous curves from the prescription of [1], using the same (2.12) but with the cutoff $\Delta = k_t/\mu$.

For completeness I also include plots of the unintegrated quark distribution functions, $f_q(x, k_t^2, \mu^2)$. The curves in Figs. 2.9 and 2.10 have all been calculated in the angular-ordered DGLAP approach, again using the MRST partons as input, at $\mu = 10$ GeV. The individual flavours of quark and antiquark have separate distributions, although at low x they are predominantly driven by the gluon (which produces light $q\bar{q}$ flavours indiscriminately). Fig. 2.9 shows the up quark distribution f_u in continuous curves and the up antiquark distribution $f_{\bar{u}}$ in dotted curves. Likewise Fig. 2.10 shows f_d and $f_{\bar{d}}$, with also, in dashed lines, the strange quark distribution f_s (one of the assumptions of the MRST partons is that $s = \bar{s}$; this of course carries through into our $f_s = f_{\bar{s}}$). Similar kinematics produce quite similar shapes of unintegrated quark, compared with the unintegrated gluon plotted before. However note that the f axis scales are much smaller than those used for the gluon plots, especially at low x, and this means that for many partonic processes at low x one can focus on processes initiated by gluons. This property is of course "inherited" from the input single-scale functions too. We also see that at low x the difference between different flavours of quark or antiquark is small, because we effectively have a "sea" of $q\bar{q}$ pairs.

We can examine the role of the Sudakov-like suppression factor more carefully by plotting the μ-dependence of the unintegrated gluon $f_g(x, k_t^2, \mu^2)$, again using the angular-ordered DGLAP version from MRST partons for simplicity. So in Fig. 2.11 I fix the transverse momentum $k_t = 3$ GeV and plot (again at four values of x) for μ from $\mu < k_t$ to $\mu \gg k_t$. Here therefore the tail $k_t > \mu$ appears on the left of the plots (before $\mu^2 = 9$ GeV^2); there is no such tail for the dashed-line plots with $\Delta = k_t/\mu$ as in [1]. In Fig. 2.11 there are notable "kinks" at $k_t = \mu$ where the slope of the tail $k_t > \mu$ is rather different from the ordinary $k_t < \mu$ region. In fact this is evident in many of the figures, such as Fig. 2.4. The effect is to do with the way the suppression factor T_a is

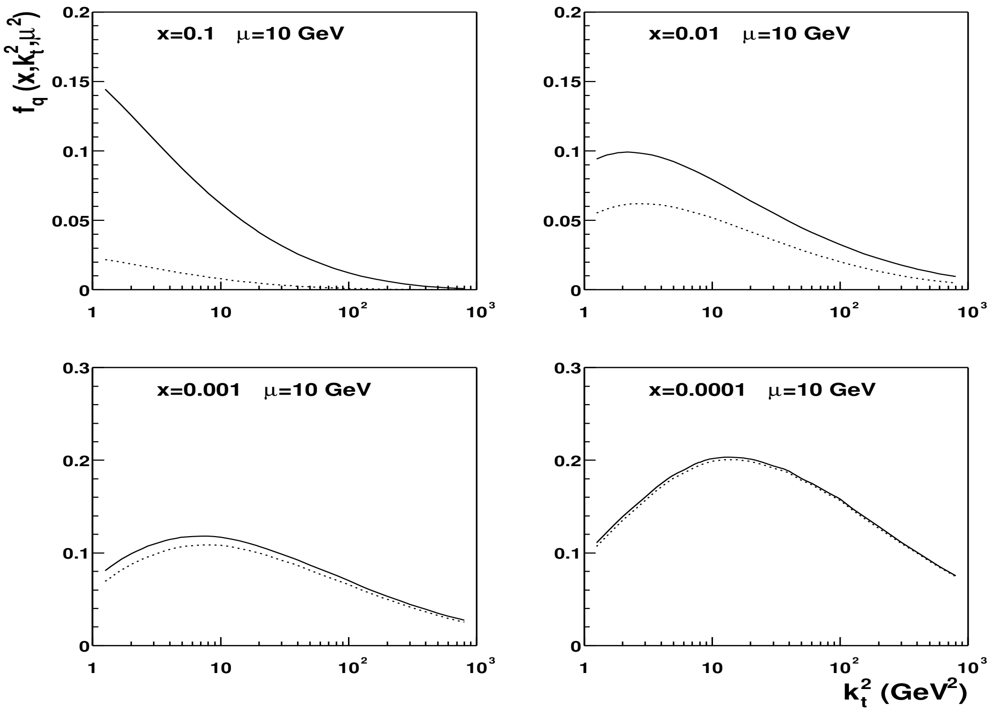

Figure 2.9: k_t dependence of unintegrated quark distributions, generated with our angular-ordered DGLAP last step from MRST parton input, at $\mu = 10$ GeV. The continuous curves are $f_u(x, k_t^2, \mu^2)$; the dotted curves are $f_{\bar{u}}(x, k_t^2, \mu^2)$.

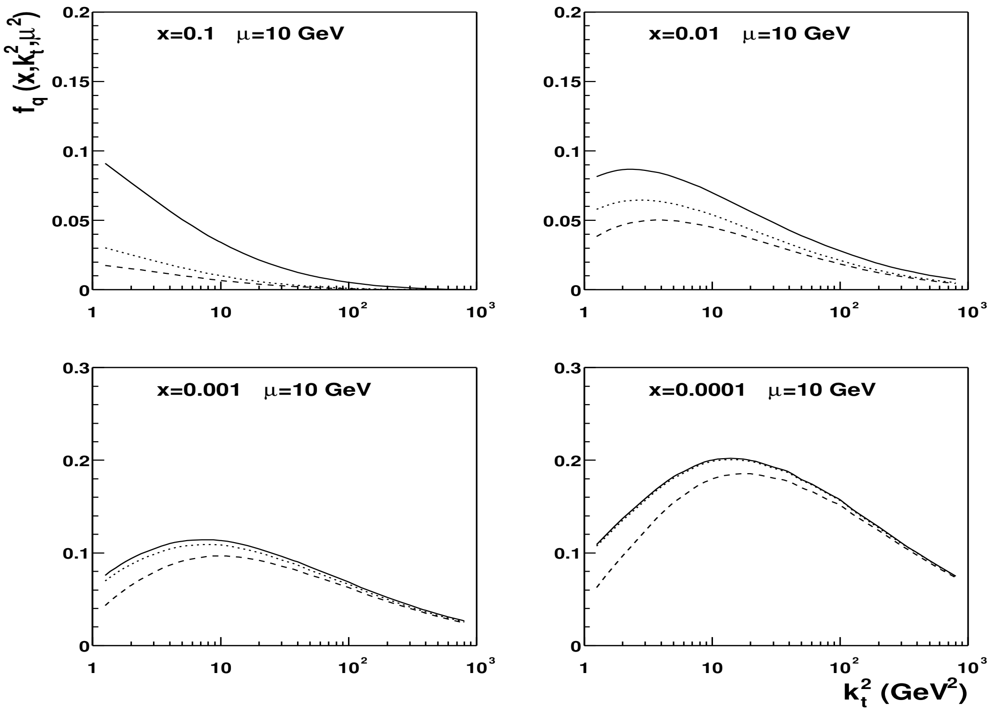

Figure 2.10: Similar to Fig. 2.9 but with continuous curves $f_d(x, k_t^2, \mu^2)$, dotted $f_{\bar{d}}(x, k_t^2, \mu^2)$, and dashed curves being $f_s(x, k_t^2, \mu^2)$.

introduced with a non-zero derivative at $\mu \geq k_t$: we see in Fig. 2.12 (dotted curves) what happens if we artificially set $T = 1$ for all k_t, μ. For physical cross section predictions we will integrate over our f_a functions, and the discontinuity in the derivative is of little significance.

We can of course also plot the section of the three dimensional function $f_g(x, k_t^2, \mu^2)$ along the line $k_t = \mu$, for various x. This is shown in Fig. 2.13. In the prescription of [1], with $\Delta = k_t/\mu$, the function is forced to be 0 here. With the new Δ we simply have evaluation of (2.12) with T_g=1 and the upper limit on x of 0.5.

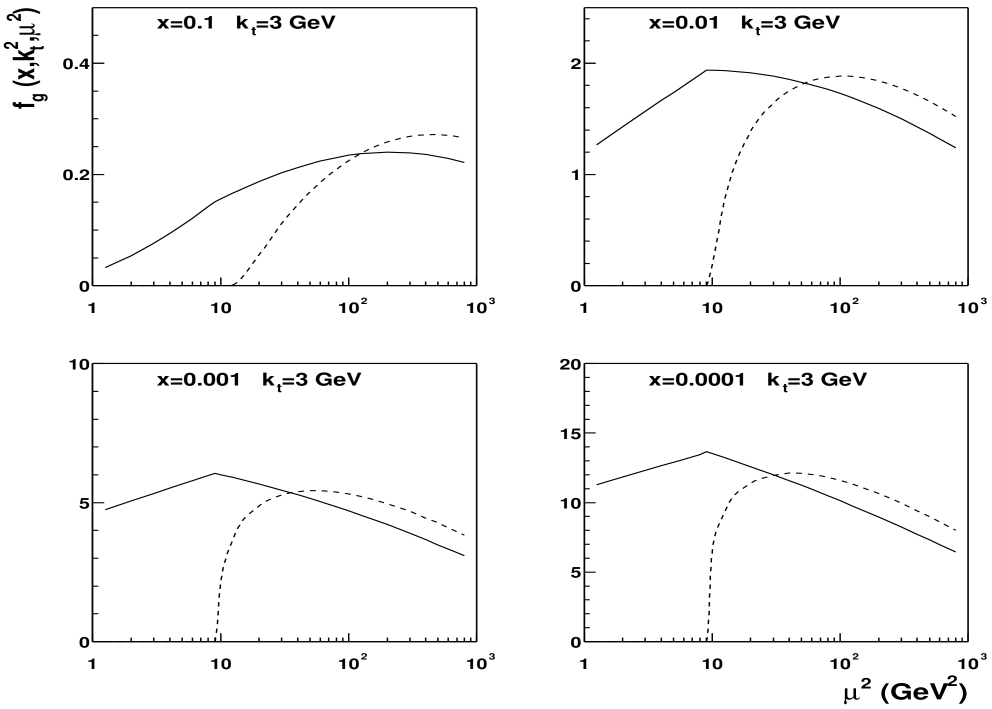

Figure 2.11: μ dependence of the unintegrated gluon distribution, generated with our DGLAP last step from MRST parton input, at $k_t = 3$ GeV. Continuous lines are for (angular-ordered) $\Delta = k_t/(k_t + \mu)$, dashed are for $\Delta = k_t/\mu$.

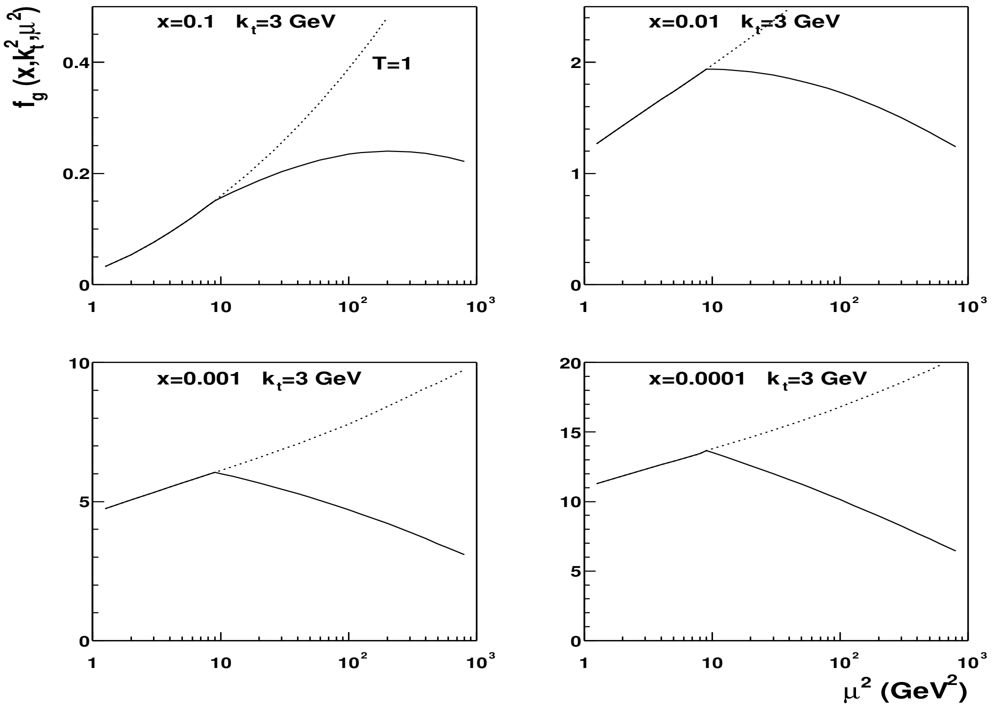

Figure 2.12: Like Fig. 2.11, but I show the (unphysical) effect of setting the suppression factor $T = 1$ everywhere, in dotted curves.

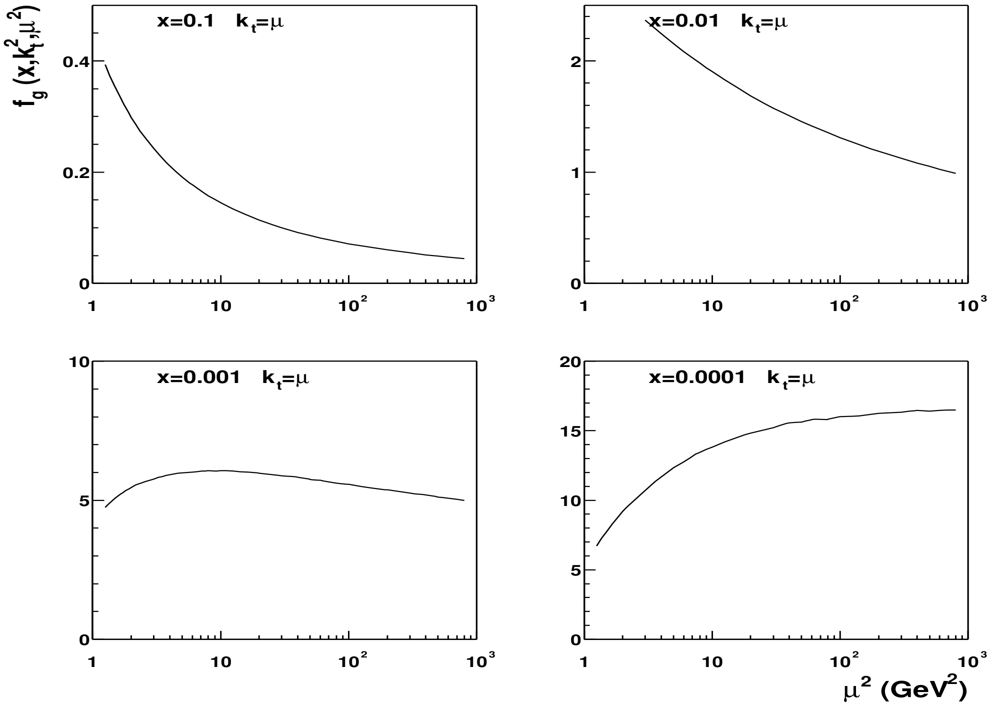

Figure 2.13: A different section of the same function $f_g(x, k_t^2, \mu^2)$; this time I plot along the line $k_t = \mu$, at which $T_g = 1$.

Chapter 3

Calculation of F_2

The deep inelastic electron-proton scattering cross section can be written (see (1.26))

$$\frac{d^2\sigma}{dx\, dQ^2} = \frac{4\pi\alpha^2}{Q^4} \left[\left(1 + (1-y)^2\right) F_1 + \frac{(1-y)}{x} \left(F_2 - 2xF_1\right) \right], \tag{3.1}$$

where we neglect the electron and proton masses, and restrict ourselves to the electromagnetic process only (considering only photon exchange, not Z^0 or charged current $W^{\pm}$ interactions). The standard DIS variables Q^2, x, and y were introduced in Section 1.4. We have also expressed the structure functions $F_{1,2}$ in terms of transverse and longitudinal structure functions F_T and F_L, where as in [18] we have $F_T = 2xF_1$ and $F_L = F_2 - 2xF_1$.

The electromagnetic interaction between the electron and proton depends on absorption of the probing photon with virtuality Q^2 by a quark with Bjorken x. This means that gluons in the proton can only contribute to F_2 via an intermediate quark, see Fig. 3.1.

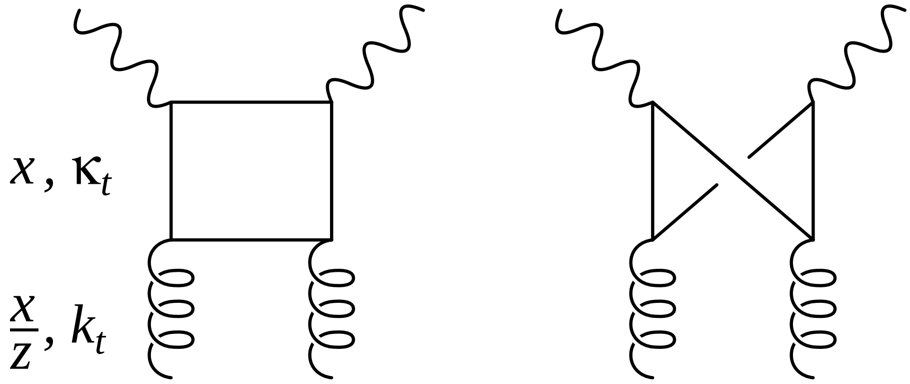

Figure 3.1: A gluon can only contribute to F_2 via an intermediate quark. There are two possible leading order diagrams, the "box" and "crossed box", shown here as the square of the amplitudes.

3.1 Unintegrated gluon through a quark box

Previous authors [18, 19, 20] have calculated the contribution to $F_2(x, Q^2)$ from a box-and-crossed-box calculation where an unintegrated gluon distribution at x/z drives the quark sea at x. In such papers only a single scale unintegrated distribution, such as $h_g(x/z, k_t^2)$, was used. We can however use our unintegrated gluon $f_g(x/z, k_t^2, \mu^2)$ as an input for such a box calculation, making some appropriate choice of the scale μ.

As in the evolution equations for our partons, we use a variable z to denote the fraction of the gluon's momentum that is transferred to the struck quark. This quark is the exchanged particle in Fig. 3.1, which couples to the virtual photon, and x, its plus momentum fraction, matches with the kinematics of the probe and thus corresponds to the first argument of $F_2(x, Q^2)$. We write k_t for the transverse momentum of the parent gluon, and κ_t for the transverse momentum of the quark. A general *Sudakov variable* decomposition of the momenta of the parent gluon and daughter quark is

$$k = ap - bq' + k_t$$

$$\kappa = \alpha p - \beta q' + \kappa_t \tag{3.2}$$

where p is the lightlike momentum of the proton, travelling down the beam axis in the positive direction, and q' is another lightlike vector constructed as $q' \equiv q + xp$, which fits the Bjorken definition[1] of x. To obtain the right plus momentum fraction, we need $a = x/z$. We consider the case of $b = 0$, which corresponds to the consistency condition (see Section A.3) where $k^2 = -k_t^2$. Further to this, we apply the quark mass-shell constraints for real outgoing quarks of mass m, eliminate α, and deduce

$$(x/z - x)\,\beta(1-\beta)\,2p\cdot q - \beta\kappa_t^2 - (1-\beta)\,(\boldsymbol{\kappa_t} - \boldsymbol{k_t})^2 = m^2. \tag{3.3}$$

A well-known variable change to $\boldsymbol{\kappa'_t} \equiv \boldsymbol{\kappa_t} - (1-\beta)\,\boldsymbol{k_t}$ can simplify computation of F_2 by enabling the dependence on the angle between $\boldsymbol{\kappa_t}$ and $\boldsymbol{k_t}$ to be integrated over analytically. In terms of Q^2, m^2, $\kappa_t'^2$, k_t^2 and the remaining Sudakov variable β, which is similar to x but describes the fraction of the photon's momentum carried by the internal quark line, (3.3) reduces to

$$\frac{1}{z} = 1 + \frac{\kappa_t'^2 + m^2}{\beta(1-\beta)Q^2} + \frac{k_t^2}{Q^2}. \tag{3.4}$$

Formally, by the k_t factorisation theorem [7] we can calculate the gluon contribution to F_2 as

$$F_2\left(x, Q^2\right) = \int_x^1 \frac{dz}{z} \int \frac{dk_t^2}{k_t^2}\, f\left(\frac{x}{z}, k_t^2\right)\, S_{box}\left(z, k_t^2, Q^2\right). \tag{3.5}$$

It is understood that S_{box}, containing the quark box-and-crossed-box approximation to the photon-gluon subprocess as shown in Fig. 3.1, involves integration over possible

[1] q is the 4-momentum of the probing virtual photon, so $q^2 = -Q^2$ and $x_{Bj} \equiv Q^2/2p\cdot q$.

intermediate transverse momenta $d^2\kappa_t$. However, existing treatments [18, 19, 20] find it is easier to use the Sudakov variable β and the new $\boldsymbol{\kappa_t'}$ variable to perform the calculation of the subprocess cross section. In this case z is no longer an explicit variable of integration, but instead we integrate $d\beta$ and $d^2\kappa_t'$ and always infer the appropriate value of z from (3.4), for fixed Q^2 and quark mass m. We sum over various quark flavours q which can appear in the box, with different masses m_q, so a separate integral is performed for each.

Reference [18] gives the result of the evaluation of the S_{box} diagrams (see also Section B.3):

$$
\begin{aligned}
F_T &= 2\sum_q e_q^2 \frac{Q^2}{4\pi^2} \int \frac{dk_t^2}{k_t^4} \int_0^1 d\beta \int d^2\kappa_t' \, \alpha_s \, f\left(\frac{x}{z}, k_t^2\right) \\
&\quad \left\{ \left[\beta^2 + (1-\beta)^2\right] \left(\frac{\kappa_t^2}{D_1^2} - \frac{\boldsymbol{\kappa_t} \cdot (\boldsymbol{\kappa_t} - \boldsymbol{k_t})}{D_1 D_2} \right) + m_q^2 \left(\frac{1}{D_1^2} - \frac{1}{D_1 D_2} \right) \right\}, \qquad (3.6)
\end{aligned}
$$

$$
F_L = 2\sum_q e_q^2 \frac{Q^4}{\pi^2} \int \frac{dk_t^2}{k_t^4} \int_0^1 d\beta \int d^2\kappa_t' \, \alpha_s \, f\left(\frac{x}{z}, k_t^2\right) \beta^2 (1-\beta)^2 \left(\frac{1}{D_1^2} - \frac{1}{D_1 D_2} \right). \qquad (3.7)
$$

The denominator factors are

$$
\begin{aligned}
D_1 &= \kappa_t^2 + \beta(1-\beta)Q^2 + m_q^2 \\
D_2 &= (\boldsymbol{\kappa_t} - \boldsymbol{k_t})^2 + \beta(1-\beta)Q^2 + m_q^2,
\end{aligned}
$$

and it is implied that $\boldsymbol{\kappa_t} = \boldsymbol{\kappa_t'} + (1-\beta)\boldsymbol{k_t}$ in these equations. A step function $\Theta(1-x/z)$ is also necessary to ensure a legitimate range for z.

These expressions are compatible, bearing in mind $F_2 \equiv F_T + F_L$, with the expression in [19, 20] for the quark sea S_q (where $F_2^{sea}(x, Q^2) = \sum_q e_q^2 S_q(x, Q^2)$)

$$S_q\left(x, Q^2\right) = \frac{Q^2}{4\pi^2} \int \frac{dk_t^2}{k_t^4} \int_0^1 d\beta \int d^2\kappa_t' \, \alpha_s \, f\left(\frac{x}{z}, k_t^2\right) \Theta\left(1 - \frac{x}{z}\right) \tag{3.8}$$
$$\left\{\left[\beta^2 + (1-\beta)^2\right]\left(\frac{\boldsymbol{\kappa_t}}{D_1} - \frac{(\boldsymbol{\kappa_t} - \boldsymbol{k_t})}{D_2}\right)^2 + \left[m_q^2 + 4Q^2\beta^2(1-\beta)^2\right]\left(\frac{1}{D_1} - \frac{1}{D_2}\right)^2\right\}.$$

We can see that we can convert (3.8) to the sum of (3.6) and (3.7) if we exploit the symmetry of the integrand under $\boldsymbol{\kappa_t} \leftrightarrow \boldsymbol{\kappa_t} - \boldsymbol{k_t}$ and $\beta \leftrightarrow 1 - \beta$, given that we integrate over all β values: this is responsible for the outermost factor of 2 in (3.6) and (3.7).

So we can work from the sum of (3.6) and (3.7) and perform the angular integration of $d^2\kappa_t'$ analytically. This uses integrals like $\int d\phi \, / (A + B\cos\phi)^2$ which are tabulated in [30]. It is helpful to define the following combinations of variables:

$$\begin{aligned} N_1 &\equiv \beta(1-\beta)Q^2 + m_q^2 \\ N_2 &\equiv \kappa_t'^2 + (1-\beta)^2 k_t^2 \\ N_3 &\equiv \kappa_t'^2 - (1-\beta)^2 k_t^2 \\ N_4 &\equiv \kappa_t'^2 + \beta(1-\beta)k_t^2. \end{aligned}$$

The result for the gluon contribution to F_2, in terms of integrals over κ_t', is therefore

$$F_2\left(x, Q^2\right) = \sum_{q=u,d,s,c} e_q^2 \frac{Q^2}{2\pi} \int \frac{dk_t^2}{k_t^4} \int_0^1 d\beta \int d\kappa_t'^2 \, \alpha_s \, f\left(\frac{x}{z}, k_t^2\right) \Theta\left(1 - \frac{x}{z}\right)$$
$$\left\{\left[\beta^2 + (1-\beta)^2\right]\left(\frac{I_1}{2\pi} - \frac{I_2}{2\pi}\right) + \left[m_q^2 + 4Q^2\beta^2(1-\beta)^2\right]\left(\frac{I_3}{2\pi} - \frac{I_4}{2\pi}\right)\right\}, \tag{3.9}$$

where

$$\frac{I_1}{2\pi} = \frac{N_1 N_2 + N_3^2}{\left(N_1^2 + 2N_1N_2 + N_3^2\right)^{3/2}}$$

$$
\begin{aligned}
\frac{I_2}{2\pi} &= \frac{N_3 - (1-2\beta)N_1}{(N_1+N_4)\sqrt{N_1^2+2N_1N_2+N_3^2}} \\
\frac{I_3}{2\pi} &= \frac{N_1+N_2}{(N_1^2+2N_1N_2+N_3^2)^{3/2}} \\
\frac{I_4}{2\pi} &= \frac{2(1-\beta)}{(N_1+N_4)\sqrt{N_1^2+2N_1N_2+N_3^2}}.
\end{aligned}
$$

However, we have to consider carefully the allowed ranges of k_t and κ_t'. Our unintegrated gluon is not defined for $k_t < k_0$, so we must impose a lower limit of k_0 on the integration over k_t. We will then account for the non-perturbative region separately. A lower limit on κ_t' would give a rather strange (β dependent) limit on the quark transverse momentum κ_t. Instead we require the restriction $\kappa_t > k_0$, and the low κ_t region will be effectively included in the non-perturbative (direct) quark contribution to F_2, see Section 3.2. Therefore it is neater to write S_{box} in terms of an integral over κ_t, and not κ_t'; the requirement $\kappa_t > k_0$ unfortunately means we can not use an analytic integral.

Thus, as in [4] we have

$$
\frac{1}{z} = 1 + \frac{\kappa_t^2 + m_q^2}{(1-\beta)Q^2} + \frac{(\boldsymbol{\kappa_t} - \boldsymbol{k_t})^2 + m_q^2}{\beta Q^2} \tag{3.10}
$$

replacing (3.4), and in place of (3.6), (3.7), (3.8), (3.9),

$$
\begin{aligned}
F_{T\ perturbative}^{\ gluon\to quark}\left(x,Q^2\right) &= \sum_{q=u,d,s,c} e_q^2 \, \frac{Q^2}{4\pi} \int_{k_0^2}^{k_{max}^2} \frac{dk_t^2}{k_t^4} \int_0^1 d\beta \int_{k_0^2}^{k_{max}^2} d\kappa_t^2 \, \frac{d\phi}{2\pi} \, \alpha_s(\mu^2) \times \qquad (3.11)\\
&f_g\left(\frac{x}{z}, k_t^2, \mu^2\right) \Theta\left(1-\frac{x}{z}\right) \left\{ \left[\beta^2 + (1-\beta)^2\right] \left(\frac{\boldsymbol{\kappa_t}}{D_1} - \frac{\boldsymbol{\kappa_t} - \boldsymbol{k_t}}{D_2}\right)^2 + m_q^2 \left(\frac{1}{D_1} - \frac{1}{D_2}\right)^2 \right\}
\end{aligned}
$$

$$
\begin{aligned}
F_{L\ perturbative}^{\ gluon\to quark}\left(x,Q^2\right) &= \sum_{q=u,d,s,c} e_q^2 \, \frac{Q^2}{4\pi} \int_{k_0^2}^{k_{max}^2} \frac{dk_t^2}{k_t^4} \int_0^1 d\beta \int_{k_0^2}^{k_{max}^2} d\kappa_t^2 \, \frac{d\phi}{2\pi} \, \alpha_s(\mu^2) \times \qquad (3.12)\\
&f_g\left(\frac{x}{z}, k_t^2, \mu^2\right) \Theta\left(1-\frac{x}{z}\right) \left\{ 4Q^2 \beta^2 (1-\beta)^2 \left(\frac{1}{D_1} - \frac{1}{D_2}\right)^2 \right\},
\end{aligned}
$$

where we still have

$$
\begin{aligned}
D_1 &= \kappa_t^2 + \beta(1-\beta)Q^2 + m_q^2 && (3.13)\\
D_2 &= (\boldsymbol{\kappa_t} - \boldsymbol{k_t})^2 + \beta(1-\beta)Q^2 + m_q^2. && (3.14)
\end{aligned}
$$

Following [19], we choose the scale μ which controls the unintegrated gluon and the QCD coupling α_s to be[2]

$$
\mu^2 = k_t^2 + \kappa_t^2 + m_q^2. \qquad (3.15)
$$

We pick an arbitrary maximum for the k_t, κ_t integrals of $k_{max} \sim 4Q$, for example; the dependence on this upper limit is weak. $m_c = 1.4$ GeV is the charm mass, and the other masses are neglected.

So (3.11) + (3.12) gives the *perturbative* gluon to quark contribution to F_2. For the contribution from the region $k_t < k_0$ we make the approximation

$$
\int_0^{k_0^2} \frac{dk_t^2}{k_t^2}\, f_g(x, k_t^2, \mu^2) \left[\frac{\text{remainder}}{k_t^2}\right] \simeq xg(x, k_0^2)\, T_g(k_0, \mu) \Big[\quad\Big]_{k_t = \langle k_t \rangle}; \qquad (3.16)
$$

in other words we compute $F_2{}^{gluon \to quark}_{perturbative} = (3.11) + (3.12)$ with (3.16), using $\langle k_t \rangle$ as a suitable "average" value of k_t between 0 and k_0. The dependence on the choice of $\langle k_t \rangle$ turns out to be numerically unimportant. The Sudakov-like factor in (3.16) roughly accounts for the difference between the integrated gluon $\int_0^{k_0^2} f_g(x/z, k_t^2, k_0^2)\, dk_t^2/k_t^2$ and what we have here, $\int_0^{k_0^2} f_g(x/z, k_t^2, \mu^2)\, dk_t^2/k_t^2$.

[2]This is intended to be representative of the subprocess pictured in Fig. 3.1, but of course there is some freedom in the choice of μ.

3.2 Unintegrated quark through a quark box

Clearly the gluon-initiated diagrams of Fig. 3.1 do not account for all the possibilities that lead to an interaction with the virtual photon. At the same perturbative order as the process where the gluon splits into a quark-antiquark pair, we have the possibility of starting with a quark which radiates a gluon away before it hits the photon[3].

Rather than a box-and-crossed-box calculation, we only need a simple box, effectively the last piece of the ladder to go from an input unintegrated quark $f_q\left(x/z, k_t^2, \mu^2\right)$ to the final state.

It is interesting to examine the concept of "valence" quarks. From the point of view of a virtual photon in deep inelastic scattering, where Q^2 is high enough to pick out structure we can describe in perturbation theory, all up quarks are the same. There may be more u quarks than $\bar{u}$ antiquarks, but we can push the distinction of valence versus sea right down to the non-perturbative parametrisation at the bottom of the ladder.

On this basis our unintegrated quarks and gluons are all generated (via our last-step formalism) from up, down, strange and charm quarks, and the corresponding antiquarks, *not* in a way that treats valence and sea quarks separately. (This is in contrast to [19, 20], for example, where valence distributions are supplied separately.) So for example, the MRST `upv` is allowed to feed in to our gluon f_g, as part of the total up contribution `up` $=$ `upv` $+$ `usea`. Similarly, our up unintegrated quark f_u is generated by a P_{qq} splitting driven by the whole up distribution at higher x (as well as by the P_{qg} part).

If we have a perturbative splitting, therefore, we can calculate a quark-to-quark

[3]We work in the axial gauge ($A^\mu q'_\mu = 0$), where other diagrams, in which the gluon and photon interaction order is interchanged, do not give leading logarithmic behaviour.

contribution to F_2 which is similar in some respects to the gluon S_{box}, but simpler as we do not include a crossed diagram:

$$F_2{}^{quark\to quark}_{perturbative}\left(x,Q^2\right) = \sum_{q=u,d,s,c} e_q^2 \int_{k_0^2}^{Q^2} \frac{d\kappa_t^2}{\kappa_t^2}\frac{\alpha_s(\kappa_t^2)}{2\pi}\int_{k_0^2}^{\kappa_t^2}\frac{dk_t^2}{k_t^2}\int_x^{Q/(Q+k_t)} dz$$
$$\left[f_q\left(\frac{x}{z},k_t^2,Q^2\right)+f_{\bar{q}}\left(\frac{x}{z},k_t^2,Q^2\right)\right]P_{qq}(z). \quad (3.17)$$

We have written an upper limit on z motivated by angular ordering, and have chosen here a scale $\mu = Q$ for the partons, although various choices of scale are possible.

Again we need to account for the non-perturbative domain $k_t < k_0$. The initial (integrated) quark distribution $xq(x, k_0^2)$ drives our final contribution. Physically the only remaining situations that we have not included are those in which a quark (or antiquark) from this initial distribution does not experience real splitting in the perturbative domain, but interacts unchanged with the photon at scale Q. Hence we write a Sudakov-like factor $T_q(k_0, Q)$ to represent the probability of evolution from k_0 to Q without radiation.

$$F_2{}^{quark\ direct}_{non\text{-}perturb.}(x,Q^2) = \sum_{q=u,d,s,c} e_q^2 \left[xq(x,k_0^2)+x\bar{q}(x,k_0^2)\right] T_q(k_0,Q). \quad (3.18)$$

To avoid double counting, it is important to put a lower limit on κ_t in both (3.11) and (3.12), to enforce $\Theta(\kappa_t^2 - k_0^2)$, as written. Without this lower limit on the final transverse momentum κ_t, equations (3.11) and (3.12) would partially include low transverse momentum κ_t quark contributions which are best incorporated in (3.18).

3.3 Numerical results for F_2

In Figs. 3.2 and 3.3 I show sample results for $F_2(x, Q^2)$ at various x and Q^2, compared with recent deep-inelastic structure function data from ZEUS, H1, NMC [13] and E665 [14]. These are *not* the results of fitting to the data, but are the predictions for F_2 as described in Sections 3.1 and 3.2, based on the input of the "DGLAP" unintegrated partons $f_g(x, k_t^2, \mu^2)$ and $f_q(x, k_t^2, \mu^2)$ that were plotted in Section 2.6. These unintegrated partons are generated by feeding the integrated MRST99 distributions $a(x, k^2)$ into the last step of the parton evolution, which is carried out with angular ordering.

The dashed curves in Figs. 3.2 and 3.3 result from the gluon-initiated box and crossed box calculation of Section 3.1. The perturbative and non-perturbative contributions have been added together: see eqns (3.11) and (3.12) and the discussion of the small approximate non-perturbative part around (3.16). We see that the gluon-driven curves rise steeply as we go to smaller x, but in themselves do not describe the data fully. We also have to include the quark contributions, shown as dotted curves, which are the sum of the perturbative quark to quark calculation (3.17) and the remaining non-perturbative piece, (3.18). The solid curves are our overall prediction for F_2. This compares reasonably well with the data for the higher Q^2 values, although the agreement at lower values of Q^2 is less good.

As they are written, (3.11) and (3.12) are suitable for computation, and these are what have been used to compute the dashed curves in Figs. 3.2 and 3.3. However we have also investigated the possibility of performing the angular integration over ϕ in the

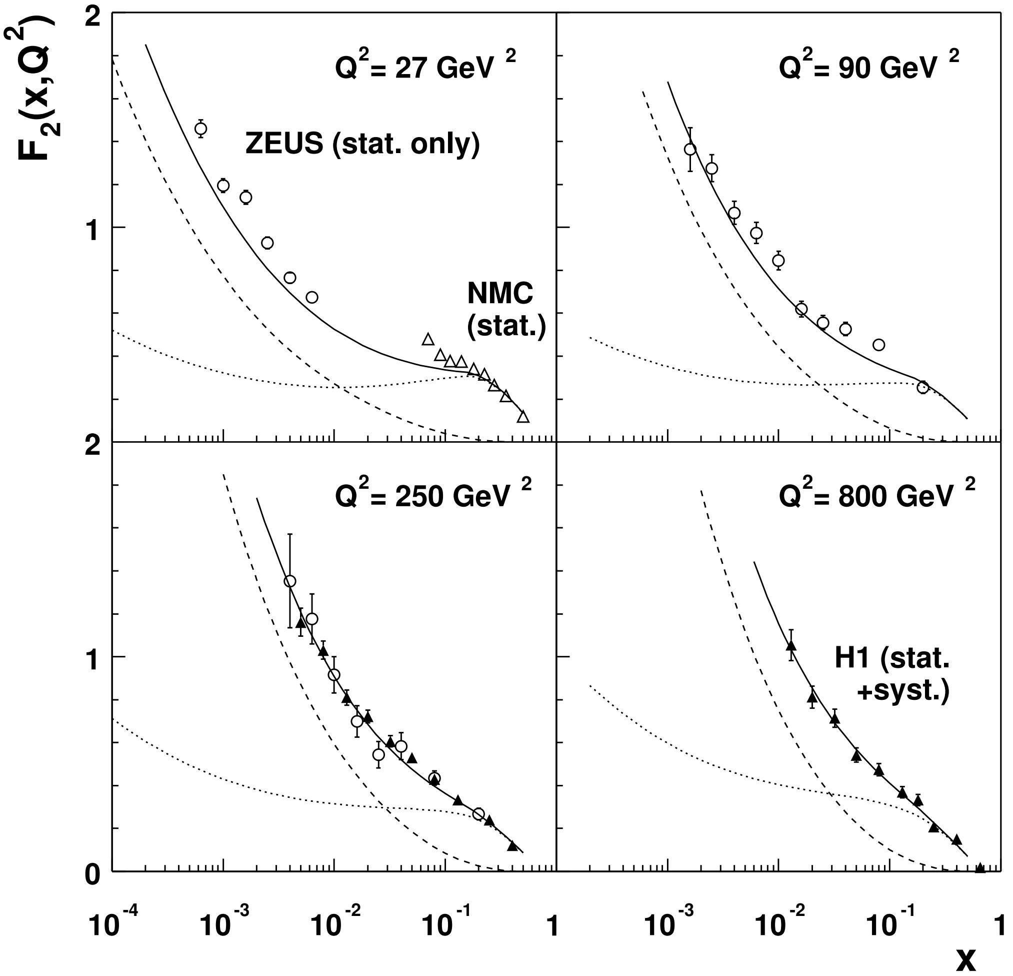

Figure 3.2: Not a fit, but the results of using our "DGLAP" unintegrated partons to calculate $F_2(x, Q^2)$; the gluon-originated contributions are shown as dashed lines and the quark-originated parts are shown as dotted lines. Recent data are plotted [13], to be compared with the continuous curves which are the sum of the gluon and quark contributions.

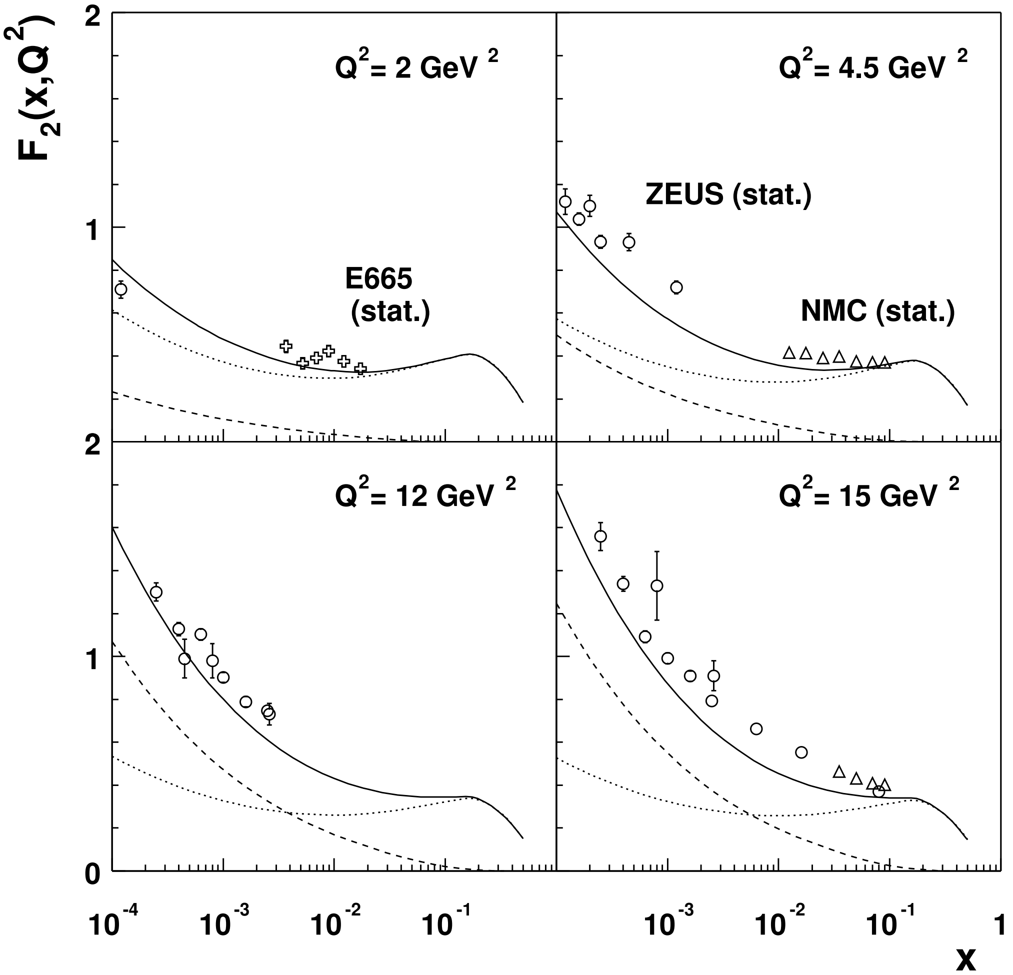

Figure 3.3: As Fig. 3.2, but for lower values of Q^2. Data from E665 [14] are included at $Q^2 = 2\ \mathrm{GeV}^2$.

following approximation, in order to speed up the calculations significantly:

$$F_{T\ \text{perturbative}}^{\ gluon\to quark}\left(x,Q^2\right) \;=\; \sum_{q=u,d,s,c} e_q^2\,\frac{Q^2}{4\pi}\int_{k_0^2}^{k_{max}^2}\frac{dk_t^2}{k_t^4}\int_0^1 d\beta\int_{k_0^2}^{k_{max}^2} d\kappa_t^2\;\alpha_s(\mu^2)\times \tag{3.19}$$
$$f_g\left(\frac{x}{\langle z\rangle},k_t^2,\mu^2\right)\,\Theta\left(1-\frac{x}{\langle z\rangle}\right)\,\left\{\left[\beta^2+(1-\beta)^2\right](J_1+J_2-J_3)\;+\;m_q^2\,(J_4+J_5-J_6)\right\}$$

$$F_{L\ \text{perturbative}}^{\ gluon\to quark}\left(x,Q^2\right) \;=\; \sum_{q=u,d,s,c} e_q^2\,\frac{Q^2}{4\pi}\int_{k_0^2}^{k_{max}^2}\frac{dk_t^2}{k_t^4}\int_0^1 d\beta\int_{k_0^2}^{k_{max}^2} d\kappa_t^2\;\alpha_s(\mu^2)\times \tag{3.20}$$
$$f_g\left(\frac{x}{\langle z\rangle},k_t^2,\mu^2\right)\,\Theta\left(1-\frac{x}{\langle z\rangle}\right)\,\left\{4Q^2\,\beta^2(1-\beta)^2\,(J_4+J_5-J_6)\right\},$$

with a representative value of z coming from choosing some "average" angle $\langle\phi\rangle$,

$$\frac{1}{\langle z\rangle}=1+\frac{\kappa_t^2+m_q^2}{(1-\beta)Q^2}+\frac{\kappa_t^2+k_t^2-2\kappa_t k_t\cos\langle\phi\rangle+m_q^2}{\beta Q^2}. \tag{3.21}$$

Then the remaining parts of the integrands of (3.11) and (3.12) can be done analytically:

$$\begin{aligned}
J_1 &= \kappa_t^2/D_1^2\\
J_2 &= \int_0^{2\pi}\frac{d\phi}{2\pi}\,\frac{\kappa_t^2+k_t^2-2\kappa_t k_t\cos\phi}{\left(D_1+k_t^2-2\kappa_t k_t\cos\phi\right)^2}\\
&= \frac{1}{\sqrt{\left(D_1+k_t^2\right)^2-4\kappa_t^2k_t^2}}-\frac{\left(D_1+k_t^2\right)\left(\beta(1-\beta)Q^2+m_q^2\right)}{\left[\left(D_1+k_t^2\right)^2-4\kappa_t^2k_t^2\right]^{3/2}}\\
J_3 &= \int_0^{2\pi}\frac{d\phi}{2\pi}\,\frac{2}{D_1}\,\frac{\kappa_t^2-\kappa_t k_t\cos\phi}{D_1+k_t^2-2\kappa_t k_t\cos\phi}=\frac{1}{D_1}\left(1+\frac{\kappa_t^2-\beta(1-\beta)Q^2-m_q^2-k_t^2}{\sqrt{\left(D_1+k_t^2\right)^2-4\kappa_t^2k_t^2}}\right)\\
J_4 &= 1/D_1^2\\
J_5 &= \int_0^{2\pi}\frac{d\phi}{2\pi}\,\frac{1}{\left(D_1+k_t^2-2\kappa_t k_t\cos\phi\right)^2}=\frac{D_1+k_t^2}{\left[\left(D_1+k_t^2\right)^2-4\kappa_t^2k_t^2\right]^{3/2}}\\
J_6 &= \int_0^{2\pi}\frac{d\phi}{2\pi}\,\frac{2}{D_1}\,\frac{1}{D_1+k_t^2-2\kappa_t k_t\cos\phi}=\frac{2}{D_1}\,\frac{1}{\sqrt{\left(D_1+k_t^2\right)^2-4\kappa_t^2k_t^2}}.
\end{aligned}$$

The main reason this saves time is that the unintegrated gluon distribution is fairly slow to compute, so choosing a representative "average" value has a big payoff in runtime.

Fig. 3.4 shows the results of this calculation for various values of $\langle\phi\rangle$. Although there is some dependence on the choice of $\langle\phi\rangle$, we find that $\langle\phi\rangle = \pi/4$ actually reproduces the "exact" calculation remarkably well.

3.4 Attempted fit to deep inelastic data

Having introduced a framework to predict the DIS observable $F_2(x, Q^2)$ in terms of the unintegrated quarks and gluons introduced in Chapter 2, it is desirable to use the available experimental data to perform a fit to determine these parton distributions. A full global unintegrated partons analysis is beyond the scope of this work, but in this section we discuss a simple approach, fitting to F_2, as an illustration of the process.

We work in terms of our "DGLAP" unintegrated partons. As described in Section 2.2, we use auxiliary functions $a(x, k^2)$ to generate the unintegrated distributions $f_a(x, k_t^2, \mu^2)$ by explicitly carrying out the last step of the evolution, with angular ordering in the last step. The functions $a(x, k^2)$ are evolved by the DGLAP equation from some starting scale k_0. This approach does not include BFKL effects, but the computation is simpler, and the indications were in Section 2.6 that BFKL effects are not particularly important in the HERA domain.

The non-perturbative input functions $a(x, k_0^2)$ contain the parameters which are to be varied in the fit. Choice of an appropriate parametrisation is of course essential for any fitting exercise. Almost the simplest choice of initial functions we can try is shown in (3.22) to (3.28). The forms of the functions $a(x, k_0^2)$ are inspired by [19, 20, 32]. I use

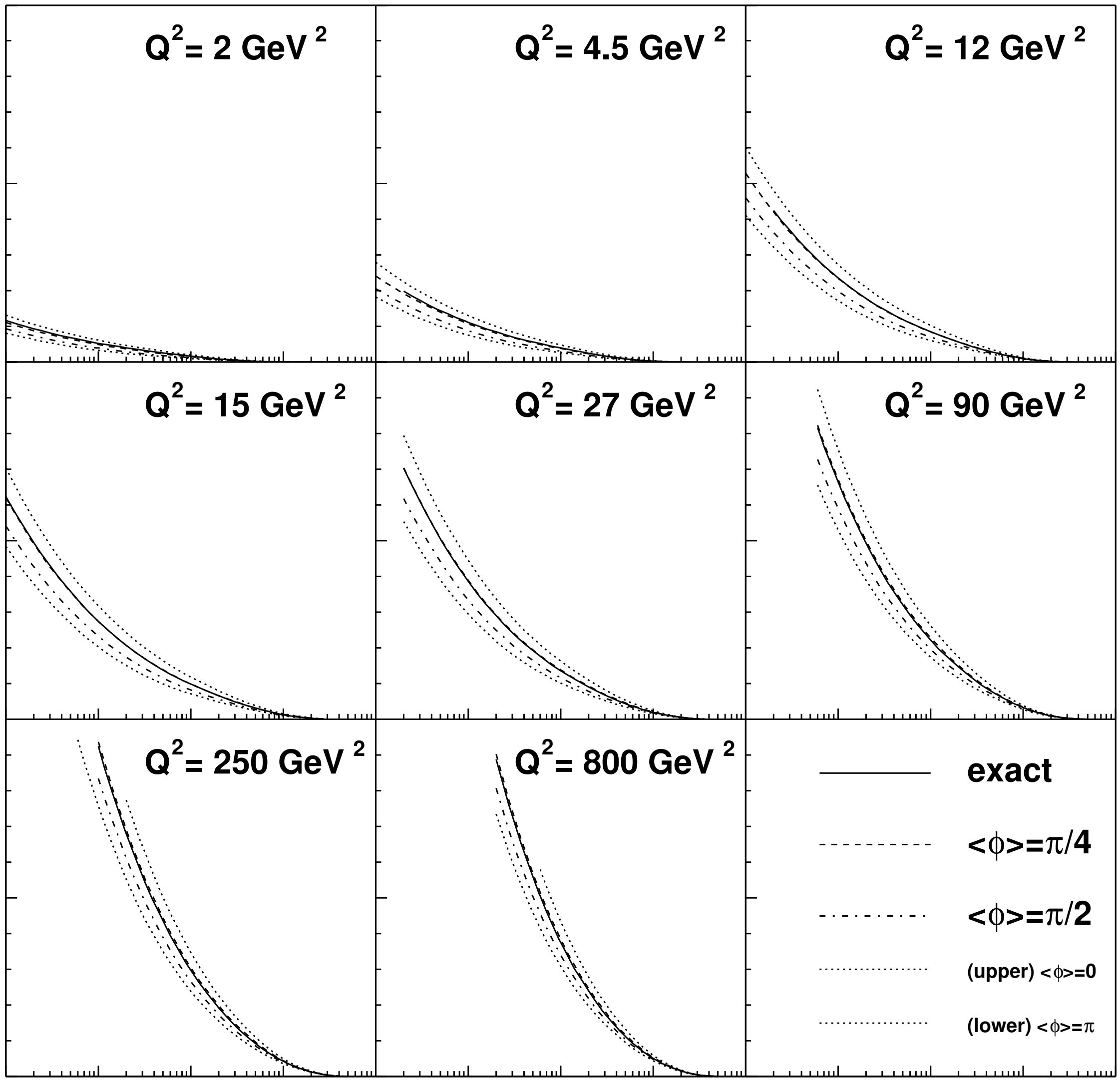

Figure 3.4: The results of using (3.19) and (3.20) to approximate (3.11) and (3.12). The approximation is based on choosing a supposedly representative value of $\langle\phi\rangle$ and only computing the unintegrated gluon once, for that value. The rest of the angular integration is performed analytically as detailed in the text. This figure shows that $\langle\phi\rangle = \pi/4$ is a suitable choice for computation of the gluon contribution to $F_2(x, Q^2)$ over the range of x and Q^2 included here.

$k_0 = 1$ GeV.

$$
\begin{aligned}
xg_0 &\equiv xg(x,k_0^2) = N_g\, x^{-\lambda_g}\, (1-x)^{\beta_g} && (3.22)\\
x\bar{u}_0 &= 2N_s\, x^{-\lambda_s}\, (1-x)^{\beta_s} && (3.23)\\
x\bar{d}_0 &= 2N_s\, x^{-\lambda_s}\, (1-x)^{\beta_s} && (3.24)\\
x\bar{s}_0 &= N_s\, x^{-\lambda_s}\, (1-x)^{\beta_s} && (3.25)\\
xu_0 &= x\bar{u}_0 \;+\; N_u\, x^{\alpha_u}\, (1-x)^{\beta_u} && (3.26)\\
xd_0 &= x\bar{d}_0 \;+\; N_d\, x^{\alpha_d}\, (1-x)^{\beta_d} && (3.27)\\
xs_0 &= x\bar{s}_0 && (3.28)
\end{aligned}
$$

The valence sum rules can be used, for instance, to constrain N_u and N_d in terms of the other parameters:

$$\int_0^1 (u_0 - \bar{u}_0)\, dx = 2; \quad \int_0^1 (d_0 - \bar{d}_0)\, dx = 1, \tag{3.29}$$

which give, for the parametrised forms we have chosen,

$$N_u = 2/B(\alpha_u, \beta_u + 1); \quad N_d = 1/B(\alpha_d, \beta_d + 1), \tag{3.30}$$

where $B(a,b)$ is the Beta function $\Gamma(a)\Gamma(b)/\Gamma(a+b)$, and the Gamma function[4] is computed by a library routine (we must have $\alpha_{u,d} > 0$, $\beta_{u,d} > -1$). The momentum sum rule is another constraint:

$$\int_0^1 (xu_0 + xd_0 + xs_0 + x\bar{u}_0 + x\bar{d}_0 + x\bar{s}_0 + xg_0)\, dx = 1; \tag{3.31}$$

[4]The Gamma function $\Gamma(a) = \int_0^\infty x^{a-1} e^{-x}\, dx$, for $a > 0$.

for this parametrisation we can therefore eliminate N_s as

$$N_s = \frac{(1 - N_u\, B(\alpha_u + 1, \beta_u + 1) - N_d\, B(\alpha_d + 1, \beta_d + 1) - N_g\, B(1 - \lambda_g, \beta_g + 1))}{10\, B(1 - \lambda_s, \beta_s + 1)}. \tag{3.32}$$

Note that we must have $\lambda_{g,s} < 1$.

We are left with the nine free parameters N_g, λ_g, β_g, λ_s, β_s, α_u, β_u, α_d and β_d. However there is also the question of how the strong coupling $\alpha_s(\mu^2)$ runs, and using (1.17) means we can also vary Λ_{QCD}, so this becomes a tenth parameter.

I have therefore performed a ten-parameter fit using a multidimensional function minimisation routine [31]. The procedure is as follows:

1. Pick a valid set of parameter values for N_g, λ_g, β_g, λ_s, β_s, α_u, β_u, α_d, β_d and Λ_{QCD}.

2. Use the parametrised $a_0 \equiv a(x, k_0^2)$ and the DGLAP evolution equation (2.6) to construct grids of evolved values of $a(x, k^2)$ for a suitable range of x and k^2.

3. Calculate the values of $F_2^{theory}(x, Q^2)$ at 52 representative points (x, Q^2) for which we have data, using the formalism described in the previous sections. The unintegrated partons $f_a(x/z, k_t^2, \mu^2)$ are computed on demand by performing the last-step integration of (2.12), with as input the functions $a(x', k^2)$, interpolated from the grids.

4. Evaluate $\chi^2 \equiv \sum_{i=1}^{52} \left(\frac{F_2^{theory} - F_2^{data}}{\delta F_2^{experimental\ error}} \right)^2$ summing over the representative points i.

These steps are then repeated as the minimisation routine explores the parameter space, moving towards the smallest value of χ^2, representing the closest match between the theoretical predictions and the measured data (weighted by the experimental errors, thus favouring data points with claimed higher accuracy). Eventually the routine finds a (possibly local) minimum and then the values of the parameters at that point give our best fit.

Figs. 3.5 and 3.6 show the curves resulting from this crude fit[5], compared to the data. The 52 points used in the fitting procedure were selected to be a representative sample of the data points shown in the figures, spread across all the Q^2 values.

The optimum values of the parameters were:

$$\begin{aligned}
N_g &= 1.22, \\
\lambda_g &= 0.0967, \\
\beta_g &= 1.85, \\
\lambda_s &= 0.0994, \\
\beta_s &= 8.56, \\
\alpha_u &= 0.986, \\
\beta_u &= 3.85, \\
\alpha_d &= 0.000275, \\
\beta_d &= 5.54, \\
\Lambda_{QCD} &= 143 \text{ MeV}.
\end{aligned}$$

The sum rules give $N_u = 9.40$, $N_d = 0.000275$, $N_s = 0.107$. Note that this value for Λ_{QCD} applies only for the LO α_s as written in (1.17).

[5]To speed up the χ^2 minimisation procedure, the $\langle\phi\rangle = \pi/4$ approximation discussed in Section 3.3 was used for the calculation of the gluon contribution to F_2. However exact angular integration for the final result produces very similar curves to those shown.

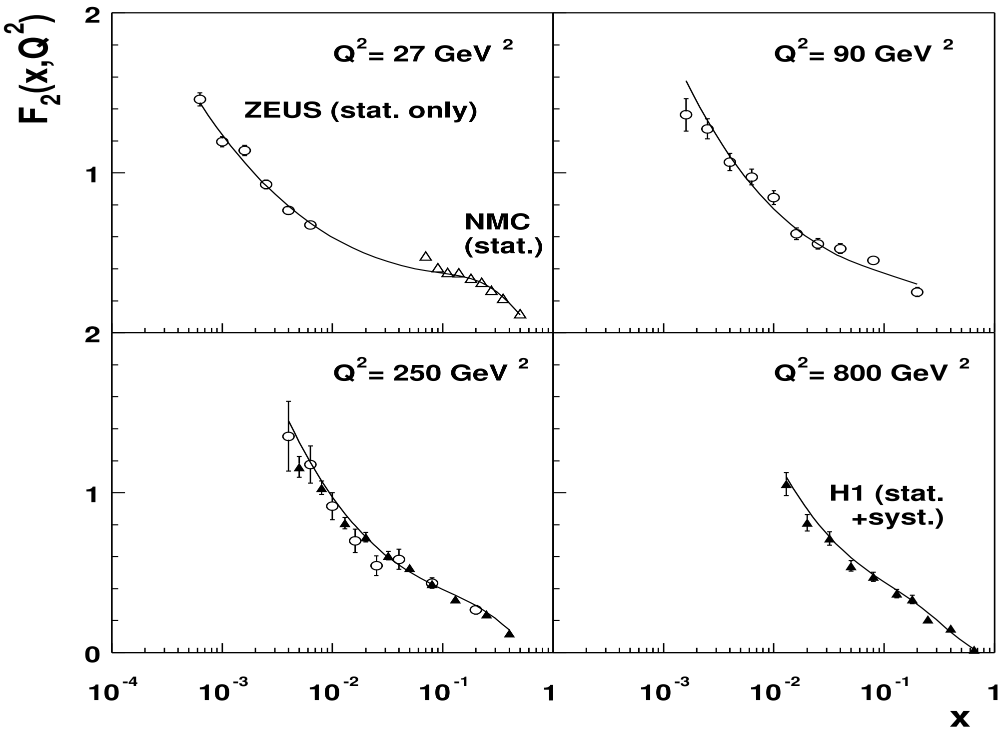

Figure 3.5: Result of our crude fit for F_2, using the new framework based on DGLAP evolution followed by an angular-ordered last step. About half of these data points were included in the fit.

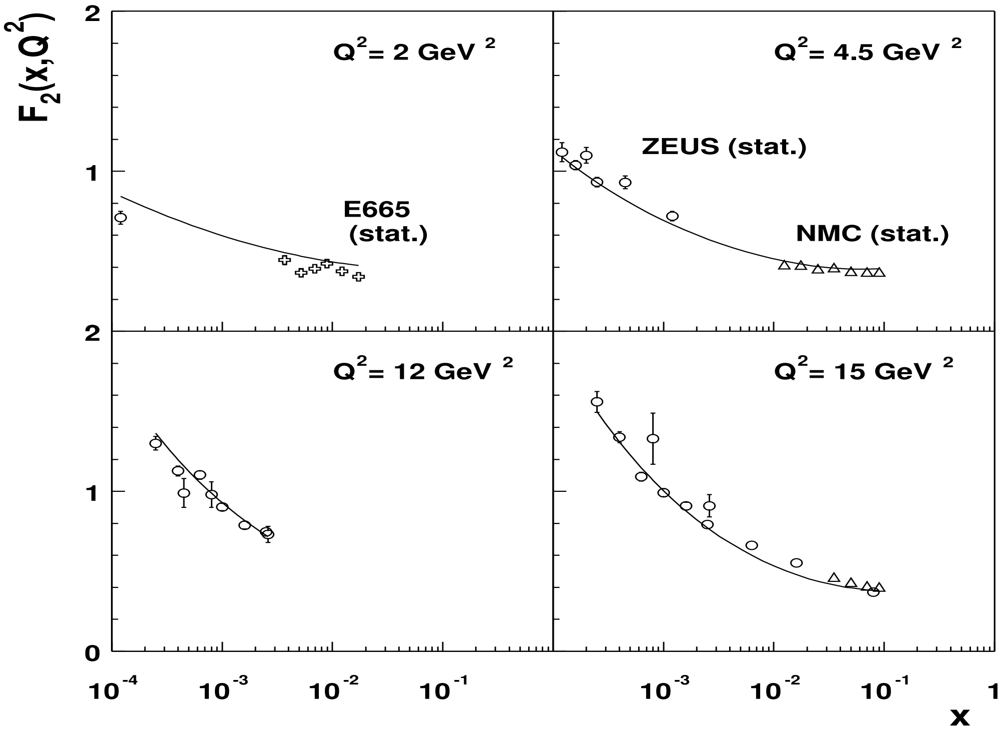

Figure 3.6: Like Fig. 3.5, but for low Q^2. About half of these data points were included in the fit.

For the 52 points for which the χ^2 value was minimised, $\chi^2 = 298$ with these parameters. For *all* the data points shown in Fig. 3.5 (higher Q^2, 52 points) χ^2 computes as 149; for *all* the data points shown in Fig. 3.6 (lower Q^2, 44 points), χ^2 computes as 394.

Such large values of χ^2 are presumably due to the fact that systematic errors have not been included in this analysis, except for the H1 data. Visually the fit in Figs. 3.5 and 3.6 seems tolerable, except perhaps at the lowest value of Q^2. More work would be needed to produce a professional fit, perhaps with a more detailed parametrisation with extra parameters. The approximate implementation of LO DGLAP evolution I have used for $a(x, k^2)$, crude thresholds for production of heavy flavours, and the LO running of $\alpha_s(\mu^2)$, are significant limitations, but the principles of fitting have been demonstrated.

For remaining calculations in this thesis it is safest to use the form of unintegrated parton plotted in Section 2.6, generated from the MRST integrated partons as input to the last step of the evolution. Although the MRST $a(x, k^2)$ have been fitted via the conventional F_2 framework to DIS data, the results are close enough to make approximate predictions for other processes.

3.5 Integrating the unintegrated partons

It is important to scrutinise the relationship between the new unintegrated partons $f_a(x, k_t^2, \mu^2)$ and conventional integrated partons distributions $a(x, \mu^2)$, as obtained in global analyses such as [32]. First we emphasise that we may use either integrated distributions or the unintegrated distributions to describe both inclusive and exclusive processes. The framework based on the unintegrated distributions is a bit more complicated. However it better accounts for the kinematics of processes, and effectively includes, even at lowest order, some of what would conventionally be NLO corrections. This hampers order-by-order comparison of computations in the different frameworks.

An important equation, sometimes cited as the defining property of unintegrated partons [2], is

$$a(x,\mu^2) = \int^{\mu^2} \frac{dk_t^2}{k_t^2}\, f_a(x,k_t^2,\mu^2), \tag{3.33}$$

where a represents xg or xq. This is in fact the first equation of [2]. In the BFKL limit, the μ dependence of f vanishes and we have $f_g(x,k_t^2,\mu^2) \to h_g(x,k_t^2)$ as in (2.16). In this case, (3.33) is clearly satisfied. However, in general the situation is complicated by the two separate momentum scales k_t and μ. The unintegrated gluons f_g of [2] were explicitly constructed to have the property (3.33), in the sense that the integral of f_g over the transverse momentum, up to the scale μ, would be the same as the integral of the input auxiliary function $h_g(x,k_t^2)$ up to the same scale. In contrast, numerical integration over k_t of our simpler, but angular-ordered unintegrated partons f_g and f_q, as defined in Chapter 2 (see also [4]), shows that (3.33) is only approximately true[6]. We typically find a discrepancy of order 25% between the right-hand side of (3.33) and the single-scale distribution that has been used to generate f_a.

In order to eliminate the discrepancy we may adjust the upper limit μ^2 of the integral in (3.33) to $c^2\mu^2$. The introduction of c is equivalent to an NLO correction. Typically in the "DGLAP" case (the first approach of Section 2.6), we require $c = 0.6$–0.8 to match the value of the original input MRST integrated gluon in the domain $\mu = 5$–10 GeV and $x \lesssim 0.01$. For the second approach of Section 2.6, $c \simeq 0.4$ is needed.

[6]Note that we cannot compute (3.33) as it is written, because we can only define the unintegrated function in the regime of perturbative $k_t > k_0$. The comparison that is made is between the integral from k_0^2 to μ^2 and the quantity $a(x,\mu^2) - a(x,k_0^2)$.

To summarise, the discrepancy between the integral (3.33) of the unintegrated parton function and the original integrated distribution is not a cause for concern. Conceptually, there are two different roles for single-scale distributions in the description of data for inclusive observables (where partonic transverse momentum is integrated out). The first role is the traditional one, in the framework of collinear factorisation, whereby integrated parton distributions are fitted directly to the data. The second role is demonstrated in this thesis, following [1, 2, 4], where we use single-scale functions as *input* to the last-step procedure; see for example (2.12); we have emphasised the need to perform a new global fit to data in terms of the new functions f_a. After this, we do not expect the input single-scale function a on the left-hand side of (3.33) to equal the integral of f_a up to μ^2, since a itself is not fitted directly to the data, but rather is used as input for the last step of the evolution, which embodies a crucial angular-ordering constraint unique to this last step. Thus our single-scale or "auxiliary" function is not a traditional parton distribution function, but simply an intermediate function.

Chapter 4

Prompt photon hadroproduction

The production of prompt photons in high energy pp collisions has long played a key role in constraining the gluon distribution of the proton at large x, through the dominance of the subprocess $gq \to \gamma q$. In contrast to the case of deep inelastic scattering, the gluon enters at leading order. However the description of the transverse momentum spectrum of the produced photons is more problematic than the inclusive DIS cross section, and has been the subject of recent controversy [32]–[41]. The observed $p_{t\gamma}$ spectrum in $pp \to \gamma X$ (or $p\bar{p} \to \gamma X$) was found to be steeper than the prediction of perturbative QCD [33, 35]. The explanation of this discrepancy was attributed to the intrinsic transverse momentum k_t of the incoming partons, which is sometimes assumed to have a Gaussian-like k_t distribution [32, 34]. Thus part of the observed $p_{t\gamma}$ comes from the initial partonic k_t such that the hard subprocess singularity $d\hat{\sigma}/d\hat{t} \sim 1/p_{t\gamma}^4$ is approached more closely, and hence leads to a steeper $p_{t\gamma}$ spectrum. However in order to describe the observed spectra in this way, it is necessary[1] to introduce a k_t spectrum with an average value which increases from $\langle k_t \rangle \sim 0.5$ GeV to more than 2 GeV [34] as

[1]The authors of [35] argue that it may not be necessary if certain data sets are rejected.

the collision energy $\sqrt{s}$ increases from UA6, E706 [39, 40] to Tevatron [41] energies. Such large partonic $\langle k_t \rangle$ cannot originate solely from the large distance confinement domain, but must also have a significant perturbative QCD component [36]. The prompt photon process is a natural problem to approach from the point of view of our unintegrated parton distributions, which describe partons with incoming k_t.

In this chapter, based on our work in [1], I discuss how we may use unintegrated parton functions to compute this hadroproduction cross section, with two hadrons in the initial state. Convenient simplifications are also of theoretical interest, and may be applied to a wider class of problems. At the end I update the work to give an indication of the effects of using the newer unintegrated partons of [4], as described in Chapter 2.

4.1 Kinematics of prompt photon production

Even a 2→2 scattering becomes non-trivial if the colliding partons are non-collinear. With a hadron-hadron collision, we have to consider the possibility of both incoming partons having non-negligible transverse momenta k_{t1} and k_{t2} relative to the beam axis.

A convenient approach, comparable with the phenomenological "smearing" methods used elsewhere [32, 34], is to define a *luminosity function* to describe the initial parton-parton state. Thus our luminosity function $\mathcal{L}$ will act as a probability density to find the initial partons with combined transverse momentum q_t (and plus momentum fractions x_1, x_2). The total initial transverse momentum q_t is the relevant quantity, not the two individual parton momenta k_{t1} and k_{t2}, if we can consistently factorise the partonic information into $\mathcal{L}$. Then we can treat the subprocess separately and boost by q_t (and also by the longitudinal momentum) to obtain cross sections in the appropriate frame.

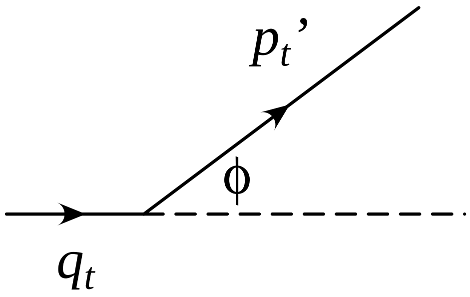

Figure 4.1: Definition of the angle ϕ, in the transverse plane relative to the beam axis. If $q_t = 0$ then ϕ has no significance, because the subprocess produces a photon with $\boldsymbol{p'_t}$ uniformly distributed in ϕ. However a significant incoming transverse momentum $\boldsymbol{q_t}$ defines a transverse direction, and the observed transverse momentum $\boldsymbol{p_t}$ in the LAB frame results from boosting the subprocess $\boldsymbol{p'_t}$ by the velocity coming from $\boldsymbol{q_t}$.

Depending on the incoming partons' momentum fractions x_1 and x_2, and also on q_t, the outgoing photon-parton system has an invariant mass M and a (longitudinal) rapidity[2] η_M. The variables we observe in the proton-proton CM are the photon's transverse momentum p_t and its rapidity η_γ. These come from the mass M, rapidity η_M and the subprocess 2→2 scattering angle θ, the whole system being Lorentz boosted sideways by q_t, then down the beam axis by η_M:

$$p_t^2 = \frac{M^2}{4}\sin^2\theta + \frac{q_t^2 + q_s^2}{4} + \frac{M_\perp q_s}{2} \tag{4.1}$$

$$\eta_\gamma = \eta_M + \frac{1}{2}\ln\left(\frac{M_\perp + q_s + M\cos\theta}{M_\perp + q_s - M\cos\theta}\right) \tag{4.2}$$

with $q_s \equiv q_t \sin\theta \sin\phi$, $M_\perp^2 \equiv M^2 + q_t^2$. The usual azimuthal symmetry associated with unpolarised hadron-hadron collisions is broken by ϕ, which is the azimuthal angle between $\boldsymbol{q_t}$ and the subprocess transverse momentum $\boldsymbol{p'_t}$ ($p'_t = M/2\ \sin\theta$), see Fig. 4.1.

[2]The rapidity η of an object with energy E and longitudinal momentum p_z is defined to be $\eta = \frac{1}{2}\ln\left[(E+p_z)/(E-p_z)\right]$.

4.2 The cross section for $pp \to \gamma X$

We convolute the luminosity function $\mathcal{L}(x_1, x_2, q_t^2)$, which contains the partonic information describing the initial state, with the appropriate hard subprocess cross section $d\hat{\sigma}/d\hat{t}$ for each of the two leading order subprocesses, which are $gq \to \gamma q$ and $q\bar{q} \to \gamma g$. There will be separate luminosities for each flavour of quark. The invariant differential cross section with respect to the photon is

$$\begin{aligned} E_\gamma \frac{d\sigma}{d^3 p_\gamma} &= \frac{d\sigma}{d\eta_\gamma \pi dp_t^2} \\ &= \frac{1}{\pi} \int \mathcal{L}(x_1, x_2, q_t^2) \frac{dx_1}{x_1} \frac{dx_2}{x_2} dq_t^2 \frac{d\hat{\sigma}}{d\hat{t}} d\hat{t} \frac{d\phi}{2\pi} \delta(\eta_\gamma - \cdots) \delta(p_t^2 - \cdots). \quad (4.3) \end{aligned}$$

We can work in terms of the variables η_M and M^2 and perform the integration over the luminosity with respect to $dM^2 d\eta_M dq_t^2$, using

$$\int \frac{dx_1}{x_1} \int \frac{dx_2}{x_2} \delta(M^2 - x_1 x_2 s + q_t^2) \delta\left(\eta_M - \tfrac{1}{2}\ln(x_1/x_2)\right) = \frac{1}{M_\perp^2}.$$

Then we have a three-dimensional integral to compute:

$$E \frac{d\sigma}{d^3 p} = \frac{1}{\pi} \int \mathcal{L}(M^2, \eta_M, q_t^2) \frac{dq_t^2}{M_\perp^2} \frac{d\phi}{2\pi} \frac{d\hat{\sigma}}{d|\hat{t}|} \left(\frac{2M^2 d\theta}{\sin\theta + (q_t/M_\perp)\sin\phi} \right). \quad (4.4)$$

For each (θ, ϕ, q_t^2) integration point, we evaluate $M_\perp$ as either (or both) solution(s) of the quadratic equation relating p_t^2 to M^2, q_t^2, θ and ϕ, viz.

$$M_\perp = -q_t \frac{\sin\phi}{\sin\theta} \pm \frac{1}{\sin\theta} \sqrt{4p_t^2 - q_t^2 \cos^2\theta \cos^2\phi}.$$

We must only use solutions which satisfy $M_\perp > q_t$. This is the first boundary condition — only certain (θ, ϕ, q_t^2) regions can generate the right p_t. Of course we must also have

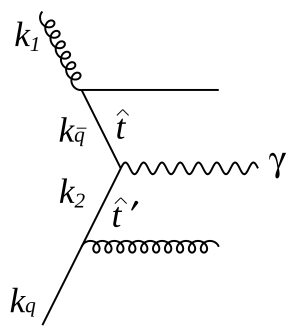

Figure 4.2: A schematic diagram describing both the subprocesses $gq \to \gamma q$ and $q\bar{q} \to \gamma g$, with either $\hat{t}$ or $\hat{t}'$ respectively representing the hard momentum transfer squared.

physical x values

$$0 < x_{1,2} < 1, \qquad x_{1,2} \equiv \frac{M_\perp}{\sqrt{s}}\, e^{\pm\eta_M}.$$

We impose two further restrictions when performing the integration of (4.4), both of which limit q_t. As in [1] it is natural to impose an ordering in transverse momenta. Inserting $\Theta(\mu^2 - q_t^2)$ prevents the total transverse momentum q_t exceeding the characteristic scale μ of the subprocess. This is somewhat approximate, and as in other perturbative QCD calculations, we have some dependence on our choice of scale. Nevertheless this picks out what we expect to be the most important configurations, with a hard subprocess and softer radiation in the parton functions. We also apply $\Theta(|\hat{t}| - q_t^2)$, which is necessary to avoid counting the same physical situation twice, as illustrated in Fig. 4.2. For the hard subprocess initiated by the gluon (k_1) and the quark (k_2) of Fig. 4.2, a strong ordering configuration implies $k_1^2, k_2^2 \ll |\hat{t}|$. This means that $q_t^2 \simeq \max(k_1^2, k_2^2) < |\hat{t}|$. Fig. 4.2 also describes the $q\bar{q} \to \gamma g$ subprocess but now $k_2^2 = \hat{t}'$ plays the role of the hard momentum transfer and strong ordering implies $k_{\bar{q}}^2, k_q^2 \ll |\hat{t}'|$.

Using our variables, we have $\hat{t} = -M^2\,(1 - \cos\theta)\,/2$ and $\hat{s} = M^2$. We make a suitable choice of scale μ for the strong coupling $\alpha_s(\mu^2)$ and for $\Theta(\mu^2 - q_t^2)$, and the same scale can act as the factorisation scale for the unintegrated parton distributions in the luminosity function. For example, $\mu = M/2$, $\mu = p_t$, or even $p_t/2$ might be thought appropriate. The two, familiar LO subprocess cross sections are [27]

$$\frac{d\hat{\sigma}}{d|\hat{t}|}(gq \to \gamma q) = \frac{C_F}{4} \frac{\pi \alpha_{em} \alpha_s(\mu^2) e_q^2}{\hat{s}^2} \left(\frac{-\hat{t}}{\hat{s}} + \frac{\hat{s}}{-\hat{t}} \right), \tag{4.5}$$

$$\frac{d\hat{\sigma}}{d|\hat{t}|}(q\bar{q} \to \gamma g) = \frac{2C_F}{3} \frac{\pi \alpha_{em} \alpha_s(\mu^2) e_q^2}{\hat{s}^2} \left(\frac{\hat{u}}{\hat{t}} + \frac{\hat{t}}{\hat{u}} \right). \tag{4.6}$$

4.3 Luminosity function

We need to construct a luminosity function to describe the probabilities of finding certain initial states. If we were happy to neglect initial k_t, we would have

$$\mathcal{L}_{gq}^{q_t=0}(x_1, x_2, q_t^2) = \delta(q_t^2)\, x_1 g(x_1, \mu^2)\, x_2 q(x_2, \mu^2) \tag{4.7}$$

using the ordinary integrated parton distribution functions at the hard interaction scale μ. In this way we obtain a standard LO cross section in the collinear factorisation approach.

However for $q_t \neq 0$ we must account for the initial transverse momenta of the partons, k_{t1} and k_{t2}. For hadron-hadron interactions, we represent the number densities of the two parton species with our unintegrated parton distribution functions $f_a(x_1, k_{t1}^2, \mu^2)$ and $f_b(x_2, k_{t2}^2, \mu^2)$. These are convoluted together to provide total transverse momentum q_t:

$$\begin{aligned} \mathcal{L}_{ab}(x_1, x_2, q_t^2) &= \int f_a(x_1, k_{t1}^2, \mu^2)\, f_b(x_2, k_{t2}^2, \mu^2)\, \pi \delta^{(2)}(\boldsymbol{k}_{t1} + \boldsymbol{k}_{t2} - \boldsymbol{q}_t)\, \frac{d^2 k_{t1}}{\pi k_{t1}^2} \frac{d^2 k_{t2}}{\pi k_{t2}^2} \\ &= \frac{1}{\pi} \int f_a(x_1, k_{t1}^2, \mu^2)\, f_b(x_2, k_{t2}^2, \mu^2)\, \frac{dk_{t1}\, d\phi_{12}}{k_{t1}\, k_{t2}^2} \end{aligned} \tag{4.8}$$

where we have constrained $k_{t2}^2 = q_t^2 + k_{t1}^2 - 2q_t k_{t1}\cos\phi_{12}$.

Most of our results in [1] were taken in the double logarithm limit (DLLA), which simplifies the luminosity and makes it considerably faster to compute. In

$$\mathcal{L}_{ab}(x_1, x_2, q_t^2) = \int f_a(x_1, k_{t1}^2, \mu^2)\, f_b(x_2, k_{t2}^2, \mu^2)\, \delta^{(2)}(\boldsymbol{k}_{t1} + \boldsymbol{k}_{t2} - \boldsymbol{q}_t)\, \frac{d^2 k_{t1}\, d^2 k_{t2}}{\pi k_{t1}^2 k_{t2}^2}, \quad (4.9)$$

to lowest order approximation, we apply strong ordering and deduce that one of the incoming partons will carry essentially all of the transverse momentum q_t. So either $k_{t1} \ll k_{t2} \simeq q_t$ and the luminosity simplifies to (see (2.18))

$$\frac{f_b}{q_t^2} \int^{q_t} f_a\, \frac{d^2 k_{t1}}{\pi k_{t1}^2} = \left[a(x_1, q_t^2)\, T_a(q_t, \mu)\right]\, \frac{f_b(x_2, q_t^2, \mu^2)}{q_t^2},$$

or $k_{t2} \ll k_{t1} \simeq q_t$, and the equivalent result.

Thus the sum of both contributions may be expressed as

$$\mathcal{L}_{ab}(x_1, x_2, q_t^2) = \frac{\partial}{\partial \lambda^2}\, \left[a(x_1, \lambda^2)\, T_a(\lambda, \mu)\, b(x_2, \lambda^2)\, T_b(\lambda, \mu)\right]\Big|_{\lambda = q_t}. \quad (4.10)$$

We refer to this convenient form as DDT, because an analogous expression for the Drell-Yan process was originally obtained[3] by Dokshitzer, Dyakanov and Troyan [15].

4.4 Variation of luminosity with q_t

We can fix x_1, x_2 at some typical value and investigate the q_t-dependence of the luminosity function, where recall q_t is the total initial (partonic) transverse momentum. The

[3]Not only do these letters DDT refer to the authors' surnames, but in [15] they contrived to write the parton functions as D and one combined Sudakov factor as T, thus spelling out their initials in the key formula of the work.

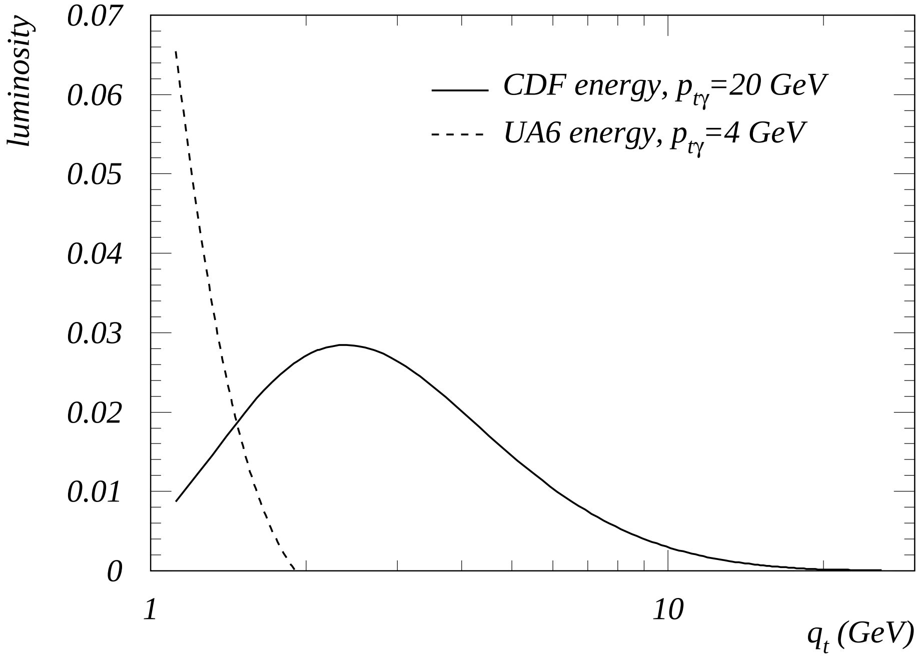

Figure 4.3: The "DDT" gluon on quark luminosity function. $x_1 = x_2 = x_T$, with the CDF energy being $\sqrt{s} = 1800$ GeV, UA6 $\sqrt{s} = 24.3$ GeV. Here the hard scale μ is taken as p_t, and the p_t values chosen are typical of the two prompt photon experiments.

appropriate x values of course depend on $\sqrt{s}$ and p_t. A convenient representative value, for the production of a single high p_t particle such as a prompt photon, is $x_T = 2p_t/\sqrt{s}$. Note that we are naturally restricted to $q_t > k_0$, where k_0 is the parton set minimum scale of order 1 GeV. The DDT luminosity from (4.10) is shown for some typical values in Fig. 4.3.

For UA6 the non-perturbative regime $q_t < k_0$ holds the bulk of the luminosity (see the next section) and the DDT formula goes negative at $q_t \sim 2$ GeV, showing the breakdown of the double logarithm approximation. At the higher energy of the Tevatron, however, non-perturbative effects become irrelevant, as most of the luminosity is in the perturbative region.

4.5 Non-perturbative luminosity region

Is $q_t < k_0$ a problem? With the DDT formula (4.10), we can define an integrated luminosity $\mathcal{L}_0(q_t)$ telling us how much luminosity comes from below a certain region q_t,

$$\mathcal{L}_0(q_t) = a(x_1, q_t^2)\, T_a(q_t, \mu)\, b(x_2, q_t^2)\, T_b(q_t, \mu).$$

$\sqrt{s}$ (GeV)	$\mathcal{L}_0(q_{max}) - \mathcal{L}_0(k_0)$ ($q_t > k_0$)	$\mathcal{L}_0(k_0)$ ($q_t < k_0$)	Fraction from $q_t < k_0$
25	0.062	0.160	**0.72**
50	0.095	0.048	**0.34**
100	0.0851	0.0103	**0.11**
500	0.0444	0.0001	$\mathbf{2 \times 10^{-3}}$
1800	0.0291	1.4×10^{-6}	$\mathbf{5 \times 10^{-5}}$
1800	1.16	0.0016	$\mathbf{1 \times 10^{-3}}$

Table 4.1: The integrated luminosity from the perturbative ($q_t > k_0$) and non-perturbative ($q_t < k_0$) domains for typical values of $\sqrt{s}, x_1, x_2$. We take $k_0^2 = 1.25$ GeV^2 and $\mu = p_t$.

Table 4.1 contains some sample numbers, showing how we can estimate what fraction of the luminosity is in the non-perturbative region. Above the dividing line we have chosen $x_1 = x_2 = 0.3$, but for the last line of the table we take $x_1 = x_2 = 0.03$, which is more physical for the Tevatron energy. At low $\sqrt{s}$, we see that the luminosity mostly comes from the region $q_t < k_0$, but at high $\sqrt{s}$ only $q_t > k_0$ is significant within this approach; compare with Fig. 4.3.

As $q_t < k_0$ *is* important for the fixed target energies (how important depends on how we choose μ), we can make phenomenological extensions to the DDT formula for the luminosity, in order to account for this non-perturbative region. Here are two simple options:

1. no intrinsic k_t —

$$\mathcal{L}\,(q_t < k_0) = \mathcal{L}_0(k_0)\,\delta(q_t^2)$$

2. wide gaussian —

$$\mathcal{L}\,(q_t < k_0) = \mathcal{L}_0(k_0)\,\frac{e^{-q_t^2/k_0^2}}{k_0^2(1 - e^{-1})}$$

Using these forms gives two possible alternative contributions to the cross section, which we may add to the cross section computed using the (perturbative $q_t > k_0$) DDT luminosity. The small difference between these two versions is shown in the prompt photon cross section curves [1] in Fig. 4.4. We note that, even in the case of the fixed target energy $\sqrt{s} = 24.3$ GeV, the main effect of the non-perturbative region is essentially the same for either option: a fairly uniform contribution to the cross section, rather than a significantly "smeared" contribution, because the shapes of the curves deriving from the "delta" and "gaussian" luminosity extensions are so similar. A simple estimate [1] shows that we would only expect the subprocess cross section to be altered by a relative correction $q_t^2/2p_t^2$, which for the non-perturbative region cannot exceed $k_0^2/2p_t^2$. Nevertheless the $q_t < k_0$ contribution must be included for such low $\sqrt{s}$ values; we see it makes up most of the cross section.

4.6 Results with DDT luminosity

Fig. 4.5 and Fig. 4.6 contain the results of the DDT-based prompt photon hadroproduction cross section calculations [1], compared with data from the UA6 [39], E706 [40] and CDF [41] experimental collaborations. We show the sensitivity of these results to the choice of the hard scale μ, which is very significant at the lower energies. With the smaller scale choice, $\mu = p_{t\gamma}/2$, both the value of α_s and the survival probability T_a are

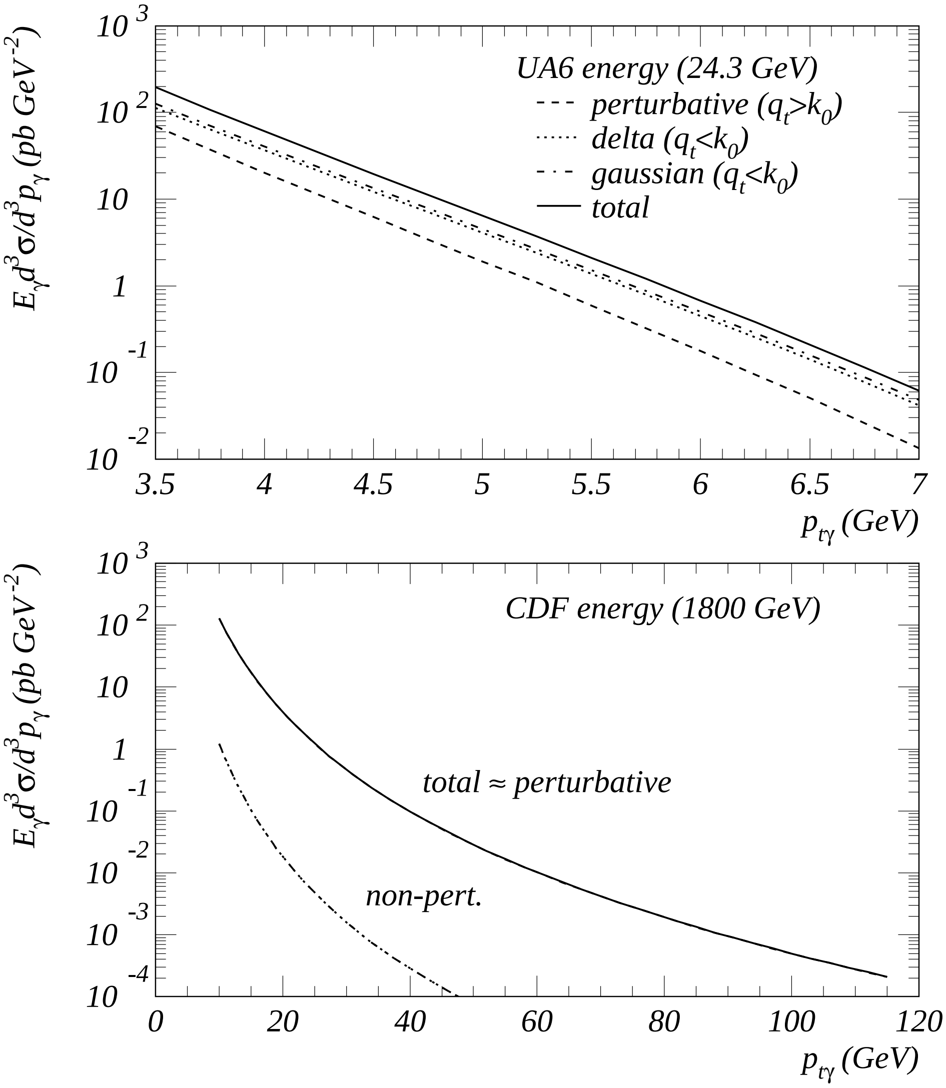

Figure 4.4: The effect of partonic q_t arising from the non-perturbative ($q_t < k_0$), perturbative ($q_t > k_0$), and total contributions to the p_t spectrum of prompt photon production in pp collisions at $\sqrt{s} = 24.3$ GeV and in $p\bar{p}$ collisions at 1800 GeV.

larger, giving a larger cross section than for $\mu = p_{t\gamma}$. (A third choice of scale, $\mu = M/2$, gives similar results to those obtained with $\mu = p_{t\gamma}$.) We also include (dashed curves in Fig. 4.5) results with the "$q_t = 0$" luminosity computed from (4.7). The major effect in going from the LO $q_t = 0$ approach to the (DLLA) unintegrated partons approach with the DDT luminosity is a shift of the cross section, rather than a change of shape. This suggests that the kinematic smearing effect is generally modest, at least with the restrictions $\Theta(\mu^2 - q_t^2)\,\Theta(|\hat{t}| - q_t^2)$ limiting our allowed q_t. An important feature of this formalism in terms of the DDT luminosity is that the integrated parton distributions are sampled at the lower scale q_t rather than, as in the $q_t = 0$ approach, at μ. This is partly responsible for the difference between the dashed and continuous curves in Fig. 4.5.

Clearly the use of unintegrated partons to predict the cross sections for hadroproduction is an area which merits further attention. We can make a few comments about Fig. 4.6, however. Comparison with the CDF data, which are taken at high $\sqrt{s}$, is reasonable, and the non-perturbative region does not present us with any difficulties. (Incidentally, the low values of x_T for such a high $\sqrt{s}$ also mean that there are not likely to be significant "threshold" effects, which we have not discussed here.) However, at the low p_t end of the spectrum there is still room for improvement for a better agreement with the CDF data. It is the E706 experiment, however, which exhibits the worst disagreement with our predictions. This is in common with other (unsmeared) analyses. The purpose of describing the prompt photon production process in terms of the k_t-dependent parton functions is to eliminate the use of phenomenological smearing, but the problem is not solved.

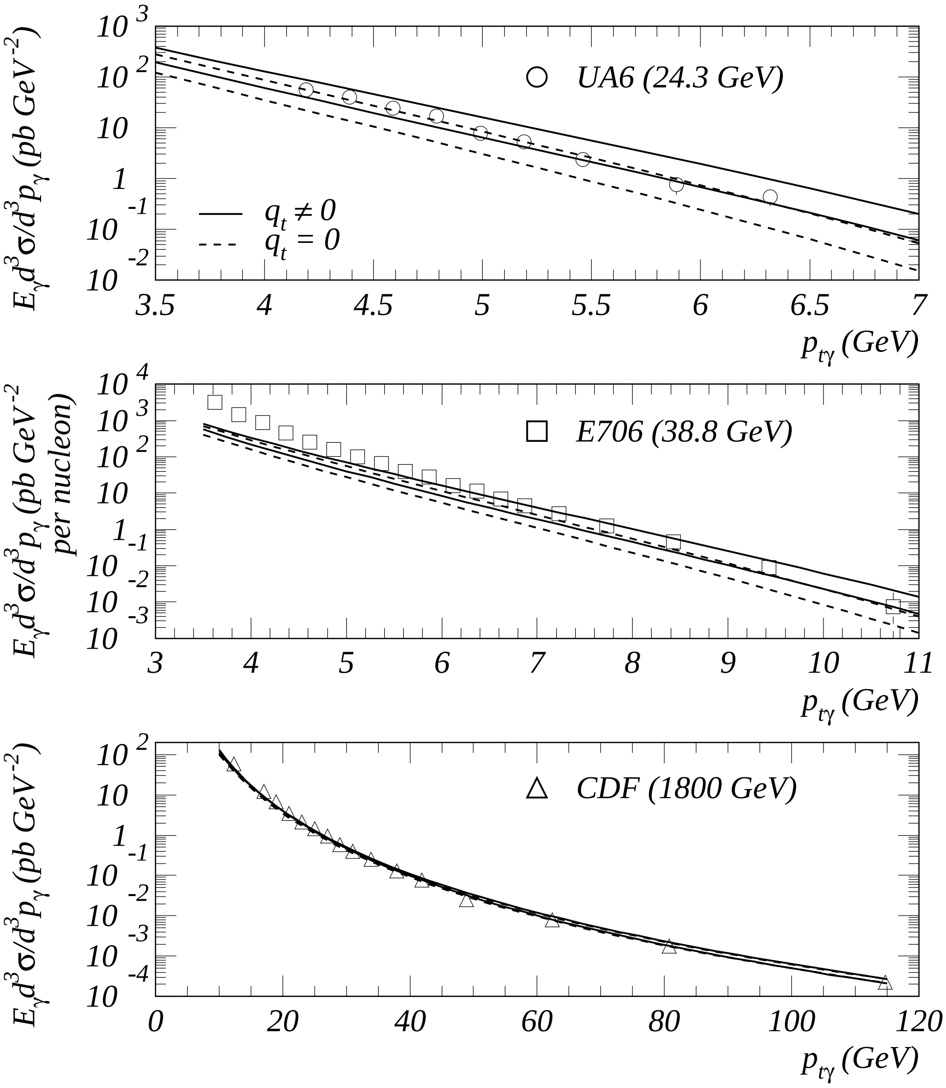

Figure 4.5: Comparison of the prompt photon cross section, computed with the DDT luminosity, with data from UA6 (pp collisions at $\sqrt{s} = 24.3$ GeV), E706 (pBe collisions at $\sqrt{s} = 38.8$ GeV) and CDF ($p\bar{p}$ collisions at $\sqrt{s} = 1.8$ TeV). The continuous curves include q_t, dashed curves are calculated with $q_t = 0$ and integrated partons sampled at scale μ. The upper curves correspond to a scale choice of $\mu = p_{t\gamma}/2$ and the lower ones to $\mu = p_{t\gamma}$, showing the greater scale dependence at lower values of $\sqrt{s}$.

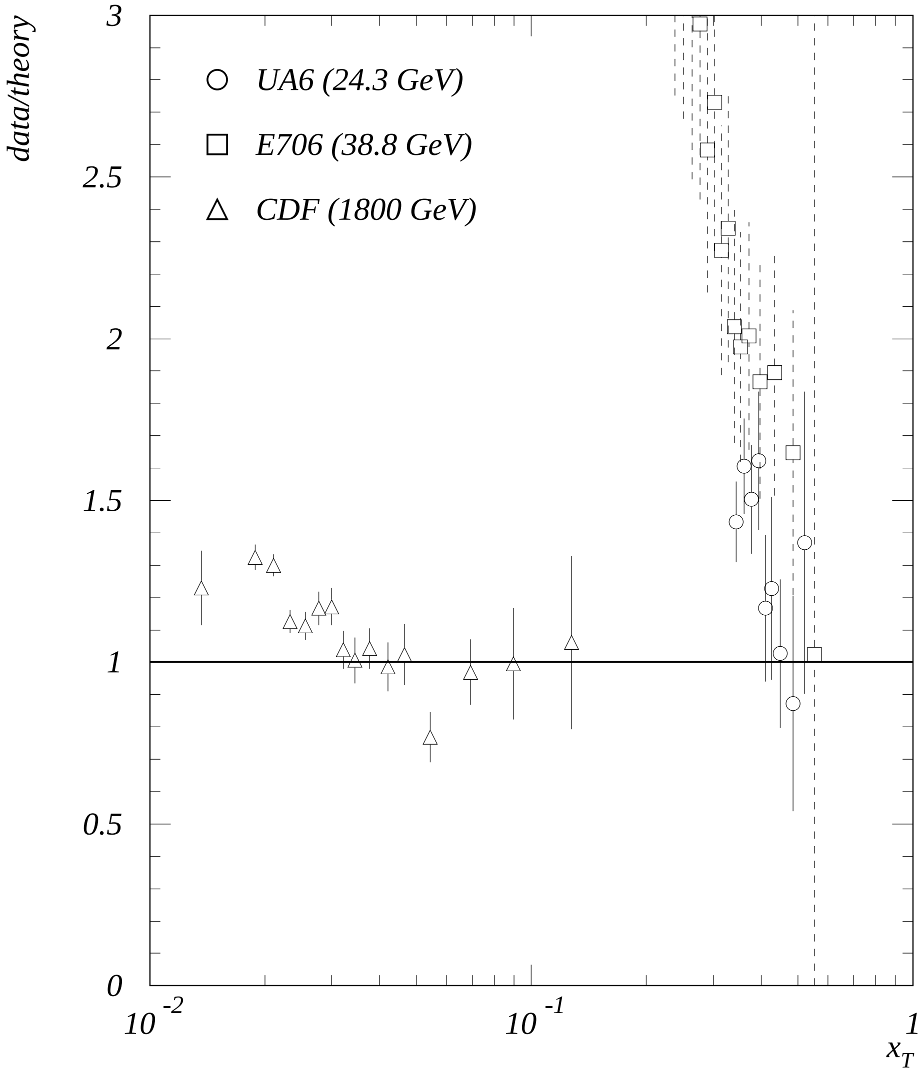

Figure 4.6: A data/theory plot, showing more clearly the discrepancies between the theoretical curves in Fig. 4.5 and the data, for $\mu = p_{t\gamma}$; the transverse momentum variable here is $x_T \equiv 2p_t/\sqrt{s}$.

4.7 Luminosity from the newer unintegrated partons

We wish to extend this work to go beyond the DLLA, and at the same time to use directly the unintegrated partons discussed in Chapter 2, which are based on angular ordering rather than the strong ordering central to [1]. The natural apparatus is still the luminosity function, but we wish to compute this explicitly as an alternative to relying on the DDT formula (4.10).

Let us return to eq. (4.8), which defines the luminosity $\mathcal{L}$ in terms of two unintegrated functions $f_a(x_1, k_{t1}^2, \mu^2)$ and $f_b(x_2, k_{t2}^2, \mu^2)$. We can perform this integral directly, choosing parton a to be an up quark, and parton b a gluon, and thus compute the up+gluon luminosity at various values of x_1, x_2, q_t. (Note in comparison with Fig. 4.3 that we plotted there the up-*valence*+gluon luminosity, but it is safer to work with the whole physical up quark distribution when using unintegrated partons.)

Our first question is what to take as the upper limit of the integral over k_{t1}. In the strong ordering approach, we would choose q_t, and the result is shown in Fig. 4.7. As in Fig. 4.3, we have chosen typical values for the Tevatron, $x_1 = x_2 = 40/1800 \simeq 0.022$, $\mu = 20$ GeV.

However, in principle we would like to include situations with larger values of k_{t1} or k_{t2} for the individual partons, provided that the vector sum results in q_t. Therefore for Fig. 4.8 we allow k_{t1} to become large[4], which has a marked effect for the lower values of q_t especially, raising the luminosity above that described by the DDT formula, unsurprisingly.

[4] To be precise, I imposed a limit of cq_t, and found the results for $c = 100$ are in close agreement with those for $c = 10$. From the form of (4.8), noting that $k_{t1} \gg q_t \Rightarrow k_{t2} \gg q_t$, we interpret this as convergence.

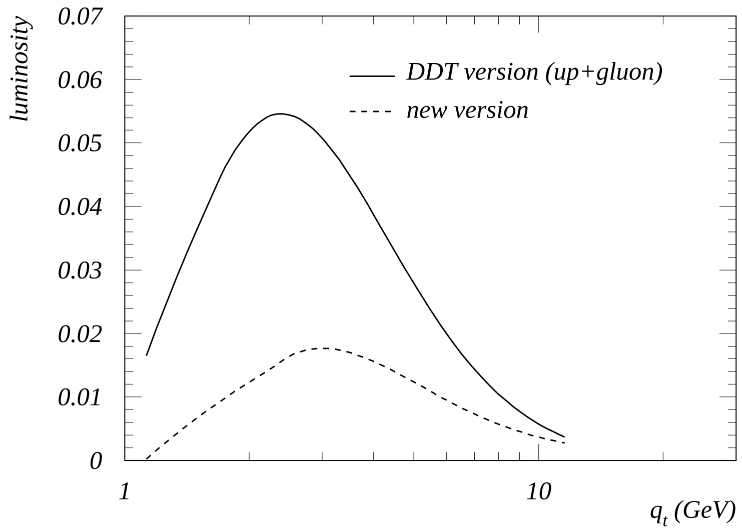

Figure 4.7: The up+gluon luminosity function, firstly (continuous curve) calculated in the DDT approach from (4.10), and then using (4.8) with our unintegrated DGLAP partons. The dashed curve has been computed with the integration limit $k_{t1} \leq q_t$.

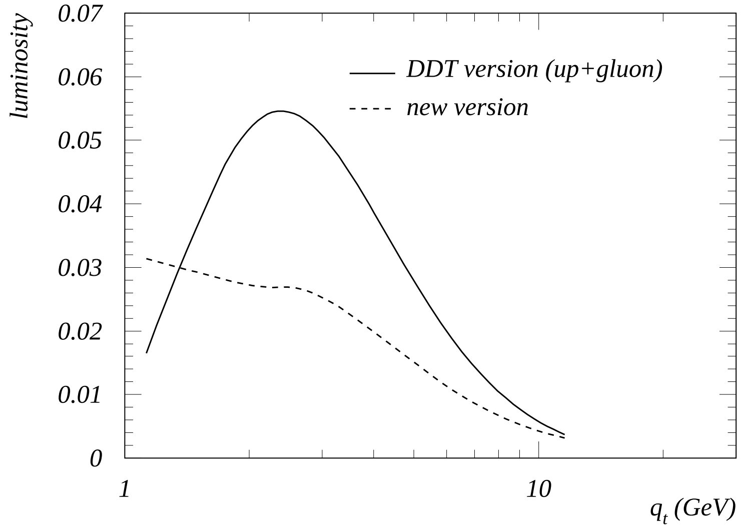

Figure 4.8: The up+gluon luminosity function, firstly (continuous curve) calculated in the DDT approach from (4.10), and then using (4.8) with our unintegrated DGLAP partons. The dashed curve has been computed with the integration limit $k_{t1} \to \infty$.

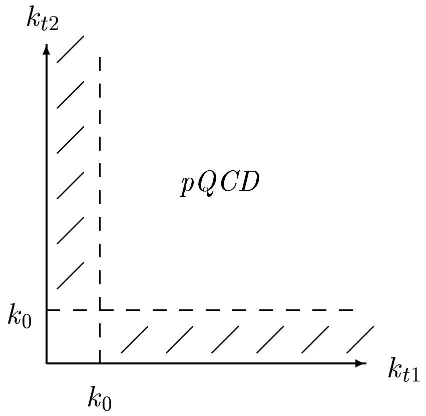

Figure 4.9: Sketch showing allowed values of k_{t1}, k_{t2}. A fully perturbative approach is only valid for $k_{t1,2} > k_0$. We can, however, make an approximation for the "off-diagonal" (shaded) region.

Even without considering what the correct value of the upper limit for k_{t1} should be, we still have a large difference between the DDT result and the new, "exact" calculation. Look for example at $q_t \sim 5$ GeV where the DDT approximation yields a significantly higher result than the new version, in Figs. 4.7 and 4.8. Because we cannot define our functions $f(x, k_t^2, \mu^2)$ for $k_t < k_0$, in computing (4.8) I have had to put a lower limit on k_{t1} of k_0, and similarly insert the cut $\Theta(k_{t2} - k_0)$. This means that although we classified the $q_t > k_0$ region plotted as "perturbative" insofar as we were using the DDT formula, we cannot compute all of it with separate unintegrated partons. Worse, the configurations omitted by restricting $k_{t1,2} > k_0$ are precisely those off-diagonal situations (see Fig. 4.9) which the (DDT) strong ordering focuses on, which clearly from the figures represent the major part of the total luminosity.

The best guess we can make for the region where $k_{t1} < k_0$ and $k_{t2} > k_0$ is, in the same spirit characterising our non-perturbative contribution to F_2 in (3.16),

$$\begin{aligned}\mathcal{L}_{ab}^{k_{t1}<k_0} &= \int_0^{k_0^2} f_a(x_1,k_{t1}^2,\mu^2)\,\frac{dk_{t1}^2}{k_{t1}^2}\,\frac{f_b(x_2,k_{t2}^2,\mu^2)}{k_{t2}^2}\,\frac{d\phi_{12}}{2\pi} \\ &\simeq a(x_1,k_0^2)T_a(k_0,\mu)\int_0^{2\pi}\frac{f_b(x_2,k_{t2}^2,\mu^2)}{k_{t2}^2}\,\frac{d\phi_{12}}{2\pi},\end{aligned} \tag{4.11}$$

where we have to pick some representative value $\langle k_{t1}\rangle$ and in the remaining integral $k_{t2}^2 = q_t^2 + \langle k_{t1}\rangle^2 - 2q_t\langle k_{t1}\rangle\cos\phi_{12}$. We can write an expression complementary to (4.11) for $\mathcal{L}_{ab}^{k_{t2}<k_0}$, proportional to $b(x_2,k_0^2)$, which also contributes. Of course we have to check that our results do not depend much on the choice of $\langle k_{t1}\rangle$ (or equivalently $\langle k_{t2}\rangle$ for the other piece). This is true for $q_t > 2$ GeV, as shown in Fig. 4.10, in which the sum of the two off-diagonal parts are shown; however we see that the choice of $\langle k_t\rangle$ does have an effect for $q_t < 2$ GeV. The lowest dashed curve is for $\langle k_t\rangle = k_0/2$, then above that is $\langle k_t\rangle = k_0/5$, and finally (highest) we set $\langle k_t\rangle = 0$, a case which is reminiscent of the intermediate step in deriving the DDT formula, with the unintegrated parton sampled at q_t^2 (and trivial ϕ_{12} integration).

It is clear that $q_t < 2k_0$ is doomed to be a tricky region to deal with. There is no obvious way to include the final region of Fig. 4.9, the lower left square where $k_{t1,2} < k_0$, unless we are confident in some phenomenological extension[5] to our unintegrated partons f below k_0. For this reason it might be plausible to take the $\langle k_t\rangle = 0$ form shown in Fig. 4.10: this is certainly an overestimate of the strictly off-diagonal contributions but perhaps numerically compensates the lack of a contribution from $k_{t1,2} < k_0$. In this case we can add this curve to our perturbative part and arrive at a luminosity that is reasonably well justified, insofar as the unintegrated DGLAP partons produced from the

[5]In Monte Carlo simulators, extrapolations are sometimes made to the unintegrated partons to account for non-perturbative regions.

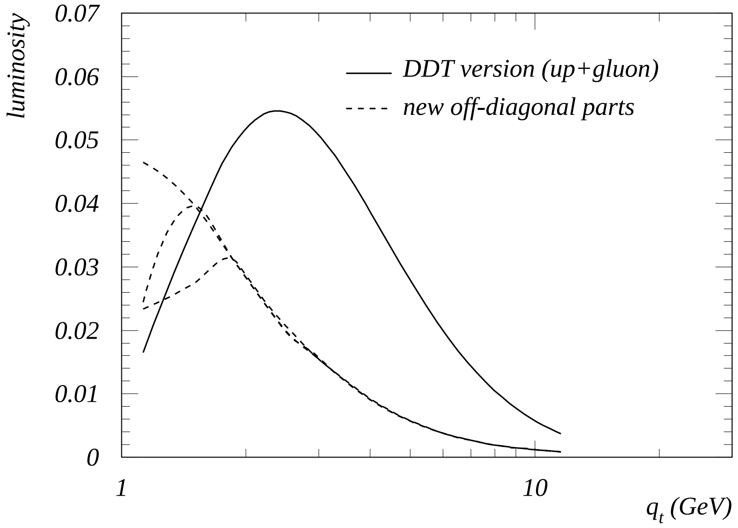

Figure 4.10: Here we show *only* the off-diagonal contributions like (4.11), computed with our unintegrated DGLAP partons. The highest dashed curve corresponds to $\langle k_t \rangle = 0$, then below that $\langle k_t \rangle = k_0/5$, followed by $\langle k_t \rangle = k_0/2$. (For reference we compare with the *total* DDT version as before.)

last-step formalism with MRST99 input are credible[6].

Figs. 4.11 and 4.12 show the final two alternatives: the former combines the perturbative contribution from Fig. 4.7, in which we limit $k_{t1} < q_t$, with the non-perturbative estimate ($\langle k_t \rangle = 0$). If instead we use the perturbative contribution from Fig. 4.8, the luminosity is rather larger, especially at small q_t, and this is shown in Fig. 4.12. The latter curve is more physical, because with the angular-ordered unintegrated partons the old restriction $q_t > k_t$ is artificial. Either way we see a somewhat different shape from the DDT luminosity approximation, but at large q_t, where we might expect the most significant smearing effects, the difference is not pronounced. In principle, it would be possible to replace the DDT luminosity with this new luminosity for the purpose of recalculating the prompt photon cross section, at least for the high $\sqrt{s}$ appropriate to

[6]We remind the reader that both the normalisation and shape of these unintegrated partons are only approximate, without a reliable global fit in the new framework as discussed in Chapter 3.

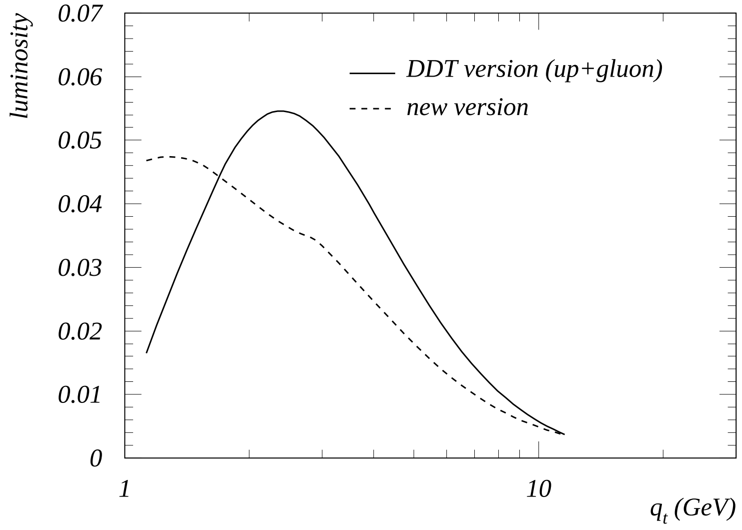

Figure 4.11: Final comparison of the DDT luminosity (for typical x values relevant at the Tevatron) with the new approach, based on direct integration of our unintegrated partons. In this figure, the new (dashed) version corresponds to a limit on k_{t1} of q_t, so this is the sum of the dashed curves in Figs. 4.7 and 4.10. Compare with Fig. 4.12.

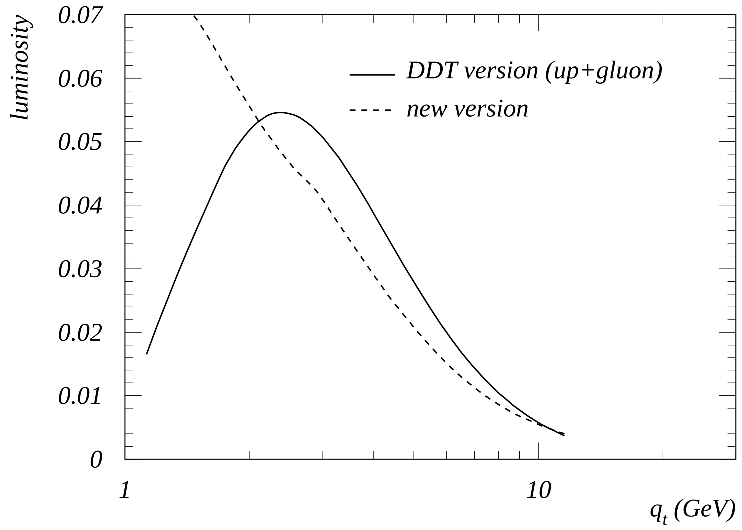

Figure 4.12: Final comparison of the DDT luminosity (for typical x values relevant at the Tevatron) with the new approach, based on direct integration of our unintegrated partons. In this figure, the new (dashed) version corresponds to no limit on k_{t1}, so this is the sum of the dashed curves in Figs. 4.8 and 4.10. Compare with Fig. 4.11.

the CDF experiment, but this is beyond the scope of the present work. There is obvious need for caution, in extending this approach beyond the leading accuracy, to ensure that the way the ordering constraints are relaxed leads to a consistent computation in which there is no double counting. It could be argued that it is easier to achieve this within collinear factorisation.

Chapter 5

Photoproduction of photons

Another environment in which prompt photons may be produced is at HERA. Electron-proton colliders produce not just interactions involving highly virtual photons (such as DIS) but an abundance of interactions in which Q^2 is very low. We therefore have the situation in which a quasi-real photon may initiate a hard scattering with the proton. Although Q^2 does not provide a hard scale for perturbative analysis of such scatterings, events can be selected when a large outgoing momentum, such as the high transverse momentum of a prompt photon, is observed, and this may be used as a hard scale enabling us to describe the incoming photon-proton interaction using perturbative QCD.

Photoproduction at HERA therefore involves the incoming electron radiating a photon along the beam axis, and it is this very low virtuality photon ($Q^2 \sim 10^{-3}$ GeV^2) that interacts with the proton. The equivalent photon approximation [21] describes the relationship between the observed electron-proton cross section σ_{ep} for the process under consideration, such as in this case the production of a prompt photon, and the cross section $\sigma_{\gamma p}$ for the incoming photon-proton interaction:

$$\sigma_{ep\to\gamma X} = \int_{y_{min}}^{y_{max}} dy\, f_\gamma^{(e)}(y)\, \sigma_{\gamma p\to\gamma X}. \tag{5.1}$$

The photon-proton cross section $\sigma_{\gamma p}$ depends on the fraction y of the electron's momentum which is transferred to the photon ($0 < y < 1$), because the invariant mass squared of the proton-photon system is

$$s_{\gamma p} = y s_{HERA}. \tag{5.2}$$

The function $f_\gamma^{(e)}(y)$ acts as a probability that a photon with this momentum fraction initiates an interaction with the proton. We use the modified [21] Weizsäcker-Williams function, which depends on the maximum Q^2 value which is allowed in the classification of photoproduction events ($Q^2_{max} = 1$ GeV^2), on the mass of the electron m_e, which provides a minimum Q^2, and of course on the electromagnetic coupling constant α_{em}:

$$f_\gamma^{(e)}(y) = \frac{\alpha_{em}}{2\pi}\left[\frac{1+(1-y)^2}{y}\ln\frac{Q^2_{max}(1-y)}{m_e^2 y^2} + \frac{2m_e^2 y}{Q^2_{max}} - \frac{2(1-y)}{y}\right]. \tag{5.3}$$

(Numerically, the term $2m_e^2 y/Q^2_{max}$ is unimportant.) We can then perform our calculation in terms of the photon and proton. However, experimental cuts, used to select the data available, may need to be simulated for theoretical calculations in terms of particle momenta in the HERA frame of reference, introducing further dependence on y.

5.1 Sample calculations

Prompt photon photoproduction data have been taken by the ZEUS collaboration, and competing groups of theorists have performed sophisticated NLO calculations (in the collinear factorisation approach) to compare with the various spectra measured; see, for example, [22]. An important feature of such calculations is the need to consider various different types of contribution, which are computed separately. The first distinction is between an outward-going photon produced immediately in the $2 \to 2$ subprocess, and the alternative of fragmentation of a final-state parton to produce this photon[1]. In the latter case, a different hard subprocess cross section is convoluted with a fragmentation function representing the probability of the outgoing parton radiating a photon with a certain fraction of its momentum. The second distinction is between hard subprocesses initiated directly by the quasi-real photon, and "resolved" interactions in which the photon itself fluctuates into further partons (such as a quark-antiquark pair), one of which participates in the reaction. The resolved contributions are thus an interesting measure of the *parton distributions of the photon*, but this complicates the analysis because another parton function needs to be included. (It may be valuable to compare the formalism in this situation with hadroproduction, see [23] for the example of $b\bar{b}$ photoproduction.)

In practice experimental cuts may be applied to select events for which $x_\gamma \simeq 1$, corresponding to mostly *direct* rather than resolved contributions. It is also the case that the photon isolation criterion, used to reject secondary photons coming from pion decay[2], serves to reduce the fragmentation component of the cross section. Nevertheless, a full analysis should include all such considerations.

In this chapter we restrict ourselves to discussing briefly how one might start to compute predictions for photon photoproduction within the framework of unintegrated par-

[1]Note that the categorisation "prompt photon" simply means that secondary photons produced after hadronisation effects, from decays of light mesons, are not included in the data.

[2]A rapidity-azimuthal angle cone is constructed around the detected photon and events are rejected if there is too much hadronic transverse energy deposited within the cone.

ton distributions, looking at the simplest contribution, which is from the direct photon-proton interaction with no subsequent fragmentation.

The appeal of prompt photon photoproduction measurements, in such a situation, is that the outgoing photon's transverse momentum has potential to give clear information about the initial k_t held by the incoming parton from the proton. In contrast to the hadroproduction calculations of Chapter 4, only one unintegrated parton function will be involved, which is a significant simplification. Measured quantities which may be particularly useful in this respect include the differential cross section with respect to the out-of-plane momentum, p_{Tout}. Events are selected with a prompt photon γ and one jet, and if the initial transverse momentum were 0, we would expect the transverse momenta of the photon and the jet to balance.

The experimental definition of the quantity p_{Tout} is [24]

$$p_{Tout} = \left| p_{\gamma(x)} p_{j(y)} - p_{\gamma(y)} p_{j(x)} \right| / E_{tj}, \tag{5.4}$$

where p_γ refers to the prompt photon's momentum, p_j refers to the jet (and E_{tj} is the transverse energy of the jet), and x and y are coordinate directions in the transverse plane. For our approach, we wish to consider the subprocess $\gamma q \to q\gamma$ (simply Compton scattering, taking the $Q^2 \to 0$ limit of the cross section derived in Section B.1). We work at the parton level, and therefore approximate the jet momentum crudely to that of the outgoing quark q, which we assume on-shell. Thus our theoretical approximation for p_{Tout} is

$$p_{Tout} = p_{t\gamma} \sin \phi_{q\gamma}. \tag{5.5}$$

Note that we define the azimuthal angle between the outgoing photon and the outgoing quark in such a way that $0 < \phi_{q\gamma} \leq \pi$.

We write down an expression for this contribution to the cross section, driven by unintegrated quark distributions (summing over all possible flavours q), which is similar in style to (4.3):

$$\frac{d\sigma_{ep\to\gamma+jet}}{dp_{Tout}} = 2p_{Tout}\sum_q \int f_q(x,k_t^2,\mu^2)\, f_\gamma^{(e)}(y)\, \delta(p_{Tout}^2 - \cdots)\, \frac{d\hat{\sigma}_{\gamma q\to q\gamma}}{d|\hat{t}|}\, d|\hat{t}|\, \frac{d\phi}{2\pi}\, dy\, \frac{dk_t^2}{k_t^2}\, \frac{dx}{x}. \tag{5.6}$$

In (5.6) the integrations over k_t^2 and x sum the possible initial states of the unintegrated quark, the integration over y sums the possible initial states of the incoming photon (which has no transverse momentum), and the integrations over $\hat{t}$ and ϕ sum the possible final states of the subprocess. ϕ is *not* the same as the angle $\phi_{q\gamma}$, but represents the azimuthal angle in the subprocess CM frame between the decay products and the boosting transverse momentum k_t.

We spent some time trying to compute the cross section in (5.6) reliably, using the Monte Carlo routine `vegas` [31]. However, there are two difficulties. Firstly, the expression for p_{Tout}^2 in terms of the other kinematic variables is far from straightforward, once the Lorentz boost has been taken into account. This means that, although the delta function in (5.6) removes one dimension of integration, the Jacobian factors introduced are complicated. A second problem is that the many experimental cuts needed to select acceptable data for this observable are necessarily messy. The phase space over which we integrate, in this approach, is peppered with holes, and with a complicated integrand which is not especially fast to compute, this makes achieving stable, credible results more difficult than one might expect.

Instead we turn here to a plausible simplification [25] which may be of more immediate use, if we are prepared to discard the overall normalisation of the cross section. In fact problems with systematic error estimation make experimentalists inclined to work with the shapes, rather than normalisations, of such spectra, anyway. By concentrating on the k_t dependence of the unintegrated quark above everything else, we yield some kind of approximation to the p_{Tout} distribution, which is very much easier to compute.

Suppose we were calculating the distribution for the overall imbalance in transverse momentum, which corresponds, if we ignore all final-state effects such as fragmentation, to our incoming k_t. In this case the cross section would be written

$$\frac{d\sigma_{ep\to\gamma+jet}}{dk_t^2} = \int f(x, k_t^2, \mu^2)\, f_\gamma^{(e)}(y)\, \frac{1}{k_t^2}\, \frac{d\hat{\sigma}_{\gamma q\to q\gamma}}{d|\hat{t}|}\, d|\hat{t}|\, \frac{d\phi}{2\pi}\, dy\, \frac{dx}{x}, \tag{5.7}$$

where we temporarily omit to write the quark flavour sum. If we can approximate that the integration of

$$f_\gamma^{(e)}(y)\, \frac{d\hat{\sigma}_{\gamma q\to q\gamma}}{d|\hat{t}|}\, d|\hat{t}|\, \frac{d\phi}{2\pi}\, dy\, \frac{dx}{x} \tag{5.8}$$

doesn't depend strongly on k_t, then we can estimate the k_t dependence of (5.7) as

$$\frac{d\sigma_{ep\to\gamma+jet}}{dk_t^2} \sim \frac{f(\overline{x}, k_t^2, \overline{\mu}^2)}{k_t^2}, \tag{5.9}$$

with $\overline{x}$ and $\overline{\mu}$ chosen as representative values of plus momentum fraction x and hard factorisation scale μ. This is far from ideal, but may give some insight into the likely k_t spectra, without invoking the full kinematics.

The observable p_{Tout} involves only one component of k_t; the other component is unconstrained. Aligning axis y in the direction of p_{Tout}, it is clear that

$$\frac{d\sigma}{dk_y} = \int \frac{d\sigma}{\pi dk_t^2}\, dk_x. \tag{5.10}$$

Write for convenience $k_x \equiv k$, and $k_y \equiv p_{Tout}$, and make the same simplification leading to (5.9). Then a tentative approximation for the p_{Tout} distribution is

$$\frac{dN}{dp_{Tout}} \sim \int \frac{f(\overline{x}, k_t^2, \overline{\mu}^2)}{k_t^2}\, dk, \tag{5.11}$$

where the appropriate total transverse momentum is given by $k_t^2 = p_{Tout}^2 + k^2$. Formally k goes from $-\infty$ to $+\infty$, but we can curtail k_t at some large value (somewhat greater than $\overline{\mu}$) and limit $|k|$ accordingly. Typical values for $\overline{x}$ and $\overline{\mu}$ are suggested from work done with `vegas` in the full integration of (5.6). $y \sim 0.12$ is a representative value, and we use $\overline{x}\,\overline{y}s \sim M^2$ with a guessed typical invariant mass squared of about 150 GeV^2 to infer $x \sim 0.014$. $\overline{\mu}$ should be therefore of order of this invariant mass. Variation of our choices $\overline{x}$ and $\overline{\mu}$ around such expected values is of course essential, to obtain an indication of the likely result.

Potentially, different flavours of quark could yield slightly different shapes in (5.11). We can easily sum the appropriate contributions to give an overall prediction:

$$\frac{dN}{dp_{Tout}} \sim \sum_q \int \frac{e_q^4\, f_q(\overline{x}, k_t^2, \overline{\mu}^2)}{k_t^2}\, dk. \tag{5.12}$$

Note that this calculation is driven exclusively by the unintegrated quark distributions, and the unintegrated gluon does not feature. We should however mention in passing that in fact the subprocess $\gamma g \to g\gamma$, which formally is a correction of higher order $\sim \alpha_s^2$ because it contains a quark loop, might produce[3] a contribution competing with (5.12) for $x \sim 0.01$, because of the larger gluon density.

[3]Certainly we have found, in studies of diphoton hadroproduction, that the related gluon-gluon fusion diagram gives a numerical correction comparable with the leading order quark-antiquark diagram for that process, although in that case there are two gluon densities to compensate for α_s^2.

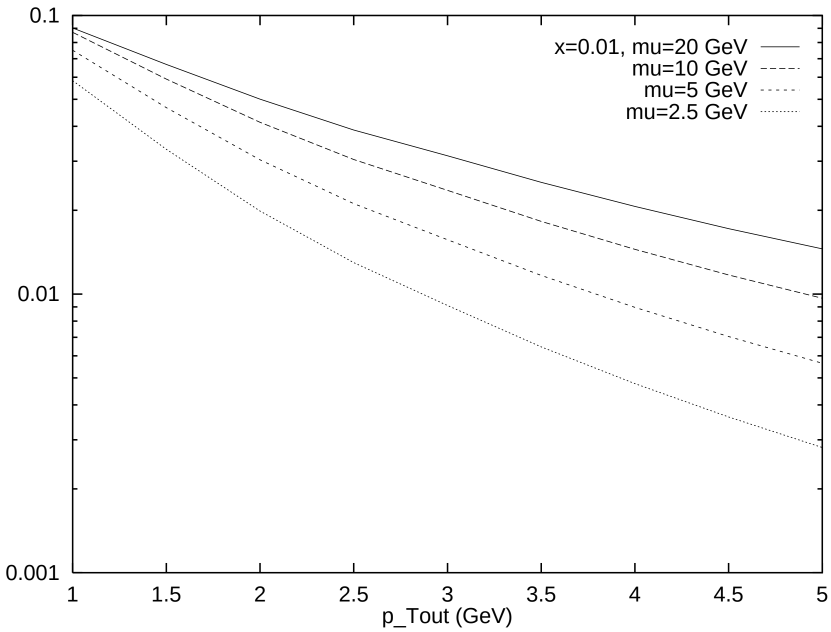

Figure 5.1: The scale dependence of (5.12) for a wide range of values of $\overline{\mu}$. The quantity plotted is an estimate of the differential rate with respect to the out-of-plane momentum p_{Tout}; there is no overall normalisation. $\overline{x} = 0.01$.

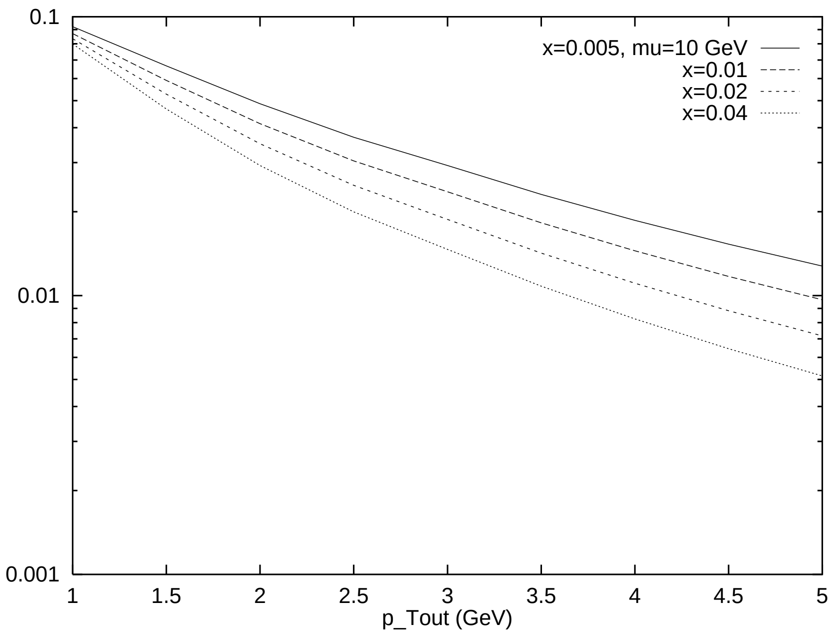

Figure 5.2: Similar to Fig. 5.1, but with a chosen scale $\overline{\mu} = 10$ GeV, showing the $\overline{x}$-dependence of (5.12). Note that x plays a significant role in the kinematics in (5.6) and so this is only a very crude guide to the likely x-dependence of a more complete calculation.

Results are presented in Figs. 5.1 and 5.2 for (5.12), plotting dN/dp_{Tout} for a suitable range of p_{Tout}. k_{tmax} is chosen as 40 GeV; the unintegrated distributions divided by k_t^2 die away rapidly as $k_t \gg \mu$ so the exact limit is unimportant. Fig. 5.1 shows the scale dependence of the result: $\overline{\mu}$ would conventionally be chosen in the range 5–10 GeV (bearing in mind that experimental cuts require $E_{tj} > 5$ GeV and we have estimated a typical invariant mass ~ 12 GeV), but we also show results for the somewhat extreme values $\overline{\mu} = 2.5$ GeV and 20 GeV. $\overline{x} = 0.01$ for this figure. With smaller scales, the spectra fall away more steeply with increasing p_{Tout}, as well as having a lower relative normalisation. The change of shape is not particularly great within the physical region. This scale dependence may be a fair reflection of the likely μ-dependence of a more complete calculation based on (5.6), because the only place the scale appears is as the final argument of the unintegrated parton function. However, the real dependence of x and k_t on the rest of the integrand, including the subprocess cross section and the detailed kinematics, may bias the calculation towards certain regions of the unintegrated parton's parameter space, in which case μ may have more or less impact on the final spectrum.

Fig. 5.2 shows the variation of the computation (5.12) with the choice of $\overline{x}$, for a fixed $\overline{\mu} = 10$ GeV. We expect going from $x = 0.005$ ($\Rightarrow y \sim 0.33$) to $x = 0.04$ ($y \sim 0.04$) to cover the likely important range of x, especially as experimentally a cut like $y > 0.1$ is required. A larger invariant mass can permit larger x values, of course. The variation shown with $\overline{x}$ in Fig. 5.2 is a little less than the variation with $\overline{\mu}$. But here, to be frank, it is difficult to draw conclusions about the likely result of a fuller calculation based on (5.6), because of the complicated kinematic role x has in the calculation, especially in determining the invariant mass for the subprocess, which may correlate x and k_t. A consolation is that the relative variation with $\overline{x}$ is rather small for the low values of p_{Tout}, which is where we anticipate better statistics experimentally, because the cross section is expected to be larger.

In conclusion, it may be worthwhile to reapproach (5.6) in the light of this limited study, and attempt to compute the direct unfragmented cross section again, perhaps imposing some simplifying cuts to concentrate on certain regions of phase space for the integration. We might in particular be interested to compare this approach with a phenomenologically "smeared" approximation, in which $f_q(x, k_t^2, \mu^2)$ is replaced by $xq(x, \mu^2)\, k_t^2 \delta(k_t^2 - \bar{k}^2)$, for choices of $\bar{k}$ such as 2 GeV, or some invented distribution, e.g. a gaussian. In contrast with our work in Chapter 4 for prompt photon hadroproduction, this problem has the merit of only one initial parton function, and therefore the effect of the k_t may be more immediately obvious than in adapting our two-parton luminosity as described in Section 4.7.

The work described in this chapter is only an exploratory study. It will be illuminating to compare refined predictions with experimental distributions for p_{Tout} when they become available.

Chapter 6

Heavy quark production

A topical problem is the cross section for the production of $b\bar{b}$ (a quark-antiquark pair of "bottom" flavour[1]) in experiments at various current colliders. The observed rates for $b\bar{b}$ production significantly exceed theoretical predictions, in a variety of environments, such as proton-antiproton, electron-proton and even electron-electron experiments. Many theorists have performed calculations in LO and NLO QCD [45] and k_t-factorisation frameworks (see the general review in [46]), and the results are generally rather lower than the data[2].

In this chapter we discuss how to make predictions for some $b\bar{b}$ cross sections using unintegrated parton distributions. We restrict ourselves to the case of heavy quark production in electron-proton collisions, which requires only one parton function. In this case, the most important subprocess contributing to the production of a $b\bar{b}$ pair is likely to be $\gamma^* g \to b\bar{b}$, because of the large number of gluons found in the proton at small

[1]Also known as "beauty" by the squeamish.

[2]An exception is [47] which claims good agreement between predictions based on k_t-factorisation and the data for hadroproduction. We feel the use of the KMS gluon in this work may be misleading (there are, for example, no suppression factors incorporated) so further investigation is needed.

Bjorken x. Therefore we shall consider this process, and illustrate how we can compute the cross section $\sigma_{\gamma^* p \to b\bar{b}X}$ using our unintegrated gluon distribution as input.

Experimental data have been taken at HERA in two different situations: $b\bar{b}$ photoproduction [42, 43], in which the virtuality Q^2 of the exchanged photon is very low, and $b\bar{b}$ production in deep inelastic scattering (DIS) [44], where Q^2 is higher (but the statistics are more limited). We start by considering the DIS case, where we can base our calculations on the expressions in Chapter 3 for the proton structure functions F_T and F_L. Then we turn our attention to the $b\bar{b}$ photoproduction cross section, which is related to the work in Chapter 5.

6.1 The production of $b\bar{b}$ pairs in DIS

When Q^2 is large, the total cross section for leptoproduction of a $b\bar{b}$ pair is part of the contribution to the structure functions $F_T(x, Q^2)$ and $F_L(x, Q^2)$ from the "box" and "crossed box" diagrams shown in Fig. 3.1. We ignore more complicated, higher order subprocesses. In Chapter 3 we used expressions for F_T and F_L driven by the unintegrated gluon; see also Section B.3. It is convenient to reuse these forms (valid in the high energy limit) specifically for $b\bar{b}$ production. The fact that our computed values of F_2 using this approach were comparable with DIS data reassures us that the normalisation is correct[3]. The relationship we need is, from (3.1),

$$\frac{d^2\sigma}{dx\, dQ^2}(ep \to b\bar{b}X) = \frac{4\pi\alpha_{em}^2}{Q^4}\left[\frac{(1+(1-y)^2)}{2x}\, F_T^{b\, box}(x, Q^2) + \frac{(1-y)}{x}\, F_L^{b\, box}(x, Q^2)\right]. \tag{6.1}$$

[3] Such an argument only applies when x is small enough that the high energy limit is appropriate, but large enough to avoid a gross extrapolation below the range of current F_2 data. For the experimental DIS $b\bar{b}$ cuts ($2\ \mathrm{GeV}^2 < Q^2 < 100\ \mathrm{GeV}^2$, $0.05 < y < 0.7$) we must be within the region $3 \times 10^{-5} < x < 0.02$, so this seems acceptable.

To be clear, by $F_T^{b\,box}(x,Q^2)$ in (6.1) I mean (3.11) calculated[4] for a given x and Q^2 with just one flavour $q = b$ (no sum). $F_L^{b\,box}(x,Q^2)$ is given in a similar way by (3.12). It follows that the total cross section for production of a $b\bar{b}$ pair can be estimated as

$$\sigma_{b\bar{b}} = \int_{y_{min}}^{y_{max}} dy \int_{\ln Q^2_{min}}^{\ln Q^2_{max}} \frac{Q^2}{sy^2} \frac{d\ln Q^2}{Q^2} 4\pi\alpha_{em}^2 \Big[\quad \Big], \tag{6.2}$$

where the square brackets refer to those in (6.1), $x = Q^2/sy$, and s is provided by HERA ($s \sim (300 \text{ GeV})^2$). Experimental cuts are responsible not just for the limits on y and Q^2, which are trivial to implement, but also restrictions on the momenta of the outgoing b and $\bar{b}$ quarks, in order for events to be identified as $b\bar{b}$ production. This means that in the code for F_T and F_L, the integrals written in terms of κ_t, k_t, β and ϕ must be modified by the insertion of Θ functions in their integrands. It turns out that these cuts are necessarily severe and only a fraction of the cross section is visible.

The quoted (preliminary) cross section in [44] is $(39 \pm 8 \pm 10)$ pb. This is based on a sample of 168 DIS events with two jets, each of which must have a transverse energy > 5 GeV. Moreover, to identify the jet sources as b and $\bar{b}$, a muon is required[5] with transverse momentum > 2 GeV and within a certain rapidity range (polar angle in HERA frame $35^\circ < \theta < 130^\circ$). (A likelihood fit is also performed using the transverse momentum of the muon relative to the jet, which marks it out as originating from the decay of something heavier than a charm (c) quark.) We approach the problem of simulating these cuts in several stages.

First we compute (6.2) as it stands with no cuts other than the experimental limits,

[4] The (probably small) contributions from $k_t < k_0$ can be included in the same way as shown in (3.16). Note that it is *not* appropriate here to perform the angular averaging described for F_2 in Section 3.3, because the $b\bar{b}$ situation is less inclusive, owing to the experimental cuts.

[5] The cross section quoted here includes the branching to the muon.

$0.05 < y < 0.7$ and $2\ \text{GeV}^2 < Q^2 < 100\ \text{GeV}^2$. This provides a total $b\bar{b}$ cross section estimate which the visible cross section cannot exceed. We find $\sigma \sim 473$ pb. About 90% of this comes from the "perturbative" region $k_t > k_0$.

At the parton level we may, to lowest order (and only as a rough approximation) simulate the rather important jet $E_t > 5$ GeV requirements by implementing transverse momentum cuts on the outgoing b quark and antiquark, $p_t > 5$ GeV. In terms of the internal quark momentum κ of the box diagram of Fig. 3.1, the outgoing transverse momenta are $\boldsymbol{\kappa_t}$ and $\boldsymbol{k_t} - \boldsymbol{\kappa_t}$.

An intermediate stage could be to require just one of these to exceed 5 GeV:

$$\text{contributions allowed if } \kappa_t > 5\ \text{GeV}\ \ \textbf{OR}\ \ |\boldsymbol{k_t} - \boldsymbol{\kappa_t}| > 5\ \text{GeV} \Rightarrow \sigma = 261\ \text{pb}.$$

However to be certain of detecting two jets we really need to insist that both the b and $\bar{b}$ have sufficient transverse momentum:

$$\text{contributions only allowed if } \kappa_t > 5\ \text{GeV}\ \ \textbf{AND}\ \ |\boldsymbol{k_t} - \boldsymbol{\kappa_t}| > 5\ \text{GeV} \Rightarrow \sigma = 128\ \text{pb}.$$

(Of that, the perturbative contribution is 112 pb, that is 88%.)

This is still significantly higher than the observed cross section; of course we have yet to account for the semileptonic decay, and the experimental cuts on the muon produced in that decay, which we expect to lead to a further large reduction. However, first we have to investigate the effect of a change of reference frame from the $\gamma^* p$ CM to the laboratory frame for the HERA experiment(s). Because the DIS photon is emitted at an angle relative to the beam axis, transverse momenta with respect to the photon may be changed when measured in the LAB frame: it is important to quantify this.

6.2 Transforming to and from the HERA frame

For our purposes it has been most convenient to work in the CM frame of the virtual photon and proton; but the experimental cuts need to be applied on momenta measured in the LAB frame ("HERA frame"), in which the electron and proton collide head-on, with an initial proton momentum of $|p| = 820$ GeV and an initial electron momentum $|k| = 27.5$ GeV.

The photoproduction case is comparatively straightforward, because the nearly-real photon is emitted along the beam axis. In this case we only need to account for its energy fraction y, and this gives a longitudinal Lorentz boost only.

However in the DIS case, the virtual photon is emitted from the electron at some finite angle. This means that to transform into a frame in which the photon and proton are of equal and opposite momenta, it is necessary to rotate our axes as well as perform a complicated Lorentz boost.

Define angles θ and ϕ representing the direction of the outgoing electron in the HERA frame. The azimuthal angle ϕ is not constrained in terms of the normal DIS variables (for inclusive measurements we are not interested in ϕ). We also define an energy fraction a such that the energy of the outgoing electron, whose momentum is denoted k', is $a|k|$. We can find the values of a and $\cos\theta$ from the definitions of the DIS variables:

$$\begin{aligned} y &= \frac{p \cdot q}{p \cdot k} = \frac{p \cdot (k - k')}{p \cdot k} = 1 - a(1 + \cos\theta)/2 \\ -Q^2 &= (k - k')^2 = -2k \cdot k' = -2|k|^2 a(1 - \cos\theta), \end{aligned}$$

giving

$$\cos\theta = \left(1 - y - \frac{Q^2}{4|k|^2}\right) \Big/ \left(1 - y + \frac{Q^2}{4|k|^2}\right) \tag{6.3}$$

$$a = 1 - y + \frac{Q^2}{4|k|^2}. \tag{6.4}$$

So the 4-momenta of the virtual photon and the proton can be written

$$q_{\mathrm{HERA}} = |k|\left(1-a,\ a\sin\theta\cos\phi,\ a\sin\theta\sin\phi,\ a\cos\theta - 1\right),$$

$$p_{\mathrm{HERA}} = |p|\left(1,\ 0,\ 0,\ 1\right)$$

in the HERA frame. To transform to the $\gamma^* p$ CM frame, we can follow the following steps:

1. Rotate about the z axis through an angle ϕ (note: *not* the same as the ϕ in $F_{T,L}$!),

$$\begin{pmatrix} p_x \\ p_y \\ p_z \end{pmatrix} \rightarrow \begin{pmatrix} p_{x'} \\ p_{y'} \\ p_{z'} \end{pmatrix} = \begin{pmatrix} p_x\cos\phi + p_y\sin\phi \\ -p_x\sin\phi + p_y\cos\phi \\ p_z \end{pmatrix}.$$

   This aligns the axes so that both momenta are in the x'-z' plane, given our definition of ϕ.

2. Rotate about the y' axis through an angle α,

$$\begin{pmatrix} p_{x'} \\ p_{y'} \\ p_{z'} \end{pmatrix} \rightarrow \begin{pmatrix} p_{x''} \\ p_{y''} \\ p_{z''} \end{pmatrix} = \begin{pmatrix} p_{x'}\cos\alpha + p_{z'}\sin\alpha \\ p_{y'} \\ -p_{x'}\sin\alpha + p_{z'}\cos\alpha \end{pmatrix},$$

choosing the angle α, in the range 0 to π, so that the x'' *velocity* components are equal (in direction as well as magnitude). We thus require

$$\frac{(a\sin\theta\cos\alpha + (a\cos\theta - 1)\sin\alpha)}{1-a} = \sin\alpha,$$

giving

$$\begin{aligned}
\cos\alpha &= \frac{2 - a(1+\cos\theta)}{\sqrt{4 + 2a(a-2)(1+\cos\theta)}} \\
\sin\alpha &= \frac{a\sin\theta}{\sqrt{4 + 2a(a-2)(1+\cos\theta)}}.
\end{aligned}$$

After this second rotation, the 4-momenta are

$$p'' = \left(|p|,\ \frac{a|p|\sin\theta}{\sqrt{4 + 2a(a-2)(1+\cos\theta)}},\ 0,\ \frac{|p|\left(2 - a(1+\cos\theta)\right)}{\sqrt{4 + 2a(a-2)(1+\cos\theta)}}\right) \tag{6.5}$$

$$\begin{aligned}
q'' = \Bigg(&(1-a)|k|,\ \frac{a(1-a)|k|\sin\theta}{\sqrt{4 + 2a(a-2)(1+\cos\theta)}},\ 0, \\
&\frac{|k|\left(-2 + a(1+3\cos\theta) - a^2(1+\cos\theta)\right)}{\sqrt{4 + 2a(a-2)(1+\cos\theta)}}\Bigg).
\end{aligned} \tag{6.6}$$

3. Now perform Lorentz boosts to the $\gamma^* p$ CM frame, in which both $\hat{x}$ momenta are 0 and the $\hat{z}$ momenta are equal and opposite. We can define a 3-vector velocity $\boldsymbol{\beta}$ of a new frame $(\hat{t}, \hat{x}, \hat{y}, \hat{z})$ relative to the current frame (written as (t, x, y, z) for clarity); and the relativistic dilation factor $\gamma \equiv 1/\sqrt{1-\beta^2}$ where $\beta^2 \equiv \boldsymbol{\beta}\cdot\boldsymbol{\beta}$. Then a general Lorentz boost into such a new frame can be written

$$\begin{aligned}
\hat{\boldsymbol{p}} &= \boldsymbol{p} + \boldsymbol{\beta}\gamma\left[\frac{\boldsymbol{\beta}\cdot\boldsymbol{p}}{\beta^2}\left(1 - \frac{1}{\gamma}\right) - p_0\right] \\
\hat{p}_0 &= \gamma\left[p_0 - \boldsymbol{\beta}\cdot\boldsymbol{p}\right].
\end{aligned} \tag{6.7}$$

Here the clearest approach is to perform *two consecutive* boosts, first in the x''

direction to make the particles collinear, then in the z'' direction to make their momenta equal in magnitude. The form of (6.7) shows that this is *not* the same as a simultaneous transformation with β_x and β_z.

Therefore step 3 is to boost by $\beta_x = \sin\alpha$, $\beta_y = 0$, $\beta_z = 0$, $\Rightarrow \gamma = \sec\alpha$, viz.

$$\begin{pmatrix} E'' \\ p_{x''} \\ p_{y''} \\ p_{z''} \end{pmatrix} \to \begin{pmatrix} E''' \\ p_{x'''} \\ p_{y'''} \\ p_{z'''} \end{pmatrix} = \begin{pmatrix} (E'' - p_{x''}\sin\alpha)/\cos\alpha \\ (p_{x''} - E''\sin\alpha)/\cos\alpha \\ p_{y''} \\ p_{z''} \end{pmatrix}.$$

After this the momenta of the proton and photon are

$$p''' = \frac{|p|\,(2 - a(1+\cos\theta))}{\sqrt{4 + 2a(a-2)(1+\cos\theta)}}\,(1,\ 0,\ 0,\ 1) \tag{6.8}$$

$$q''' = \frac{|k|}{\sqrt{4 + 2a(a-2)(1+\cos\theta)}}\left(\frac{(1-a)\,(4 - 4a(1+\cos\theta) + a^2(1+\cos\theta)^2)}{2 - a(1+\cos\theta)},\right.$$
$$\left. 0,\ 0,\ \left(-2 + a(1+3\cos\theta) - a^2(1+\cos\theta)\right)\right). \tag{6.9}$$

A useful check at this point is to go to the case of photoproduction. In this situation the first three steps collapse to identity transformations, because the photon and proton are already collinear. If we take the $Q^2 \to 0$ limit, then $\theta \to 0$ and $a \to 1 - y$, simplifying the expressions so that $p''' = p'' = |p|(1,0,0,1)$ and $q''' = q'' = |k|(y,0,0,-y)$.

4. Finally we boost along z''' to get to the CM frame. The z'''-velocity $\hat{\beta}$ of the centre of momentum of the two particles is $(p_{z'''} + q_{z'''})/(E'''_p + E'''_q)$. Thus $\hat{\beta} =$

$$\frac{|p|\,(2 - a(1+\cos\theta))^2 + |k|\,(2 - a(1+\cos\theta))\,(-2 + a(1+3\cos\theta) - a^2(1+\cos\theta))}{|p|\,(2 - a(1+\cos\theta))^2 + |k|\,(1-a)\,(4 - 4a(1+\cos\theta) + a^2(1+\cos\theta)^2)}, \tag{6.10}$$

which reduces to $(|p| - |k|y)/(|p| + |k|y)$ for photoproduction. We compute (6.10) numerically (and the associated $\hat{\gamma}$) to perform the final Lorentz boost.

The procedure to transform our outgoing particles from the $\gamma^* p$ CM frame to the HERA frame, in which the experimental cuts are applied, is the reverse of the procedure detailed, with the same values for $\hat{\beta}$, β_x, and α, but the boosts and rotations apply in the opposite directions, and the transformations are taken in the opposite order. In fact the H1 and ZEUS detectors are approximately cylindrically symmetric, so the angle ϕ is of little significance, as the cuts do not depend on it. Therefore, for the DIS kinematics, we perform the reverse of steps 4, 3 and then 2:

$$\begin{pmatrix} E \\ p_x \\ p_y \\ p_z \end{pmatrix}_{\text{HERA}} = \begin{pmatrix} 1 & 0 & 0 & 0 \\ 0 & \cos\alpha & 0 & -\sin\alpha \\ 0 & 0 & 1 & 0 \\ 0 & \sin\alpha & 0 & \cos\alpha \end{pmatrix} \begin{pmatrix} \sec\alpha & \tan\alpha & 0 & 0 \\ \tan\alpha & \sec\alpha & 0 & 0 \\ 0 & 0 & 1 & 0 \\ 0 & 0 & 0 & 1 \end{pmatrix} \times \begin{pmatrix} \hat{\gamma} & 0 & 0 & \hat{\beta}\hat{\gamma} \\ 0 & 1 & 0 & 0 \\ 0 & 0 & 1 & 0 \\ \hat{\beta}\hat{\gamma} & 0 & 0 & \hat{\gamma} \end{pmatrix} \begin{pmatrix} E \\ p_x \\ p_y \\ p_z \end{pmatrix}_{\gamma^* p\ \text{CM}}.$$

Now the outgoing 4-momenta of the b and $\bar{b}$ are $\kappa + q$ and $k - \kappa$ (see (3.2) and Section B.2). In terms of the integration variables κ_t and (Sudakov) β, the $\gamma^* p$ CM 4-momenta decompose as

$$\begin{aligned} p_1 \equiv \kappa + q &= \frac{x(\kappa_t^2 + m^2)}{(1-\beta)Q^2}\, p + (1-\beta) q' + \boldsymbol{\kappa_t} \\ p_2 \equiv k - \kappa &= \left(\frac{x}{z} - \frac{x(\kappa_t^2 + m^2)}{(1-\beta)Q^2} - x \right) p + \beta q' + \boldsymbol{k_t} - \boldsymbol{\kappa_t}. \end{aligned}$$

We take these momenta and numerically perform the transform to yield new vectors for the HERA frame, and then the requirement $p_{1\perp} > 5$ GeV **AND** $p_{2\perp} > 5$ GeV is imposed. For the perturbative contribution, we find a cross section 110 pb. Comparing this with the untransformed computation where the restrictions were applied directly to κ_t and $|\boldsymbol{k_t} - \boldsymbol{\kappa_t}|$, which gave a perturbative contribution of 112 pb, we are encouraged that for the typical values of Q^2 and y in this analysis, the effect of the Lorentz transform on the transverse momenta is fairly minor. Presumably the actual angles and boost velocities involved are modest.

6.3 The role of the gluon jet

An interesting concern that became apparent during our study of $b\bar{b}$ production can be summed up in the question, *What happens to the gluon radiated "in the last step of the evolution"?* Such a gluon is intrinsic to our approach, using unintegrated partons as described in Chapter 2. Even if unintegrated parton distributions are produced in other ways, there remains the possibility of radiation with significant transverse momentum; this is not a feature of collinear factorisation unless it is explicitly added in the factorised subprocess (with, e.g., matrix elements for $q\bar{q}g$ production), or alternatively if a Monte Carlo simulation is used to generate a cascade of initial state radiation.

For the description of inclusive processes, the radiated gluon is not very important. However, in the context of $b\bar{b}$ production, we have to consider the possibility that the last-step gluon, generated in our formalism with transverse momentum $-\boldsymbol{k_t}$, produces a jet that is captured in the detector. In this case, one of the two jets required by the cuts may not originate from a b or $\bar{b}$ quark at all!

This immediately suggests a new form of cut that we can apply to our crude estimate of the $b\bar{b}$ cross section. Back in the $\gamma^* p$ CM frame, we may impose a requirement somewhat intermediate between our previous "AND" and "OR" cuts, to imitate at least two jets with transverse energy exceeding 5 GeV, out of a possible *three* jets:

$$\text{contributions allowed if (at least) } \mathbf{TWO} \text{ of } \{\kappa_t, |\boldsymbol{k_t} - \boldsymbol{\kappa_t}|, k_t\} > 5 \text{ GeV} \Rightarrow \sigma = 187 \text{ pb.}$$

In this calculation we found that 70% of that cross section corresponded to situations where $\kappa_t > k_t$, which one might describe as normal, and 30% came from $\kappa_t < k_t$. If we repeat the calculation for $c\bar{c}$ pairs, the total charm cross section with the same cut is 2.26 nb, of which 46% has the abnormal ordering $\kappa_t < k_t$. The ramifications are potentially serious since the experimentalists use the muon relative transverse momentum to select supposed $b\bar{b}$ events from amongst the large background of $c\bar{c}$ production. A significant proportion of "abnormal" configurations introduces the possibility that a muon, emitted with a small transverse momentum relative to a decaying c quark, will be misidentified as originating from the gluon jet and hence with possibly a rather larger relative transverse momentum. In other words, gluon jets in some $c\bar{c}$ events may be classed as b jets, thus artificially boosting the measured $b\bar{b}$ cross section above theoretical expectations. This possibility is currently being investigated in the experimental analysis, which uses various Monte Carlo programs to simulate initial state radiation.

Note that our approach is limited in one respect: although our last-step formalism generates a radiated gluon with transverse momentum $-\boldsymbol{k_t}$ for free, along with the unintegrated parton, we have no information about the longitudinal momentum of this gluon. This means that it is not possible to see the effect of transforming this third jet particle into the HERA frame, whilst retaining the factorised form with our unintegrated parton. Of course we could "undo" the last step of the evolution, looking at the z integration of the final splitting in the ladder, and impose a detailed cut including this z. However in that case our approach reduces to a collinear factorisation calculation with a rather approximate matrix element. The Monte Carlo cascades do not suffer from this problem, because they simulate all the particles produced and the momenta are available for further manipulation. Nevertheless, the indications from this study are that the frame transformation has little effect, so we perhaps achieve an approximate description by allowing a gluon jet with transverse momentum $-\boldsymbol{k_t}$.

6.4 Implementing the semileptonic decay

The HERA experiments classify $b\bar{b}$ events by detecting a muon from the decay of the b or $\bar{b}$. This has two ramifications for our computations. Firstly, we need to include a branching ratio for the decay; only about 10% of b quarks produced will generate a muon (thus 19% of the $b\bar{b}$ pairs will produce muons). Roughly, we can compensate for this by dividing our $b\bar{b}$ cross sections by a factor like 5. Thus 128 pb corresponds to a predicted visible cross section of 26 pb, or 187 pb (including the gluon jet and cutting on two out of a possible three jets) corresponds to a predicted visible 37 pb. These numbers are now much more like the experimental value of 39 pb.

However, the second feature is that some fraction of the semileptonic decays will fail the cuts imposed on the muon, depending on the momenta of the b or $\bar{b}$, and also depending on the random direction and magnitude of the muon momentum from the three-body decay. The experimental requirements are that the muon has a transverse momentum more than 2 GeV, and a HERA polar angle between 35° and 130°. In addition to this the transverse momentum of the muon *relative to the jet* is used in a likelihood fit, to reduce contamination from $c\bar{c}$ events. Simulation of these cuts will necessarily lower our cross section prediction, but the question is, by how much? Unfortunately, implementing the muon decay (with a known momentum spectrum[6] and uniformly distributed in direction in the decaying particle's rest frame) in the integrand of `vegas` makes it rather harder to find non-zero contributions, and this work is still in progress. It is possible that our comparison will not be significantly different from the existing NLO QCD predictions, which undershoot the data substantially [44].

6.5 $b\bar{b}$ photoproduction

For the case of $b\bar{b}$ photoproduction, it is possible to compute similar cross sections in terms of $F_{T,L}$ as we have done for DIS. We may replace (6.2) by

$$\sigma_{b\bar{b}} = \int_{y_{min}}^{y_{max}} dy \, \ln\left(\frac{Q^2_{max}}{y^2 m_e^2}\right) \frac{4\pi\alpha_{em}^2}{sy^2} \Big[\quad \Big]_{\langle Q^2 \rangle}, \tag{6.11}$$

where the logarithm containing Q^2_{max} and m_e^2 is like a crude Weizsäcker-Williams distribution, and we compute the expressions[7] for F_T and F_L inside the square brackets using the median value for Q^2, which is 10^{-3} GeV^2. It is not clear to what extent we can trust the structure function expressions for very low values of x and Q^2, but it is convenient to try to adapt the previous work in this way.

Various related cross sections are quoted in the ZEUS and H1 papers for $b\bar{b}$ photoproduction [42, 43]. The basic results are similar in form to the visible ep cross section quoted in the DIS case in [44], that is $\sigma_{vis}(ep \to b\bar{b}X \to \mu X)$. The H1 result for pho-

[6] I am grateful to Felix Sefkow for providing code which approximates the measured muon momentum spectrum.

[7] Note that a fixed arbitrary upper limit of 50 GeV is imposed on the k_t and κ_t integrations.

toproduction, with $0.1 < y < 0.8$, is $\sigma_{vis} = (170 \pm 25)$ pb. (Such a cross section can then be extrapolated using Monte Carlo models to give predicted total cross sections for $\sigma(ep \to b\bar{b}X)$, but the extrapolation is somewhat model dependent, and not necessarily easier to compare with theoretical predictions.) The most similar quantity quoted by ZEUS in [42] is $(24.9 \pm 6.4\ ^{+4.2}_{-7.3})$ pb. However, this is for $0.2 < y < 0.8$, with electrons rather than muons being used to identify the b decays, and in addition slightly more severe cuts on the jets.

Using (6.11), and cutting on the b and $\bar{b}$ transverse momenta, we compute some estimates in the same spirit as before:

$$\begin{aligned}
\text{total with no transverse momentum cuts} &\Rightarrow \sigma = 2.4 \text{ nb;}\\
\text{contributions only allowed if } \kappa_t > 5 \text{ GeV } \textbf{AND } |\boldsymbol{k_t} - \boldsymbol{\kappa_t}| > 5 \text{ GeV} &\Rightarrow \sigma = 604 \text{ pb;}\\
\text{contributions allowed if (at least) } \textbf{TWO} \text{ of } \{\kappa_t, |\boldsymbol{k_t} - \boldsymbol{\kappa_t}|, k_t\} > 5 \text{ GeV} &\Rightarrow \sigma = 930 \text{ pb.}
\end{aligned}$$

These results are for $0.1 < y < 0.8$; if we restrict to $0.2 < y < 0.8$ the relevant numbers are 1.7 nb, 444 pb and 697 pb respectively. The indications are that including the branching ratio to produce a muon (and the cuts on the muon) would bring these predicted cross sections down to significantly below the measured results, as is the situation for existing NLO QCD calculations [42, 43].

6.6 Another approach to $b\bar{b}$ photoproduction

Rather than adapting the $F_{T,L}$ computation, it is of interest to consider recomputing the photoproduction cross section from first principles, using the same strategy as in Chapter 5.

We wish to calculate the cross section for $\gamma p \to b\bar{b}X$ as

$$\sigma_{\gamma p \to b\bar{b}X} = \int f_g\left(\frac{x}{z}, k_t^2, \mu^2\right) \frac{d\hat{\sigma}}{d|\hat{t}|}\, d|\hat{t}|\, \frac{d^2k_t}{\pi k_t^2}\, \frac{dz}{z}. \tag{6.12}$$

In this expression x is fixed (as Q^2/sy; s is supplied by HERA). The scale μ is representative of the subprocess. We then obtain $\sigma_{ep \to b\bar{b}X}$ as $\int f_\gamma^{(e)}(y)\, \sigma_{\gamma p \to b\bar{b}X}\, dy$. The $2 \to 2$ cross section for $\gamma g \to b\bar{b}$ is derived in Section B.2.

Let us examine the kinematics afresh, in the centre of mass frame of the photon-proton system. We assume the mass of the proton is negligible and so it is described by a lightlike vector $p^\mu = (\mathcal{P}, 0, 0, \mathcal{P})$. The photon's 4-vector is $q^\mu = (\sqrt{\mathcal{P}^2 - Q^2}, 0, 0, -\mathcal{P})$ in this frame; we can construct another lightlike vector $q'^\mu \equiv q^\mu + xp^\mu$, where the variable x is exactly Bjorken $x = Q^2/2p \cdot q$.

In terms of these lightlike vectors we can describe the outgoing and incoming particles with Sudakov variables:

$$\begin{aligned}
p_1^\mu &= \alpha_1 p^\mu + \beta_1 q'^\mu + p_{1\perp} \\
p_2^\mu &= \alpha_2 p^\mu + \beta_2 q'^\mu + p_{2\perp} \\
q^\mu &= -xp^\mu + q'^\mu \\
k^\mu &= \frac{x}{z} p^\mu - bq'^\mu + k_t.
\end{aligned} \tag{6.13}$$

We have defined a splitting fraction z in such a way that the plus momentum fraction of the proton p held by the gluon, k^+/p^+, is x/z. We will then be able to perform calculations driven by the unintegrated gluon distribution corresponding to these kinematics, $f_g(x/z, k_t^2, \mu^2)$.

Notice that we can relate the momentum $\mathcal{P}$ to the invariants Q^2 and x, using the definition of the invariant mass squared of the photon and the proton, $s_{\gamma p}$:

$$s_{\gamma p} = (q^\mu + p^\mu)^2 = Q^2\left(\frac{1}{x} - 1\right) = 2\mathcal{P}^2 - Q^2 + 2\mathcal{P}\sqrt{\mathcal{P}^2 - Q^2} \quad \Rightarrow \mathcal{P} = \frac{Q/2}{\sqrt{x(1-x)}}. \tag{6.14}$$

The typical x values, $x = Q^2/(s_{\gamma p} + Q^2) \simeq Q^2/(y s_{\mathrm{HERA}})$, probed in photoproduction are small, such as 10^{-8}. Nevertheless, small z values tend to compensate these so that x/z is reasonable.

What are the constraints on the Sudakov parameters? Conservation of momentum gives

$$\begin{aligned} \alpha_1 + \alpha_2 &= x\left(\frac{1}{z} - 1\right) && (6.15)\\ \beta_1 + \beta_2 &= 1 - b && (6.16)\\ \boldsymbol{p_{1\perp}} + \boldsymbol{p_{2\perp}} &= \boldsymbol{k_t}; && (6.17) \end{aligned}$$

we can interpret (6.15) as the defining constraint on z. The outgoing quark and antiquark, with transverse momenta $\boldsymbol{p_{1\perp}}$ and $\boldsymbol{p_{2\perp}}$, are real particles with mass m (m_b), so

$$\begin{aligned} p_1^2 &= \alpha_1\beta_1\frac{Q^2}{x} - p_{1\perp}^2 = m^2 && (6.18)\\ p_2^2 &= \alpha_2\beta_2\frac{Q^2}{x} - p_{2\perp}^2 = m^2 && (6.19) \end{aligned}$$

which fixes α_1 and α_2 in terms of the other variables. Combining (6.15), (6.18) and (6.19) gives

$$\frac{1}{z} = 1 + \frac{p_{1\perp}^2 + m^2}{\beta_1 Q^2} + \frac{p_{2\perp}^2 + m^2}{\beta_2 Q^2}, \tag{6.20}$$

which is a similar constraint to (3.10), but now written in the external momenta only.

As before, we choose $b = 0$; this gives a simple connection between β_1 and β_2. Working with k_t as the transverse momentum of the incoming gluon, we introduce an angle ϕ_{gb} (from d^2k_t in (6.12)) and retain $p_{1\perp}$ and β_1, using (6.16) and (6.17) to write $\beta_2 = 1 - \beta_1$ and $p_{2\perp}^2 = k_t^2 + p_{1\perp}^2 - 2k_t p_{1\perp}\cos\phi_{gb}$. To perform the integration over β_1 and $p_{1\perp}$, we use

$$\begin{aligned}
|\hat{t}| &= Q^2(1-\beta_1) + \frac{p_{1\perp}^2 + m^2}{\beta_1} - m^2 && (6.21)\\
\frac{1}{z} &= 1 + \frac{p_{1\perp}^2 + m^2}{\beta_1 Q^2} + \frac{k_t^2 + p_{1\perp}^2 - 2k_t p_{1\perp}\cos\phi_{gb} + m^2}{(1-\beta_1)Q^2} && (6.22)
\end{aligned}$$

(see Section B.2), and obtain the Jacobian for $d|\hat{t}|\,dz \to \mathcal{J}\,d\beta_1\,dp_{1\perp}^2$ as

$$\begin{aligned}
\mathcal{J} &= z^2\left\{\frac{1}{\beta_1} + \frac{1 - \dfrac{k_t}{p_{1\perp}}\cos\phi_{gb}}{1-\beta_1}\right.\\
&\quad\left. + \frac{\left(1 - \dfrac{k_t}{p_{1\perp}}\cos\phi_{gb}\right)(p_{1\perp}^2 + m^2)}{\beta_1^2(1-\beta_1)Q^2} + \frac{k_t^2 + p_{1\perp}^2 - 2k_t p_{1\perp}\cos\phi_{gb} + m^2}{\beta_1(1-\beta_1)^2 Q^2}\right\}. && (6.23)
\end{aligned}$$

Here, and in the expression (B.33) for $d\hat{\sigma}/d|\hat{t}|$, the value of z is computed from (6.22).

Therefore we rewrite (6.12) as

$$\sigma_{\gamma p} = \int f_g\left(\frac{x}{z}, k_t^2, \mu^2\right)\frac{d\hat{\sigma}}{d|\hat{t}|}\,\frac{\mathcal{J}}{z}\,d\beta_1\,dp_{1\perp}^2\,\frac{d\phi_{gb}}{2\pi}\,\frac{dk_t^2}{k_t^2}. \qquad (6.24)$$

We compute this, choosing $\mu^2 = p_{1\perp}^2 + m^2$, and convolute with the Weizsäcker-Williams function to obtain an estimate of the ep cross section. (The range $0.1 < y < 0.8$ is taken, as in the H1 experiment.) We have only implemented the cuts $p_{1\perp} > 5$ GeV, $p_{2\perp} > 5$ GeV. Our result is 610 pb, which compares well with our previous result of

604 pb via (6.11). However, there may be some dependence on the choice of scale μ, both in this calculation and in the previous ones based on $F_{T,L}$.

6.7 The Sudakov parameter b

Sometimes b is approximated to 0. Note, however, that in principle there are separate roles for the incoming transverse momentum, k_t, and the typical scale of the subprocess, μ, which we set to, for example, $\mu = c\sqrt{p_{1\perp}^2 + m^2}$ where c is an arbitrary constant. Keeping transverse momentum and virtuality distinct, let the gluon have spacelike virtuality $-\mu^2$. Then, from (6.13),

$$k^2 = \frac{-bQ^2}{z} - k_t^2 = -\mu^2, \tag{6.25}$$

then this determines $b = (\mu^2 - k_t^2)z/Q^2$, which is non-zero unless $k_t = \mu$. This of course gives a different relationship for β_2 in terms of β_1, via (6.16), than the previous $\beta_2 = 1 - \beta_1$.

Consider the ranges of the parameters. Our use of z as a splitting fraction necessitates $z > x$. From (6.18) we see that α_1 and β_1 must have the same sign, as $\alpha_1\beta_1 > 0$; and to obtain a positive energy for the b quark we must therefore have $\alpha_1 > 0$ and $\beta_1 > 0$; similarly we can show $\alpha_2 > 0$ and $\beta_2 > 0$. This means that $z < 1$, which is suitable for a splitting fraction. From (6.15) it follows that $\alpha_1 < 1$ and $\alpha_2 < 1$, and from (6.16) we see $b < 1$.

We need a lower limit on b too. From the requirement that the partons radiated in the evolution (the "rungs" of the ladder) are timelike (invariant mass squared $m^2 \geq 0$) it can be shown that $b \geq 0$. (This means that the new constraint (6.25) prevents the region $k_t > \mu$ from contributing[8]. The consequences of this have not been investigated.) It follows that $\beta_1 \leq 1$, $\beta_2 \leq 1$.

The connection between β_1 and β_2 is complicated: we need to combine the relation from (6.25)

$$\beta_1 + \beta_2 - 1 = \frac{z\,(k_t^2 - \mu^2)}{Q^2}$$

with (6.20), giving

$$(\beta_1 + \beta_2 - 1)\left(Q^2 + \frac{m_{t1}^2}{\beta_1} + \frac{m_{t2}^2}{\beta_2}\right) = k_t^2 - \mu^2, \tag{6.26}$$

where I write $m_{t1}^2 \equiv p_{1\perp}^2 + m^2$, $m_{t2}^2 \equiv p_{2\perp}^2 + m^2$.

Equation (6.26) is quadratic, specifying β_2 in terms of β_1 and the other variables:

$$\begin{aligned} \beta_2^2\left(\beta_1 Q^2 + m_{t1}^2\right) &+ \beta_2\left(\beta_1(\beta_1 - 1)Q^2 + (\beta_1 - 1)m_{t1}^2 + \beta_1\left(m_{t2}^2 + \mu^2 - k_t^2\right)\right) \\ &+ \beta_1(\beta_1 - 1)m_{t2}^2 = 0. \end{aligned} \tag{6.27}$$

So in terms of the coefficients q_a, q_b, q_c,

$$\begin{aligned} q_a &\equiv \beta_1 Q^2 + m_{t1}^2, \\ q_b &\equiv \beta_1(\beta_1 - 1)Q^2 + (\beta_1 - 1)m_{t1}^2 + \beta_1\left(m_{t2}^2 + \mu^2 - k_t^2\right), \quad \text{and} \\ q_c &\equiv \beta_1(\beta_1 - 1)m_{t2}^2, \end{aligned}$$

[8]However, note that the scale μ does not have to be chosen as the virtuality, so this need not be a fixed limit.

we could potentially have two β_2 solutions for given β_1,

$$\beta_2 = \frac{-q_b \pm \sqrt{q_b^2 - 4q_a q_c}}{2q_a}. \tag{6.28}$$

However, $q_c < 0$ implies that only one of the two possible solutions in (6.28) is positive, and this is the physical value of β_2 corresponding to a given β_1.

It would be possible to use the new relationship between β_1 and β_2, in the case $b \neq 0$ discussed in this section, to make more predictions for cross sections, in which the virtuality of the incoming parton is not restricted to $-k_t^2$, and to compare the results with those calculated in the $b = 0$ approximation. However, in investigating higher order effects, there are a great number of separate concerns to be resolved, and this is probably not the most important approximation to improve upon.

6.8 Final points

In this chapter we have illustrated our efforts to make predictions, using the unintegrated gluon from the last-step prescription based on DGLAP evolution, for various observed $b\bar{b}$ cross sections. Implementation of the appropriate experimental cuts is particularly demanding, and the work is incomplete. Our approach, based at the parton level, would have to be incorporated in a hadronisation Monte Carlo simulation before definite conclusions could be drawn. (Differences between different simulations' predictions for the extrapolation between parton and hadron level are responsible for a significant part of the errors quoted on the experimental measurements.) There are as yet no indications that using unintegrated partons would generate a significantly higher prediction than existing NLO QCD calculations.

Nevertheless, this type of calculation is viable within the unintegrated parton approach. It is attractive to include incoming transverse momentum, and although this complicates the kinematics, the framework can be used for all[9] values of x. Our studies (Section 6.3) have prompted a question as to possible misidentification of c decays in the present experimental analyses when a gluon jet is present, which is an important detail to be investigated. We have discussed this with the experimentalists and they are also studying this problem.

We stress one important point about the two scales k_t and μ in the unintegrated parton distributions: even though in practice the region $k_t \gg \mu$ does not play a significant role in typical calculations, such as those in this and the previous chapter, we nevertheless should include $k_t > \mu$, in other words the region where k_t is of the order of up to a few times μ. In computations using unintegrated parton functions where $f(x, k_t^2, \mu^2)$ is artificially forced to zero at $k_t \geq \mu$, this is a potential source of large scale dependence on μ, because the kinematics of the process become overconstrained by the choice of factorisation scale.

[9]Results in the literature are commonly derived in the small x approximation, but there need be no dichotomy between small- and large-x work.

Chapter 7

Shadowing effects at very low x

In this chapter we discuss briefly the likely nature of shadowing corrections to parton distributions at very small values of x, following closely our work in [3].

As expected in both the DGLAP and BFKL evolution frameworks, it is well verified experimentally that parton distributions $a(x, Q^2)$, particularly the gluon, increase rapidly as x decreases. However it has long been anticipated [48, 49] that linear evolution equations must eventually break down at some sufficiently small value of x. The critical region for a given Q^2 is when [50]

$$\frac{a(x, Q^2)}{Q^2} \sim \pi R^2,$$

that is when the number of partons per unit rapidity, multiplied by the typical transverse area occupied by one parton, is of order of the transverse area available to be populated within the hadron. The radius R should not exceed that of the hadron, although it is possible that it could be smaller (with the low-x partons concentrated in one or more "hot-spots"). For such a region of small x, non-linear screening corrections could be expected to modify the evolution equations and halt the growth, leading to saturation of the parton distribution functions. This is called shadowing, and has not yet been experimentally observed. We note that at lower values of Q^2, saturation effects are likely to become significant for larger, that is, less tiny values of x.

At such small x, the natural quantity is the single-scale unintegrated gluon distribution $h_g(x, k^2)$, and quarks are irrelevant, provided in both cases that we are interested in the leading behaviour only. For this chapter we shall therefore work with the KMS "unified" BFKL-DGLAP gluon [19], which for convenience we write as $f(x, k^2)$ as in [19] and [3]. We also write the same function as $f(Y, k^2)$ where $Y \equiv \ln 1/x$ is closely related to the gluon rapidity (a parton 4-vector like (A.13) has rapidity η such that $\delta\eta = -\delta Y$, if the other variables remain constant). From the unintegrated gluon one may of course obtain an integrated distribution

$$xg(x, Q^2) = xg(x, k_0^2) + \int_{k_0^2}^{Q^2} \frac{dk^2}{k^2} f(x, k^2); \tag{7.1}$$

from the fit of [19, 20] the starting non-perturbative distribution was determined to be the surprisingly flat $xg(x, k_0^2 = 1 \text{ GeV}^2) = 1.57(1-x)^{2.5}$.

The original Gribov-Levin-Ryskin (GLR) work [48] found a shadowing contribution to $f(Y, k^2)$ of the form

$$\frac{\partial f_{shad}(Y, k^2)}{\partial Y} = -\frac{\alpha_s^2}{R^2 k^2} \left[xg(x, k^2) \right]^2. \tag{7.2}$$

Insight may be gained into the origin of (7.2) by considering the probability of gluon recombination [51]. The gluon-gluon cross section is $\sim \pi\alpha_s^2/k^2$, which we must divide by the transverse area πR^2 to get a pure probability, and then multiply by the square

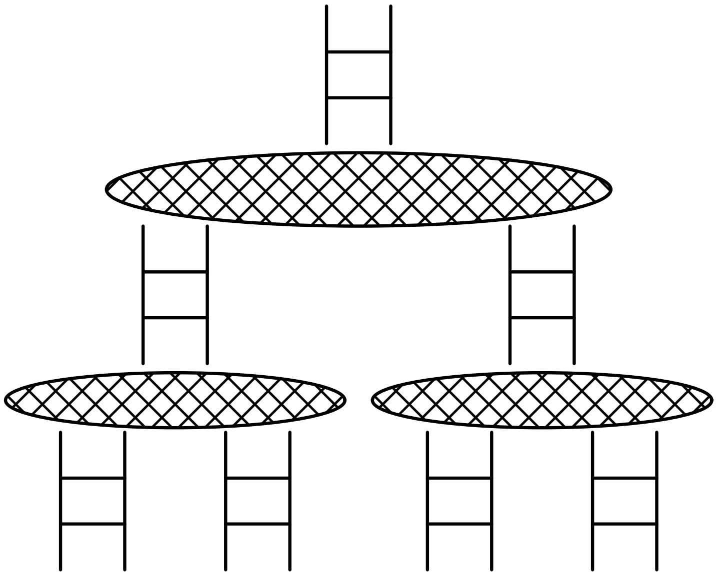

Figure 7.1: A possible pomeron fan diagram. At the top will be a hard interaction, for example with a colour dipole.

of the gluon number density (per unit rapidity) $xg(x, k^2)$. Then a quadratic term in xg seems physically plausible. So we combine this shadowing term with DGLAP evolution in the double leading log approximation (DLLA) to obtain the GLR equation for the integrated gluon at scale k^2

$$\frac{\partial xg(x,k^2)}{\partial Y\, \partial \ln(k^2/\Lambda^2)} = \frac{N_C\, \alpha_s}{\pi}\, xg(x,k^2) - \frac{\alpha_s^2}{R^2 k^2}\, \left[xg(x,k^2)\right]^2 . \tag{7.3}$$

Effectively the GLR equation resums the "fan" diagrams generated by the branching of QCD pomerons, which correspond in the GLR approach to gluonic ladders in the DLLA to DGLAP evolution. See Fig. 7.1. The pomeron is an important concept for small-x physics, and is the subject of the book [29]. It is not a particle in the same way that a quark or gluon is, but a particular type of collective behaviour, described in Regge theory as a reggeon: a superposition of possible exchanges of gluons (gluons according to QCD). In particular the pomeron corresponds to an exchange with total cross section (in the high energy limit $s \gg |t|$) $\sigma_{tot} \sim s^{(\alpha_P(0)-1)}$ which grows slowly with s, thus with "intercept" $\alpha_P > 1$, and with vacuum quantum numbers only. The most economical approximation we can make to the QCD pomeron is a ladder of two interacting gluons, and Fig. 7.1 shows separate ladders merging.

In the GLR approach, the triple-pomeron vertex, which couples the ladders and governs the recombination, is computed in the leading $\ln k^2$ approximation. The GLR equation has stimulated an enormous literature [52]–[70] connected with shadowing effects in deep inelastic and related hard scattering processes. One of the important results to emerge from these studies is the computation of the triple-pomeron vertex beyond leading $\ln k^2$, but staying within the more appropriate leading $\ln 1/x$ approximation.

Here, following [3], we use this improved knowledge of the triple-pomeron vertex to perform a quantitative estimate of the gluon shadowing effects which can be probed in the low x domain accessible at the LHC.

7.1 Triple-pomeron vertex

The colour dipole model has provided a phenomenologically successful [69] formulation for treating saturation in DIS. The physical picture is of the virtual photon fluctuating into a $q\bar{q}$ dipole, and this dipole interacts with the proton [50]:

$$\sigma_{\gamma^* p}(x, Q^2) \sim \int dz\, dr^2\, |\psi(r, Q, z)|^2\, \sigma_{q\bar{q}}(r, x), \tag{7.4}$$

where ψ denotes the wavefunction of the virtual photon, r is the transverse size of the dipole and z is the momentum fraction of the photon carried by the quark. Effectively we have partly transformed into the coordinate representation: transverse momentum has been replaced by transverse separation.

The structure of the triple-pomeron vertex can be extracted from an equation, formulated by Kovchegov [66], for the quantity $N(\boldsymbol{r},\boldsymbol{b},Y)$. N is closely related to the dipole cross section $\sigma(r,Y)$ describing the interaction of the $q\bar{q}$ dipole with the proton target. To be precise

$$\sigma(r,Y) = 2\int d^2b\, N(\boldsymbol{r},\boldsymbol{b},Y), \tag{7.5}$$

where b is the impact parameter for the interaction. This dipole cross section is given in terms of the unintegrated gluon distribution by [60]

$$\sigma(r,Y) = \frac{8\alpha_s\pi^2}{N_c}\int\frac{dk}{k^3}\,[1-J_0(kr)]\; f(Y,k^2). \tag{7.6}$$

In the large N_c limit, the function N satisfies the integral equation [67]

$$\begin{aligned} N(\boldsymbol{r}_{01},\boldsymbol{b},Y) &= N_0(\boldsymbol{r}_{01},\boldsymbol{b},Y) + \frac{\alpha_s N_c}{2\pi}\int_0^Y dy\left\{-2\ln\frac{r_{01}^2}{\rho^2}\,N(\boldsymbol{r}_{01},\boldsymbol{b},y) + \right. \qquad (7.7)\\ &\left.\int_\rho\frac{d^2r_2}{\pi}\frac{r_{01}^2}{r_{02}^2r_{12}^2}\left[2N\left(\boldsymbol{r}_{02},\boldsymbol{b}+\tfrac{1}{2}\boldsymbol{r}_{12},y\right) - N\left(\boldsymbol{r}_{02},\boldsymbol{b}+\tfrac{1}{2}\boldsymbol{r}_{12},y\right)\,N\left(\boldsymbol{r}_{12},\boldsymbol{b}-\tfrac{1}{2}\boldsymbol{r}_{20},y\right)\right]\right\}, \end{aligned}$$

which is the unfolded version of eqn. (15) of [66][1]. The linear part of this equation corresponds to the BFKL equation in dipole transverse coordinate space. The term containing the log denotes the virtual correction responsible for the reggeisation of the gluon, while the linear term under the dr_2 integral corresponds to real gluon emission. ρ is the ultraviolet cut-off parameter. The subscripts 01, 02 and 12 enumerate scattering off $q\bar{q}$, qg and $\bar{q}g$ systems respectively. The equation resums fan diagrams through the quadratic shadowing term.

[1]An equation similar to (7.7) can be found in [63].

If we rewrite (7.7) in terms of the transformed function

$$\tilde{N}(\ell, b, Y) = \int_0^\infty \frac{dr}{r}\, J_0(\ell r)\, N(r, b, Y), \tag{7.8}$$

then the shadowing term has a much simpler form: we have

$$\tilde{N}(\ell, b, Y) = \tilde{N}_0(\ell, b, Y) + \frac{\alpha_s N_c}{\pi} \int_0^Y dy\, \left[K \otimes \tilde{N}(\ell, b, y) - \tilde{N}^2(\ell, b, y)\right], \tag{7.9}$$

where K is the BFKL kernel[2] in momentum space [11]. Here we have made the short-distance approximation in which we neglect the $\boldsymbol{r}_{ij}$ terms in comparison to $\boldsymbol{b}$, so that N is only a function of the magnitudes r and b, and $\tilde{N}$ of ℓ and b.

We may resum the linear BFKL effects and rearrange (7.9) in the form

$$\tilde{N}(\ell, b, Y) = \tilde{N}_L(\ell, b, Y) - \frac{\alpha_s N_c}{\pi} \int_0^Y dy\, G(Y - y) \otimes \tilde{N}^2(\ell, b, y), \tag{7.10}$$

where $\tilde{N}_L$ is the solution of the linear part of (7.9) with the shadowing term neglected, and G is the Green function of the BFKL kernel

$$G(Y - y) = \exp\left(\frac{\alpha_s N_c}{\pi}\,(Y - y) K\right). \tag{7.11}$$

Eq. (7.10) may be solved by iteration. At large $Y (\equiv \ln 1/x)$ the dominant region of integration is $y \sim Y$, where $G \simeq 1$, and so the first iteration gives

$$\tilde{N}(\ell, b, Y) = \tilde{N}_L(\ell, b, Y) - \frac{\alpha_s N_c}{\pi} \int_0^Y dy\, \tilde{N}_L^2(\ell, b, y). \tag{7.12}$$

[2]See Section 7.4.

We now assume that the b dependence can be factored out of $\tilde{N}_L$ as a profile function $S(b)$

$$N_L(\ell, b, Y) = S(b)\, n_L(\ell, Y), \tag{7.13}$$

where we use the normalisation $\int d^2b\, S(b) = 1$. Integrating (7.12) over d^2b then gives

$$\tilde{n}(\ell, Y) = \tilde{n}_L(\ell, Y) - \frac{\alpha_s N_c}{\pi} \frac{1}{\pi R^2} \int_0^Y dy\, \tilde{n}_L^2(\ell, y), \tag{7.14}$$

where

$$\frac{1}{\pi R^2} \equiv \int d^2b\, S^2(b). \tag{7.15}$$

7.2 Results for the gluon distributions

We use (7.6) and (7.5) to write (7.14) in terms of the unintegrated gluon distribution. We obtain

$$f(Y, k^2) = f_L(Y, k^2) - \frac{\alpha_s^2}{R^2} \left(1 - \frac{d}{d\ln k^2}\right)^2 k^2 \int_0^Y dy \left[\int_{k^2}^{\infty} \frac{d\ell^2}{\ell^4} \ln\left(\frac{\ell^2}{k^2}\right) f_L(y, \ell^2)\right]^2, \tag{7.16}$$

where we have used the identities

$$\int_0^{\infty} \frac{dr}{r} J_0(kr)\, [1 - J_0(\ell r)] = \tfrac{1}{2} \ln\left(\frac{\ell^2}{k^2}\right) \Theta(\ell^2 - k^2), \tag{7.17}$$

$$\left(1 - \frac{d}{d\ln k^2}\right)^2 k^2 \int_{k^2}^{\infty} \frac{d\ell^2}{\ell^4} \ln\left(\frac{\ell^2}{k^2}\right) f(Y, \ell^2) = f(Y, k^2). \tag{7.18}$$

Note that the term in square brackets in (7.16) is proportional to $n_L(k, y)$. Formula (7.16) is valid in the large N_c limit. For finite N_c we multiply the shadowing term by a factor $N_c^2/(N_c^2 - 1) = 9/8$. However, merely a change of the normalisation of the shadowing term does not exhaust possible corrections beyond the large N_c limit. We expect that there will be other contributions beyond those leading to equation (7.7). The general structure of those corrections is unfortunately not entirely known, and after taking them into account it may no longer be possible to obtain a closed equation for N since other independent and more complicated dynamical quantities will need to be introduced. It should also be observed that the non-linear equation (7.7) does not contain possible effects generated by the compound states of more than two reggeised gluons [70].

The second term on the right-hand-side of (7.16) is simply the shadowing contribution $-f^{(0)}_{shad} =$

$$-\frac{2\alpha_s^2}{R^2}\frac{9}{8}\int_x^{x_0}\frac{dx'}{x'}\left\{k^2\left[\int_{k^2}^{\infty}\frac{d\ell^2}{\ell^4}\,f(x',\ell^2)\right]^2+f(x',k^2)\int_{k^2}^{\infty}\frac{d\ell^2}{\ell^4}\,\ln\left(\frac{\ell^2}{k^2}\right)\,f(x',\ell^2)\right\}, \tag{7.19}$$

and we approximately resum such contributions using a simple (1,1) Padé-type representation

$$f=\frac{f_L}{1+f^{(0)}_{shad}/f_L}. \tag{7.20}$$

(This represents an approximation to the series whose first two terms are given on the right hand side of (7.16).)

In Fig. 7.2 we show the results for the integrated gluon $xg(x,Q^2)$ obtained from (7.20). The shadowing term $-f^{(0)}_{shad}$ is computed from the unintegrated gluon f_L of [19], assuming a running coupling $\alpha_s(k^2)$; we cut off the x' integration in (7.19) at an upper value of $x_0 = 10^{-2}$ (rather than 1) and the ℓ^2 integration at $100k^2$ (rather than ∞).

Several features of the results of Fig. 7.2 are noteworthy. First we see, as expected, that the effect of shadowing on $xg\,(x,Q^2)$ decreases with increasing Q^2. Second, with increasing $\ln(1/x)$, the start of the "turn-over" towards the saturation limit is evident in the $Q^2 = 4$ GeV^2 curves. The major uncertainty in the predictions arises from the choice of the value of R, as a consequence of the $1/R^2$ dependence of the shadowing term. We have chosen values of R that are consistent with the radius of the proton[3]. The results of Fig. 7.2 show that the effects of shadowing are rather small and difficult to identify at HERA where, at best, the domain $x \sim 10^{-4} - 10^{-3}$ at $Q^2 \sim 5$ GeV^2 can be probed. On the other hand shadowing leads to up to a factor of 2 suppression of $xg\,(x, Q^2)$ in the $Q^2 \sim 5$ GeV^2 and $x \sim 10^{-6} - 10^{-5}$ domain accessible to the LHC experiments. Typically, this domain may be probed by observing prompt photon production ($gq \to \gamma q$) or Drell-Yan production both at very large rapidities [71]. Of course the latter process involves a convolution to allow for the $g \to q\bar{q}$ transition, which is required for a gluon-initiated reaction; consequently somewhat larger values of the gluon x are probed.

7.3 Connection with the GLR equation

For completeness we summarise how the Kovchegov equation (7.7) [66] may be reduced to the GLR form [48]. We start with (7.6) and approximate $1 - J_0(kr)$ by $(kr)^2/4$, which is valid provided $k^2 \ll 4/r^2$. Then we obtain

$$\sigma(r, Y) = \frac{\alpha_s \pi^2}{N_c} r^2 \int^{4/r^2} \frac{dk^2}{k^2} f(Y, k^2), \tag{7.21}$$

where the integral can be identified with the integrated gluon $xg(x, 4/r^2)$. Thus, from (7.5), we have

$$\int d^2 b\, N(\boldsymbol{r}, \boldsymbol{b}, Y) \simeq \frac{\alpha_s \pi^2}{2N_c} r^2\, xg(x, 4/r^2). \tag{7.22}$$

[3]If the gluons were concentrated in "hot-spots" within the proton, then shadowing effects would, of course, be correspondingly larger.

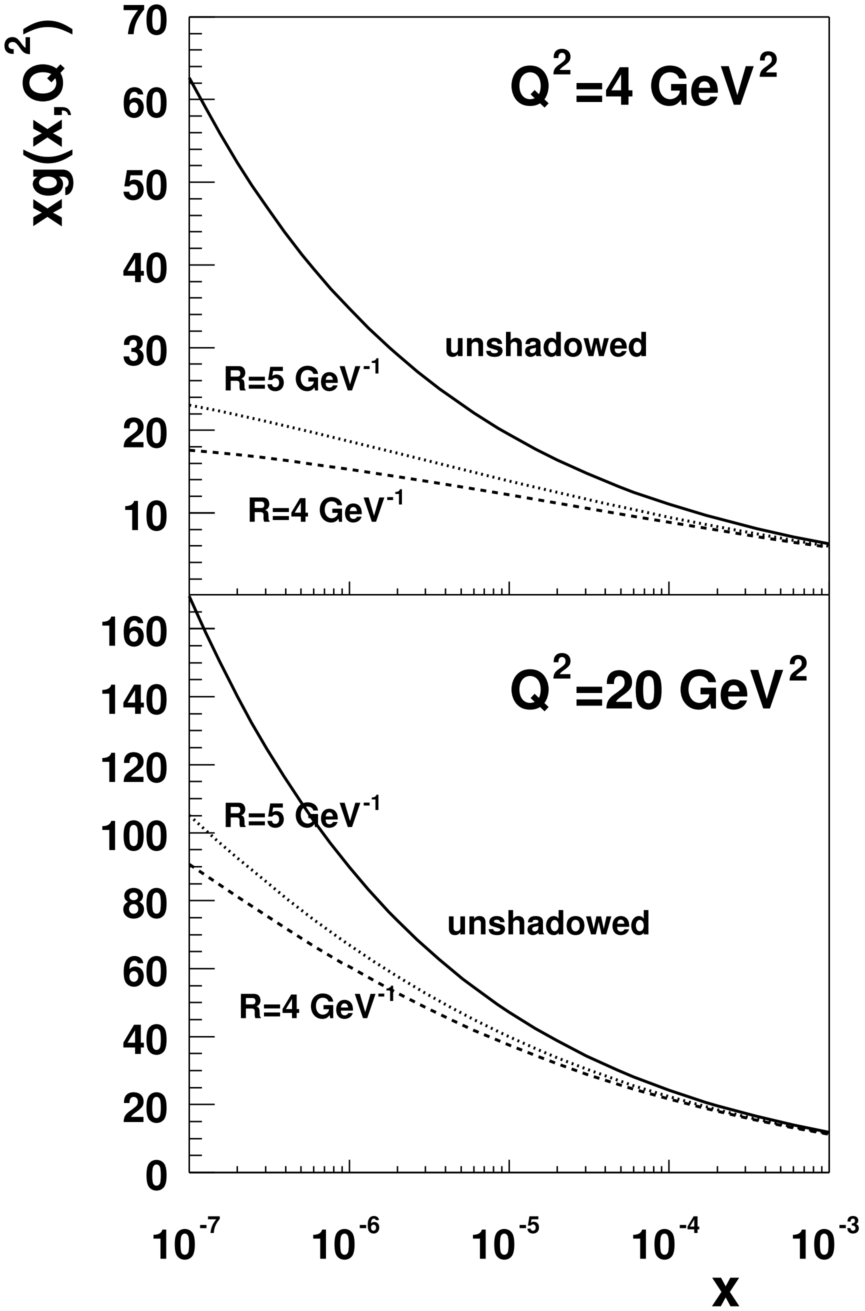

Figure 7.2: The effect of shadowing on the integrated gluon distribution $xg(x, Q^2)$, at $Q^2 = 4$ GeV^2 and 20 GeV^2. The continuous line is simply the unshadowed xg obtained from f_L [19]. The dashed and dotted lines show the result of shadowing with $R = 4$ and 5 GeV^{-1} respectively, where the "radius" R is defined in terms of the proton profile function, $S(b)$.

Now if (7.7) is evaluated in the strongly-ordered approximation ($r_{01}^2 \ll r_{02}^2 \sim r_{12}^2$), it can be shown that it reduces to the GLR form[4]

$$\frac{\partial xg(x,Q^2)}{\partial Y\,\partial\ln(Q^2/\Lambda^2)} = \frac{N_c\alpha_s}{\pi}\,xg(x,Q^2) - \frac{\alpha_s^2\pi}{\pi R^2}\,\frac{1}{Q^2}\left[xg(x,Q^2)\right]^2 . \tag{7.23}$$

7.4 A brief note on the BFKL equation

We define the BFKL kernel $K(k,k')$ so that the single-scale unintegrated gluon $f(x,k^2)$ ($\equiv h_g(x,k^2)$ in the notation of Chapter 2) evolves as

$$f(x,k^2) = f_0(x,k^2) + \frac{\alpha_s}{2\pi}\int_x^1 dz\,\frac{2N_c}{z}\int\frac{dk'^2}{k'^2}\,K(k,k')\,f\left(\frac{x}{z},k'^2\right). \tag{7.24}$$

In the DLLA we would just have the kernel $K = \Theta(k^2 - k'^2)$, which imposes strong ordering in transverse momenta, and the resulting evolution would be written (omitting the driving term f_0)

$$\frac{\partial xg(x,k^2)}{\partial\ln k^2} = \frac{\alpha_s}{2\pi}\int_x^1 dz\,\frac{2N_c}{z}\,xg\left(\frac{x}{z},k^2\right);$$

compare with (2.6). However, the BFKL kernel has a more complicated structure [11]:

$$K(k,k') = \frac{k^2}{|k'^2 - k^2|} - k'^2\,\delta(k^2 - k'^2)\int\frac{dk''^2}{k''^2}\left(\frac{k^2}{|k''^2 - k^2|} - \frac{k^2}{\sqrt{4k''^4 + k^4}}\right). \tag{7.25}$$

This leads to the BFKL equation

$$\frac{\partial f(x,k^2)}{\partial\ln 1/x} = \frac{N_c\alpha_s}{\pi}\int\frac{dk'^2}{k'^2}\,k^2\left(\frac{f(x,k'^2) - f(x,k^2)}{|k'^2 - k^2|} + \frac{f(x,k^2)}{\sqrt{4k'^4 + k^4}}\right). \tag{7.26}$$

[4]Note that [49] defines the shadowing term with an extra factor of $4N_c^2/(N_c^2-1)$, however.

Chapter 8

Summary and conclusions

In this thesis we have developed and illustrated the theory of parton distributions $f_a(x, k_t^2, \mu^2)$, unintegrated with respect to transverse momentum k_t. In particular we have demonstrated a "last-step" formalism whereby such distributions may be approximately obtained by performing a final evolution step explicitly, paying careful attention to the effect of applying an angular ordering constraint to relate the two hard scales k_t and μ. The form of the last step of the evolution is derived from the evolution equations used to evolve single-scale auxiliary functions which enter the last step procedure as input. Thus this last-step formalism can be applied in the context of different evolution schemes, such as DGLAP or "unified" BFKL-DGLAP evolution.

Taking for convenience the MRST99 set of (integrated) partons $a(x, \mu^2)$ $(a = q, g)$ as a possible input to our procedure, we have computed and plotted the resulting unintegrated quark and gluon functions. We have developed a framework based on k_t-factorisation to predict the deep inelastic scattering observable $F_2(x, Q^2)$ using not only our unintegrated gluon distributions, but also our unintegrated quark distributions. This is unconventional, but has the merit of being a more symmetrical treatment of quarks and gluons than traditional approaches. It may be preferred at intermediate values of x. Note in particular that our physical unintegrated parton distributions are positive, unlike single-scale unintegrated partons (effectively the derivatives of corresponding integrated functions) which can become negative at higher values of x. At very low x gluons dominate numerically, and also the dependence on μ can be expected to be less important. There are also necessarily contributions to F_2 from the integrated starting distributions, $xg_0(x, k_0^2)$ and $xq_0(x, k_0^2)$, which represent the region $k_t < k_0$, where k_0 is the minimum allowed scale for perturbative QCD analysis, typically chosen of order 1 GeV. Because our analysis is based on perturbative QCD, we have not investigated possible phenomenological extensions to our distributions for k_t less than k_0, but we make approximations to account for the $k_t < k_0$ region at the level of the cross section, using the starting distributions. It is not a serious limitation of our formalism, but comes inevitably when trying to describe the kinematics of processes where a non-negligible transverse momentum is accounted for in the parton densities.

We have also compared briefly our angular-ordered partons produced from the input of MRST99 partons with an equivalent approach, based on the "unified" BFKL-DGLAP evolution equation derived in [19]. In this case we incorporate BFKL effects in the evolution. We find that, provided we impose angular ordering in our formalism for the last step of the evolution, the distributions obtained allowing for these BFKL effects are not very different from those we generate from DGLAP evolution, at least down to $x = 10^{-4}$. We have not exhaustively investigated the differences, but it seems that a correct treatment of the kinematics of angular ordering is rather more important than the reggeisation of gluons, in the intermediate x region. More work in this area would be beneficial, because we would expect that at some low value of x, the approach incorporating BFKL effects should be preferred. In practice, it is easier to compute the DGLAP-based unintegrated partons and we use the DGLAP version through most of the work described in the thesis.

It is important to stress that the adoption of the MRST99 integrated partons, used as input to our last-step procedure, is a matter of convenience. These partons $a(x, Q^2)$ have been generated by a global fit to data, using the traditional collinear factorisation approach at NLO. We have introduced an alternative framework in which $a(x, Q^2)$ play a different role, as auxiliary functions for the last-step procedure. In particular the angular ordering is subtly different from the strong ordering of transverse momenta assumed in DGLAP evolution. As a result, the MRST99 partons are only used as auxiliary functions as a leading approximation. The ideal situation would be to refit to data in terms of this new, alternative framework with unintegrated partons $f_a(x, k_t^2, \mu^2)$ regarded as fundamental objects. We have illustrated a crude example of such a fit to a sample of F_2 data, but further work is needed to produce optimum unintegrated distributions.

In Chapters 4, 5, and 6, we have demonstrated ways in which unintegrated parton distributions may be used to make predictions for various experimental cross sections. As mentioned before, this research is ongoing. The work is based on LO matrix elements, but the use of k_t-dependent parton distributions means that accurate kinematics are allowed for even at starting order. This has potential impact on studies such as prompt photon production, where traditionally phenomenological "smearing" has been applied to account for incoming transverse momentum. We argue that perturbative QCD should be used to describe $k_t > k_0$, although we also have had to estimate a contribution from $k_t < k_0$ which is phenomenological in nature.

For hadroproduction, two incoming parton distributions are needed. We have described how the initial state in a hadron-hadron collision can be factorised into a parton luminosity function. Our calculations for prompt photon hadroproduction cross sections were based on the "DDT" approximation, whereby to double logarithmic accuracy only we approximated the product of unintegrated parton functions by a derivative expression first derived in [15]. We have made some comparisons with the more accurate luminosity function, but we found that some difficulties are introduced for the non-perturbative region, which contributes heavily to the cross section for the hadroproduction of prompt photons at fixed target experiments. It would be appropriate to continue this study to make more comparisons with Tevatron prompt photon data. It should be emphasised, however, that a development of our work to incorporate higher order effects in a systematic way (NLO, NNLO, etc.) would be more challenging than in the collinear factorisation framework, and it should be carried out with great care to avoid double counting.

Our work on $b\bar{b}$ production, in which we have concentrated on deep inelastic scattering and photoproduction at HERA, has been of a preliminary nature. We have made clear the enormous importance of an accurate simulation of experimental cuts, which are so essential for more exclusive measurements, in any theoretical approach. Our initial estimates of cross sections seem likely to yield results which do not improve significantly on the existing situation, in which NLO QCD predictions are somewhat low compared to the data points (although the data have large errors and this discrepancy is probably not a sign of anything fundamentally wrong with QCD or current calculations). We found one interesting question, to do with possible jet misidentification at HERA, which has bearing on the experimental analysis of these measurements. At the same time, we realised that our last-step formalism throws up a spare particle in the final state with significant transverse momentum, and for further implementation of this approach, we need to investigate the possible impact of this radiation in physical cross sections. We note the relation of our work to Monte Carlo simulations, which are favoured by experimentalists because they can include (sometimes to low order approximation only) a large number of effects relevant to experimental analysis. Nevertheless we feel that independent, self-contained theoretical calculations with explicit analytic perturbative QCD expressions are valuable, in comparison with Monte Carlo studies, to isolate and highlight the particular effects of different approximations and assumptions.

Finally, in Chapter 7 we have performed a new computation of the likely magnitude of shadowing corrections to parton distributions at very low x values, implementing the work of Kovchegov [66], and others, on the triple-pomeron vertex, to produce an estimate of shadowing at HERA and at the LHC. For the purposes of this estimate we used the single-scale unintegrated KMS gluon [19]. Our conclusion is that shadowing is not expected to be particularly noticeable for the kinematic range of HERA, but that at the low-x, low-Q^2 region accessible at the pending LHC, shadowing effects may well begin to show up in the measured gluon distribution.

Appendix A

Some kinematics

In this appendix I include a few details of the kinematic restrictions on parton evolution.

A.1 z cutoff of $\mu/(\mu + k_t)$ from angular ordering

The premise is that we should naturally adopt a factorisation scale μ, characterising the end of the parton evolution, which is expressed as a "rescaled" transverse momentum "q". In the ladder of emitted gluons with transverse momenta q_{tn}, we find that angular ordering is most conveniently imposed in terms of

$$q_n \equiv \frac{q_{tn}}{1 - z_n}. \tag{A.1}$$

z_n is the longitudinal[1] momentum fraction inherited by parton n from its parent $n-1$, thus $(1 - z_n)$ is the fraction of that parent's "x" which was lost to the radiated gluon along with transverse momentum q_{tn}. Fig. A.1 should clarify the definitions.

[1] Or more precisely, $z_n = k_n^+/k_{n-1}^+$, where $k_n^+ \equiv k_n^0 + k_n^3$ is the positive light-cone variable momentum of the parton with x_n, k_{tn}.

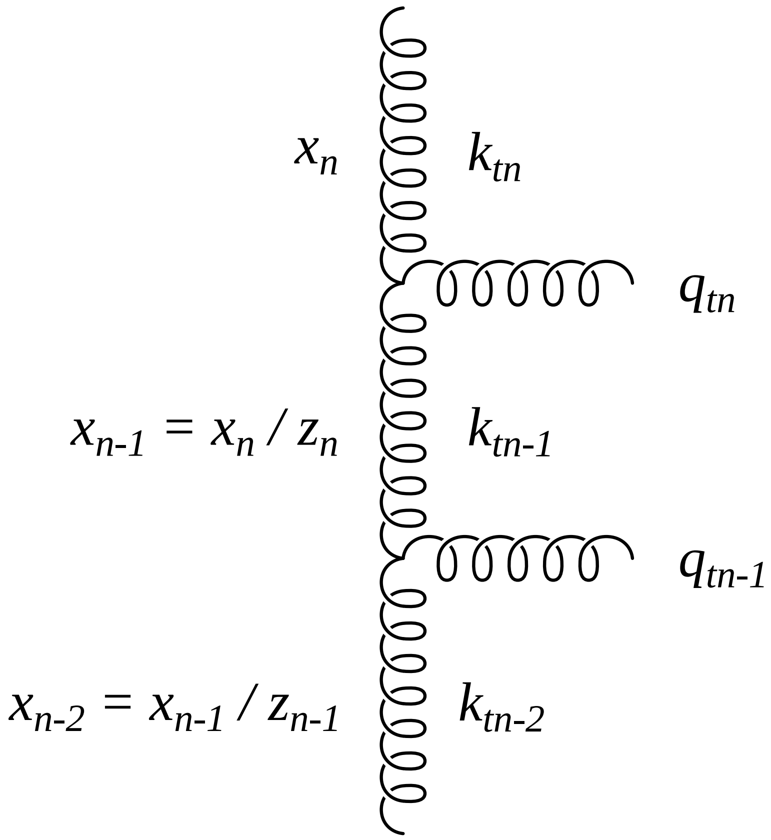

Figure A.1: A section of the evolution ladder and the variables used. The final parton shown has plus momentum x_n and transverse momentum k_{tn}. The suggestion is that the upwards evolution can be performed in the variable $q_n \equiv q_{tn}/(1 - z_n)$.

The physics of the coherent radiation of gluons [6, 12] generates an angular ordering of the emitted gluons as we go up the ladder:

$$\cdots\ \theta_n > \theta_{n-1} > \theta_{n-2}\ \cdots \tag{A.2}$$

These angles are between the direction of motion of the radiated gluons n, $n-1$, $n-2$ and the beam axis (see Fig. 2.2), that is the direction of motion of the whole proton with conventional 4-vector $p^\mu = k_0^\mu = (p, 0, 0, p)$. Of course the parton gluons in the ladder also recoil when the radiated gluons move off at an angle, but the constraint in the form given applies to the real emitted radiation, and the ordered angles are relative to p.

If the angles are quite small we may approximate $\sin\theta_n \simeq \theta_n$, and if we can relate the parton energies[2] as $E_{n-1} \simeq z_{n-1}\, E_{n-2}$, then the angular ordering in (A.2) can be written

$$q_n > z_{n-1}\, q_{n-1}. \tag{A.3}$$

How can we apply equation (A.3) to the hard process at the top of the ladder? We have proposed that the scale μ should be treated as a q variable so our final restriction should appear as

$$\mu > z\, q, \tag{A.4}$$

with z and q pertaining to the last emission before the hard interaction.

Now the two-scale unintegrated parton functions $f_a(x, k_t^2, \mu^2)$ only describe the final parton emerging from the QCD evolution. This parton has been generated in the last piece of the ladder by a real splitting from a parent parton with x/z, k_t', and this z is the

[2] See section A.2 for the physical 4-vectors. Small angles imply small q_t compared to the longitudinal momentum and then z approximately operates as an energy fraction.

variable appearing in (A.4). However, we do not directly access q_t, which is the transverse momentum radiated *away* at this last step. By conservation of transverse momentum at the last vertex before the hard interaction we have, in terms of the parent's k'_t,

$$\boldsymbol{k'_t} = \boldsymbol{k_t} + \boldsymbol{q_t} = \boldsymbol{k_t} + (1-z)\,\boldsymbol{q}, \tag{A.5}$$

or equivalently we can write our final parton's transverse momentum as the vector sum of all the recoils away from the initially collinear state[3]:

$$\boldsymbol{k_t} = -\sum_i \boldsymbol{q_{ti}} = -\sum_i (1-z_i)\,\boldsymbol{q}_i. \tag{A.6}$$

Within the framework of angular ordering, if the values of z are not too near 0 or 1, then (A.3) effectively reduces to the familiar DGLAP strong ordering in angular momenta along the ladder,

$$\cdots\; k_{tn} \gg k_{tn-1} \gg k_{tn-2}\;\cdots \tag{A.7}$$

and it follows from (A.5) that

$$k_t \simeq q_t \tag{A.8}$$

(in the notation of (A.6) the same physics is described by $q_{tn} \gg |\sum_i^{n-1} \boldsymbol{q_{ti}}|$).

In Section 2.3 we apply a restriction on the splitting variable z of the last step to ensure the angular ordering condition in (A.3) is satisfied. In this case we will have a maximum z, describing the largest proportion of longitudinal momentum which our parton can inherit, consistent with the constraints of kinematics and the additional requirement that the radiated gluon is emitted in a suitable physical direction for the

[3] *Intrinsic* transverse momentum, as discussed in Chapter 4, could be included by a fictitious splitting $q_{t0} \sim \Lambda_{QCD}$.

coherence argument. We must also bear in mind that we have assumed that the angle of this radiated gluon is not too large for equations (A.3) and (A.4) to be accurate. If the kinematics were genuinely collinear then (A.3) would have no meaning and there would be no reason to prevent $z = 1$.

It therefore seems appropriate to adopt $k_t \simeq q_t$ as a suitable approximation to insert into our final angular ordering constraint (A.4), leading to the requirement

$$\mu > \frac{z\, k_t}{1-z}. \tag{A.9}$$

The function $z/(1-z)$ increases monotonically with z (and is finite and positive when $0 < z < 1$) and therefore we can infer that the maximum value of z occurs when $\mu = z\, k_t/(1-z)$, which implies

$$z_{max} = \frac{\mu}{\mu + k_t}. \tag{A.10}$$

It is not clear how accurate this cutoff is when k_t is large, say $k_t \gg \mu$, but the vanishing behaviour as $k_t/\mu \to \infty$ is sensible. In addition the limit when $k_t \ll \mu$ is of course $1 - k_t/\mu$, in accordance with the motivation in [1].

A.2 General parton 4-vectors

In the parton evolution ladder, we wish to use general 4-vectors which contain transverse as well as longitudinal momentum [17]. The appropriate apparatus is that of light-cone variables[4], where $k^{\pm} \equiv k^0 \pm k^3$, and the transverse momentum k_t is unaffected.

Our essential definition is the splitting fraction z, which describes the way the x

[4]Some authors include an extra $1/\sqrt{2}$ in this definition. With our definition, $k \cdot p = \frac{1}{2}(k^+p^- + k^-p^+) - k_t \cdot p_t$, and in particular $k^2 = k^+k^- - k_t^2$.

variable changes at a vertex in the parton ladder. The established usage, for a parent parton with 4-momentum k' and a daughter with k, such as k_{n-1} and k_n in Fig. A.1, is the definition

$$z \equiv \frac{k^+}{k'^+}. \tag{A.11}$$

We seek a general form of 4-vector for both k and k' which satisfy (A.11). As these are virtual partons $k^2 \equiv k_\mu k^\mu$ is non-zero, and so enters as a parameter. Writing the proton momentum as p, we have

$$k^+ = 2xp, \quad k'^+ = \frac{2xp}{z}, \quad k^- = \frac{k^2 + k_t^2}{2xp}, \quad k'^- = \frac{k'^2 + k_t'^2}{2xp/z}, \tag{A.12}$$

and that gives conventional 4-vectors *(energy, vector momentum)*

$$\begin{aligned} k^\mu &= \left(xp + \frac{k^2 + k_t^2}{4xp} \,,\, \boldsymbol{k_t} \,,\, xp - \frac{(k^2 + k_t^2)}{4xp} \right) \\ k'^\mu &= \left(\frac{xp}{z} + \frac{k'^2 + k_t'^2}{4xp/z} \,,\, \boldsymbol{k_t'} \,,\, \frac{xp}{z} - \frac{(k'^2 + k_t'^2)}{4xp/z} \right). \end{aligned} \tag{A.13}$$

Clearly x in this framework is not purely a longitudinal momentum fraction, or an energy fraction, unless $k^2 + k_t^2 \ll xp$. However, even when x is quite small, it is likely that at a collider experiment the beam momentum p is enormous compared to the transverse momenta of partons or their virtualities, and this interpretation will be valid to good approximation. In addition, the "kinematic" or "consistency" constraint plays a role whereby the spacelike negative virtuality squared is dominated by the transverse momentum squared.

A.3 Consistency condition

In the context of low x evolution, it has been found appropriate [17, 20] to apply a constraint of kinematical origin to the exchanged particles in the t channel. This has been called variously "the kinematic constraint" or "the consistency condition". It acts as a subleading modification to the BFKL equation, which itself describes parton evolution in the $x \to 0$ limit in terms of effective ladder diagrams where reggeised gluons are exchanged. Staśto writes [20] that the multi-Regge configuration forces the longitudinal components of the exchanged particles in the t-channel to be small and only transverse components can dominate the overall particle's momentum.

The principle of the consistency condition, which seems appealing to obtain a consistent framework in terms of (A.13), is therefore that $|k^2| \simeq k_t^2$, or as an inequality,

$$k_t^2 > \left| k_t^2 + k^2 \right| . \tag{A.14}$$

In light-cone momenta this is written $k_t^2 > |k^+ k^-|$.

Applying conservation of momentum separately for the $+$ and $-$ momenta, combined with the condition that the radiated object is on-shell, gives

$$k^- = k'^- - \frac{q_t^2}{q^0 + q^3} = k'^- - \frac{q_t^2}{k'^+ - k^+} . \tag{A.15}$$

Now insofar as we can argue $k'^- \ll k^-$, it follows from (A.15) that

$$k^+ k^- = \frac{k^+}{k'^+ - k^+}\, q_t^2 = -\frac{z}{1-z}\, q_t^2 . \tag{A.16}$$

Then the imposition of (A.14) via (A.16) gives the precise formulation of the consistency constraint,

$$q_t^2 < \frac{(1-z)k_t^2}{z}. \tag{A.17}$$

However we only expect to apply this constraint for low z, in which case the condition

$$q_t^2 < \frac{k_t^2}{z} \tag{A.18}$$

will suffice.

Appendix B

Calculation of Feynman diagrams

We present sample derivations of the theoretical expressions for the cross sections for two different parton-level processes, $\gamma^* q \to q\gamma$ and $\gamma^* g^* \to b\bar{b}$. The derivation of the expressions for F_L and F_T in deep inelastic scattering, which involves different techniques, is also discussed.

B.1 (Virtual) Compton scattering: $\gamma^* q \to q\gamma$

For the $2 \to 2$ subprocess illustrated in Figure B.1, the differential cross section with respect to the Mandelstam invariant $\hat{t} < 0$ is given by [27]

$$\frac{d\hat{\sigma}}{d|\hat{t}|} = \frac{\overline{|\mathcal{M}|^2}}{16\pi \left(\hat{s}^2 - 2\hat{s}(m_A^2 + m_B^2) + (m_A^2 - m_B^2)^2\right)} \tag{B.1}$$

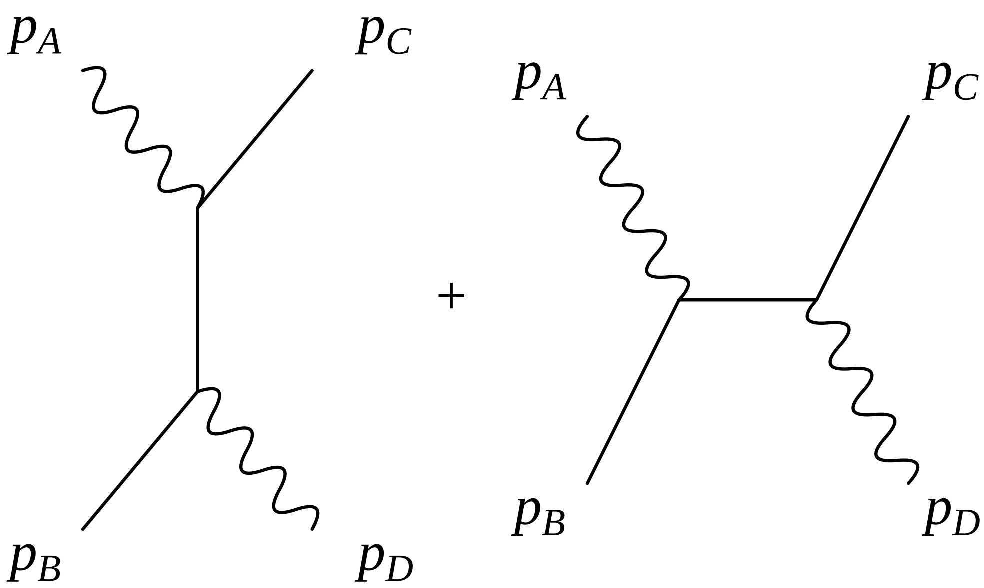

Figure B.1: Lowest order diagrams for $\gamma^* + q \to q + \gamma$

where m_A^2 and m_B^2 are the squared masses (or virtualities) of the incoming particles A and B. For the amplitudes shown in Fig. B.1, we write down the matrix element $\mathcal{M}$ as

$$i\mathcal{M} = e_q^2 \left(\sqrt{4\pi\alpha_{em}}\right)^2 \mathcal{E}_A^\mu \mathcal{E}_D^{*\nu} \left(\bar{u}_C\, i\gamma_\mu \frac{i(\not{p}_B - \not{p}_D)}{(p_B - p_D)^2}\, i\gamma_\nu u_B + \bar{u}_C\, i\gamma_\nu \frac{i(\not{p}_A + \not{p}_B)}{(p_A + p_B)^2}\, i\gamma_\mu u_B\right), \tag{B.2}$$

with quark spinors u_B, Dirac gamma matrices γ_μ, and $\not{p}_A \equiv \gamma_\mu p_A^\mu$. e_q is the fractional charge of the quark, such as $-1/3$ or $2/3$. In unpolarised situations we sum over the possible polarisations $\mathcal{E}$ of the external photons, using (in a covariant gauge)

$$\sum_{pol.\,D} \mathcal{E}_D^{*\nu} \mathcal{E}_D^{\sigma} \to -g^{\nu\sigma}, \qquad \sum_{pol.\,A} \mathcal{E}_A^{\mu} \mathcal{E}_A^{*\rho} \to -g^{\mu\rho}$$

where particle A is a virtual photon and particle D is a real photon. This means that the spin-averaged[1] matrix element squared is given by

$$\overline{|\mathcal{M}|^2} = \frac{1}{2} \times e_q^4\, 16\pi^2 \alpha_{em}^2 \sum_{spin\ B} \sum_{spin\ C} \left(M_{11} + M_{12} + M_{21} + M_{22}\right), \tag{B.3}$$

where the pieces M_{ij} come from squaring (B.2) and applying the polarisation sums:

$$\begin{aligned}
M_{11} &= \bar{u}_C\, \gamma_\mu \frac{(\not{p}_B - \not{p}_D)}{(p_B - p_D)^2}\, \gamma_\nu u_B \bar{u}_B\, \gamma^\nu \frac{(\not{p}_B - \not{p}_D)}{(p_B - p_D)^2}\, \gamma^\mu u_C \\
M_{12} &= \bar{u}_C\, \gamma_\mu \frac{(\not{p}_B - \not{p}_D)}{(p_B - p_D)^2}\, \gamma_\nu u_B \bar{u}_B\, \gamma^\mu \frac{(\not{p}_A + \not{p}_B)}{(p_A + p_B)^2}\, \gamma^\nu u_C \\
M_{21} &= \bar{u}_C\, \gamma_\nu \frac{(\not{p}_A + \not{p}_B)}{(p_A + p_B)^2}\, \gamma_\mu u_B \bar{u}_B\, \gamma^\nu \frac{(\not{p}_B - \not{p}_D)}{(p_B - p_D)^2}\, \gamma^\mu u_C \\
M_{22} &= \bar{u}_C\, \gamma_\nu \frac{(\not{p}_A + \not{p}_B)}{(p_A + p_B)^2}\, \gamma_\mu u_B \bar{u}_B\, \gamma^\mu \frac{(\not{p}_A + \not{p}_B)}{(p_A + p_B)^2}\, \gamma^\nu u_C.
\end{aligned}$$

The spinors obey

$$\sum_{spin\ B} u_B \bar{u}_B = \not{p}_B + m_B, \tag{B.4}$$

which is to be understood as an equation in terms of 4×4 matrices. Here we take the quark mass $m_B = 0$. M_{ij} here are numbers, not matrices, and rearranging the order of the matrices and vectors, by moving u_C whilst keeping track of the spinor indices, shows that once we combine the spinors using (B.4), the expressions can be computed as a trace of products of gamma matrices, such as

$$\sum_{spins} M_{11} = \mathrm{Tr}\, \left(\not{p}_C \gamma_\mu \frac{(\not{p}_B - \not{p}_D)}{(p_B - p_D)^2}\, \gamma_\nu \not{p}_B \gamma^\nu \frac{(\not{p}_B - \not{p}_D)}{(p_B - p_D)^2}\, \gamma^\mu \right).$$

[1] We normally sum over final state spin possibilities, and average the incoming ones. The factor of 1/2 is to average over the incoming quark's spin; however, we do not include here a factor to average over the incoming photon's polarisation states, because the virtual photon is understood to come from leptoproduction (with the *electron's* spin averaged in the leptonic tensor), or, as in Chapter 5, in photoproduction where the factor of 1/2 is effectively contained within the Weizsäcker-Williams function.

These traces can be evaluated using the known properties of gamma matrices, for example

$$\mathrm{Tr}\, \gamma^\mu = 0, \quad \mathrm{Tr}\, \gamma^\mu \gamma^\nu = 4 g^{\mu\nu}, \quad \text{and } \gamma^\mu \gamma^\nu \gamma_\mu = -2\gamma^\nu, \tag{B.5}$$

and it is often most convenient to use a computer package such as FORM [72] to evaluate them. At the same time, we can apply conservation of momentum and substitute the Mandelstam variables $\hat{s}$, $\hat{t}$, and $\hat{u}$ for expressions involving the scalar products of the various 4-vectors. In this case we specify $p_A^2 = m^2$, $p_B^2 = p_C^2 = p_D^2 = 0$:

$$\hat{s} = p_A^2 + 2 p_A \cdot p_B = 2 p_C \cdot p_D \tag{B.6}$$

$$\hat{t} = p_A^2 - 2 p_A \cdot p_C = -2 p_B \cdot p_D \tag{B.7}$$

$$\hat{u} = p_A^2 - 2 p_A \cdot p_D = -2 p_B \cdot p_C \tag{B.8}$$

with $\hat{s} + \hat{t} + \hat{u} = p_A^2$.

Performing these manipulations, we find

$$\begin{aligned}
\sum_{spins} M_{11} &= -8\hat{s}\hat{t}/\hat{t}^2 \\
\sum_{spins} M_{12} &= \left\{-8m^4 + 8m^2\hat{s} + 8m^2\hat{t}\right\} \Big/ \hat{s}\hat{t} \\
\sum_{spins} M_{21} &= \sum_{spins} M_{12} \\
\sum_{spins} M_{22} &= -8\hat{s}\hat{t}/\hat{s}^2
\end{aligned} \tag{B.9}$$

which sum to give the result

$$\sum_{spins} \sum_{ij} M_{ij} = -8\frac{\hat{s}}{\hat{t}} - 8\frac{\hat{t}}{\hat{s}} + 16m^2 \left(\frac{1}{\hat{t}} + \frac{1}{\hat{s}} - \frac{m^2}{\hat{s}\hat{t}} \right). \tag{B.10}$$

An alternative is to work in an axial gauge. In this case the polarisation sum for the virtual photon A becomes

$$\sum_{pol.\,A} \mathcal{E}_A^{\mu} \mathcal{E}_A^{*\rho} \rightarrow -g^{\mu\rho} + \frac{n^{\mu} p_A^{\rho} + n^{\rho} p_A^{\mu}}{n \cdot p_A} - \frac{n^2 \, p_A^{\mu} p_A^{\rho}}{(n \cdot p_A)^2}, \tag{B.11}$$

where n^{μ} is an arbitrary 4-vector satisfying $n \cdot \mathcal{E} = 0$. A suitable choice in this case is $n = p_B$, which has the advantage that $n^2 = 0$. Thus the combination

$$\left(\gamma^{\mu} - \frac{p_A^{\mu} \not{p}_B + \not{p}_A p_B^{\mu}}{p_A \cdot p_B} \right)$$

replaces γ^{μ} in the second halves of the expressions for M_{ij}. We can also perform the polarisation sum for the photon D in the same way. Here a convenient choice for n is $n = p_C$, giving

$$\left(\gamma^{\nu} - \frac{p_C^{\nu} \not{p}_D + \not{p}_C p_D^{\nu}}{p_C \cdot p_D} \right)$$

instead of γ^{ν} in the second halves of the expressions. The individual $\sum_{spins} M_{11}$, $\sum_{spins} M_{12}$, ... give more complicated answers than those in (B.9), but nevertheless the sum of the M_{ij} remains the same as (B.10).

From (B.10) it follows, using $m^2 = -Q^2$ for the incoming photon, that the differential cross section for the photoproduction subprocess shown in Fig. B.1 is

$$\frac{d\hat{\sigma}}{d|\hat{t}|} = \frac{4\pi e_q^4 \alpha_{em}^2}{(\hat{s} + Q^2)^2} \left(\frac{\hat{s}}{|\hat{t}|} + \frac{|\hat{t}|}{\hat{s}} + \frac{2Q^2}{\hat{s}|\hat{t}|} \left(\hat{s} + \hat{t} + Q^2 \right) \right). \tag{B.12}$$

A similar result is derived by Field [27], p122.

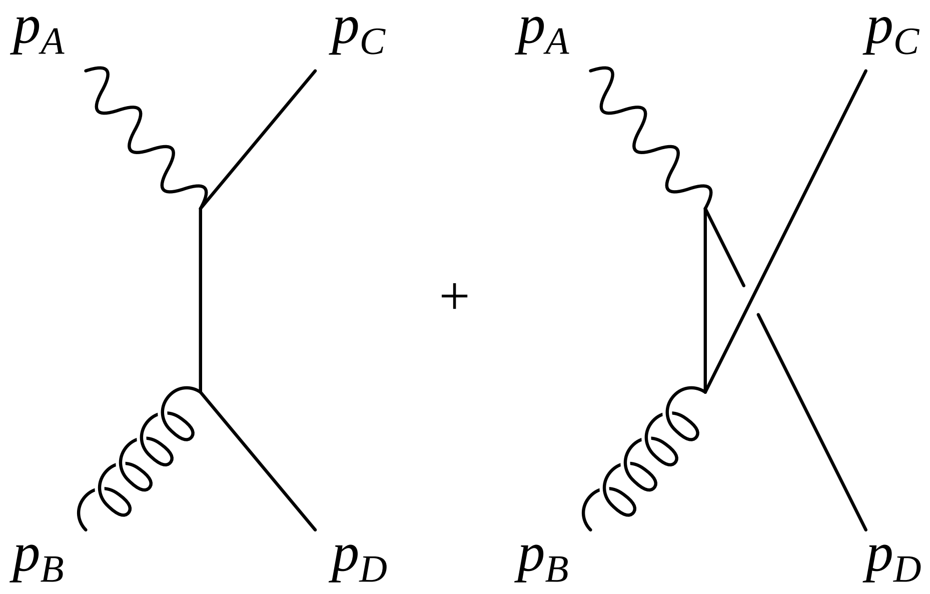

Figure B.2: Lowest order diagrams for $\gamma^* + g \to q + \bar{q}$

B.2 $b\bar{b}$ production: $\gamma^* g^* \to b\bar{b}$

For the amplitudes shown in Fig. B.2, we write down the matrix element for $b\bar{b}$ production initiated by a gluon

$$\begin{aligned} i\mathcal{M} &= e_b\,\sqrt{4\pi\alpha_{em}}\sqrt{4\pi\alpha_s}\,t^a_{ij}\,\mathcal{E}^\mu_A\mathcal{E}^\nu_B \\ & \left(\bar{u}_C\,i\gamma_\mu\frac{i(\not{p}_B-\not{p}_D+m_b)}{(p_B-p_D)^2-m_b^2}\,i\gamma_\nu v_D+\bar{u}_C\,i\gamma_\nu\frac{i(\not{p}_A-\not{p}_D+m_b)}{(p_A-p_D)^2-m_b^2}\,i\gamma_\mu v_D\right) \end{aligned} \tag{B.13}$$

where i and j are quark colour indices (run from 1 to 3) of the colour matrix t^a (a runs from 1 to 8 and denotes the (bi)colour of the gluon). When we sum $|\mathcal{M}|^2$ over final colour states i and j, and average the incoming colour a, we obtain the colour factor $\frac{1}{8}t^a_{ij}t^a_{ji} = \frac{1}{8}\mathrm{Tr}\ t^at^a = \delta^{aa}/16 = \frac{1}{2}$. Here we are only interested in bottom quarks so the fractional charge is $e_b = -\frac{1}{3}$. The quantity m_b appearing in the quark propagator is the mass of the b quark. The antiquark spinor v_D will satisfy

$$\sum_{spin\ D} v_D \bar{v}_D = \not{p}_D - m_b, \tag{B.14}$$

and for the quark we will need

$$\sum_{spin\ C} u_C \bar{u}_C = \not{p}_C + m_b; \tag{B.15}$$

we use the polarisation sums (covariant gauge[2])

$$\sum_{pol.\ A} \mathcal{E}^{\mu}_{A} \mathcal{E}^{*\rho}_{A} \quad \to \quad -g^{\mu\rho} \tag{B.16}$$

$$\sum_{pol.\ B} \mathcal{E}^{\nu}_{B} \mathcal{E}^{*\sigma}_{B} \quad \to \quad -g^{\nu\sigma} \tag{B.17}$$

in the expression for the matrix element squared.

So the averaged, squared matrix element, including the colour factor, is

$$\overline{|\mathcal{M}|^2} = \frac{1}{2} \times \frac{1}{2} \times e_b^2\, 16\pi^2 \alpha_s \alpha_{em} \sum_{spin\ C} \sum_{spin\ D} \left(M_{11} + M_{12} + M_{21} + M_{22} \right), \tag{B.18}$$

with separate parts

$$\begin{aligned}
M_{11} &= \bar{u}_C \gamma_\mu \frac{(\not{p}_B - \not{p}_D + m_b)}{(p_B - p_D)^2 - m_b^2} \gamma_\nu v_D \bar{v}_D \gamma^\nu \frac{(\not{p}_B - \not{p}_D + m_b)}{(p_B - p_D)^2 - m_b^2} \gamma^\mu u_C \\
M_{12} &= \bar{u}_C \gamma_\mu \frac{(\not{p}_B - \not{p}_D + m_b)}{(p_B - p_D)^2 - m_b^2} \gamma_\nu v_D \bar{v}_D \gamma^\mu \frac{(\not{p}_A - \not{p}_D + m_b)}{(p_A - p_D)^2 - m_b^2} \gamma^\nu u_C \\
M_{21} &= \bar{u}_C \gamma_\nu \frac{(\not{p}_A - \not{p}_D + m_b)}{(p_A - p_D)^2 - m_b^2} \gamma_\mu v_D \bar{v}_D \gamma^\nu \frac{(\not{p}_B - \not{p}_D + m_b)}{(p_B - p_D)^2 - m_b^2} \gamma^\mu u_C \\
M_{22} &= \bar{u}_C \gamma_\nu \frac{(\not{p}_A - \not{p}_D + m_b)}{(p_A - p_D)^2 - m_b^2} \gamma_\mu v_D \bar{v}_D \gamma^\mu \frac{(\not{p}_A - \not{p}_D + m_b)}{(p_A - p_D)^2 - m_b^2} \gamma^\nu u_C
\end{aligned}$$

[2]It is again convenient to use this simple projection, because we do not need to include ghost loops for these diagrams.

With these masses and virtualities, the Mandelstam variables are

$$\hat{s} = (p_A + p_B)^2 = p_A^2 + p_B^2 + 2p_A \cdot p_B = 2p_C \cdot p_D + 2m_b^2 \tag{B.19}$$

$$\hat{t} = (p_B - p_D)^2 = p_B^2 + m_b^2 - 2p_B \cdot p_D = p_A^2 + m_b^2 - 2p_A \cdot p_C \tag{B.20}$$

$$\hat{u} = (p_A - p_D)^2 = p_A^2 + m_b^2 - 2p_A \cdot p_D = p_B^2 + m_b^2 - 2p_B \cdot p_C \tag{B.21}$$

with $\hat{s}+\hat{t}+\hat{u} = p_A^2+p_B^2+2m_b^2$. The incoming particles are spacelike, so we use $p_A^2 = -Q^2$ and $p_B^2 = -\mu^2$.

Again we can compute the relevant traces and contractions with FORM. For the purposes of the calculation in Chapter 6 it is most convenient to express the momenta in terms of the Sudakov variables in (6.13), and working in the photon-proton CM frame, to use (6.14) so that the proton momentum is

$$p^\mu = \left(\frac{Q/2}{\sqrt{x(1-x)}},\ \mathbf{0},\ \frac{Q/2}{\sqrt{x(1-x)}} \right), \tag{B.22}$$

and the other lightlike momentum is

$$q'^\mu = \left(\frac{Q/2\ (1-x)}{\sqrt{x(1-x)}},\ \mathbf{0},\ \frac{Q/2\ (x-1)}{\sqrt{x(1-x)}} \right); \tag{B.23}$$

the condition that the outgoing b and $\bar{b}$ are on-shell (writing m for mass m_b) implies

$$\alpha_1 = \frac{x(m^2+p_{1\perp}^2)}{\beta_1 Q^2}, \quad \alpha_2 = \frac{x(m^2+p_{2\perp}^2)}{\beta_2 Q^2}.$$

First let us look at the denominators in M_{ij}. We find

$$\hat{t} - m^2 = -\left(Q^2(1-\beta_1) + \frac{m^2+p_{1\perp}^2}{\beta_1} \right) \equiv -\Delta_1 \tag{B.24}$$

$$\hat{u} - m^2 \quad = \quad -\left(Q^2(1-\beta_2) + \frac{m^2 + p_{2\perp}^2}{\beta_2}\right) \equiv -\Delta_2 \tag{B.25}$$

without making any assumptions about the value of the Sudakov parameter b for the incoming gluon. Then

$$\sum_{spins} M_{11} = \tag{B.26}$$

$$8\Big(p_{1\perp}^2 p_{2\perp}^2 + p_{1\perp}^2 m^2(1+2\beta_2) + p_{2\perp}^2 m^2 + p_{1\perp}^2 Q^2\beta_2(1-\beta_2) + p_{2\perp}^2 Q^2\beta_1(1-\beta_1)$$
$$+m^2Q^2\left(\beta_1(1-\beta_1) + \beta_2(1-\beta_2) + 4\beta_1\beta_2 - 2\beta_1^2\beta_2\right) + 2\mu^2 m^2\beta_1\beta_2 - \mu^2 Q^2\beta_1\beta_2$$
$$+m^4\left(1+2\beta_2 - 4\beta_1\beta_2\right) + Q^4\beta_1\beta_2\left(1-\beta_1-\beta_2+\beta_1\beta_2\right)\Big)\Big/\beta_1\beta_2\Delta_1^2$$

$$\sum_{spins} M_{12} = \sum_{spins} M_{21} = \tag{B.27}$$

$$8\Big(\left(p_{1\perp}^2\beta_2 + p_{2\perp}^2\beta_1\right)(m^2 - \mu^2 - Q^2) - \mu^2 m^2(\beta_1+\beta_2)$$
$$+m^2Q^2\left(2\beta_1\beta_2 - \beta_1 - \beta_2 - \beta_1^2\beta_2 - \beta_1\beta_2^2\right) + \mu^2Q^2\beta_1\beta_2(\beta_1+\beta_2)$$
$$+m^4(\beta_1+\beta_2-4\beta_1\beta_2) + \mu^4\beta_1\beta_2 + Q^4\beta_1\beta_2(\beta_1+\beta_2-1)\Big)\Big/\beta_1\beta_2\Delta_1\Delta_2$$

$$\sum_{spins} M_{22} = \tag{B.28}$$

$$8\Big(p_{1\perp}^2 p_{2\perp}^2 + p_{1\perp}^2 m^2 + p_{2\perp}^2 m^2(1+2\beta_1) + p_{1\perp}^2 Q^2\beta_2(1-\beta_2) + p_{2\perp}^2 Q^2\beta_1(1-\beta_1)$$
$$+m^2Q^2\left(\beta_1(1-\beta_1) + \beta_2(1-\beta_2) + 4\beta_1\beta_2 - 2\beta_1\beta_2^2\right) + 2\mu^2 m^2\beta_1\beta_2 - \mu^2 Q^2\beta_1\beta_2$$
$$+m^4\left(1+2\beta_1 - 4\beta_1\beta_2\right) + Q^4\beta_1\beta_2\left(1-\beta_1-\beta_2+\beta_1\beta_2\right)\Big)\Big/\beta_1\beta_2\Delta_2^2.$$

These are symmetric expressions, but we wish to simplify them. By setting the Sudakov parameter b to 0, which corresponds to the consistency condition $\mu^2 = k_t^2$ for the incoming gluon[3], we can eliminate β_2 by conservation of momentum as $1-\beta_1$, and obtain

$$\sum_{spins} M_{11} = \tag{B.29}$$

$$8\Big(p_{1\perp}^2\left|\boldsymbol{k_t}-\boldsymbol{p_{1\perp}}\right|^2 + p_{1\perp}^2 m^2(3-2\beta_1) + \left|\boldsymbol{k_t}-\boldsymbol{p_{1\perp}}\right|^2 m^2 + \left|\boldsymbol{k_t}-\boldsymbol{p_{1\perp}}\right|^2 Q^2\beta_1(1-\beta_1)$$
$$+p_{1\perp}^2 Q^2\beta_1(1-\beta_1) + m^2Q^2\left(6\beta_1(1-\beta_1) - 2\beta_1^2(1-\beta_1)\right) + 2k_t^2m^2\beta_1(1-\beta_1)$$
$$-k_t^2Q^2\beta_1(1-\beta_1) + m^4\left(3-2\beta_1-4\beta_1(1-\beta_1)\right) + Q^4\beta_1^2(1-\beta_1)^2\Big)\Big/\beta_1(1-\beta_1)\Delta_1^2$$

$$\sum_{spins} M_{12} = \sum_{spins} M_{21} = \tag{B.30}$$

$$8\Big(\left(p_{1\perp}^2(1-\beta_1) + \left|\boldsymbol{k_t}-\boldsymbol{p_{1\perp}}\right|^2\beta_1\right)(m^2-k_t^2-Q^2) - k_t^2m^2 + m^2Q^2\left(\beta_1(1-\beta_1)-1\right)$$
$$+k_t^2Q^2\beta_1(1-\beta_1) + m^4\left(1-4\beta_1(1-\beta_1)\right) + k_t^4\beta_1(1-\beta_1)\Big)\Big/\beta_1(1-\beta_1)\Delta_1\Delta_2$$

$$\sum_{spins} M_{22} = \tag{B.31}$$

$$8\Big(p_{1\perp}^2\left|\boldsymbol{k_t}-\boldsymbol{p_{1\perp}}\right|^2 + p_{1\perp}^2 m^2 + \left|\boldsymbol{k_t}-\boldsymbol{p_{1\perp}}\right|^2 m^2(1+2\beta_1) + \left|\boldsymbol{k_t}-\boldsymbol{p_{1\perp}}\right|^2 Q^2\beta_1(1-\beta_1)$$
$$+p_{1\perp}^2 Q^2\beta_1(1-\beta_1) + m^2Q^2\left(6\beta_1(1-\beta_1) - 2\beta_1(1-\beta_1)^2\right) + 2k_t^2m^2\beta_1(1-\beta_1)$$
$$-k_t^2Q^2\beta_1(1-\beta_1) + m^4\left(1+2\beta_1-4\beta_1(1-\beta_1)\right) + Q^4\beta_1^2(1-\beta_1)^2\Big)\Big/\beta_1(1-\beta_1)\Delta_2^2,$$

and of course the expression (B.25) for Δ_2 is written in terms of β_1, $\boldsymbol{p_{1\perp}}$ and k_t.

The invariant mass for the photon–*gluon* subprocess is

$$\hat{s} = (p_\gamma + p_g)^2 = (q+k)^2 = \left(\frac{1}{z}-1\right)Q^2 - k_t^2, \tag{B.32}$$

[3]We approximate the incoming virtuality to $-k_t^2$ in much the same spirit as parton calculations conventionally approximate the incoming virtuality to 0, as far as the matrix element is concerned.

where x/z is the fraction of the proton's plus momentum held by the gluon. We can therefore describe the subprocess scattering in terms of $d\hat{\sigma}/d\hat{t}$ as in (B.1),

$$\begin{aligned}\frac{d\hat{\sigma}}{d|\hat{t}|} &= \frac{4\pi^2 e_b^2 \alpha_s \alpha_{em} \sum_{ij} \sum_{spins} M_{ij}}{16\pi \left(\left[\left(\frac{1}{z} - 1 \right) Q^2 - k_t^2 \right]^2 + 2 \left[\left(\frac{1}{z} - 1 \right) Q^2 - k_t^2 \right] \left(k_t^2 + Q^2 \right) + \left(k_t^2 - Q^2 \right)^2 \right)} \\ &= \frac{\pi e_b^2 \alpha_s \alpha_{em} \sum_{ij} \sum_{spins} M_{ij}}{4Q^2 \left(\frac{Q^2}{z^2} - 4k_t^2 \right)}. \end{aligned} \tag{B.33}$$

B.3 Squared diagram approach

Here we discuss how the photon-gluon subprocess may be approached in terms of squared diagrams as in Fig. 3.1. This yields the expressions for F_T and F_L in Chapter 3, with suitable approximations, and provided that we embed our diagrams in the factorisation framework. Much of this section is inspired by similar treatments in [29], see also [18].

The general scattering matrix S includes both scattering from one in-state $|a\rangle$ to a different out-state $|b\rangle \neq |a\rangle$, and the no-change (forward amplitude) case $|b\rangle = |a\rangle$. Conventionally the non-identity part is labelled the T-matrix:

$$S = 1 + iT.$$

In terms of the "matrix element" $\mathcal{M}$ written elsewhere,

$$T_{ab} = (2\pi)^4 \, \delta^{(4)} \left(\sum p_a - \sum p_b \right) \mathcal{M}_{ab}.$$

The S-matrix must be unitary, for conservation of probability, so

$$\begin{aligned} S^\dagger S &= \left(1 - iT^\dagger\right)(1 + iT) = 1 \\ &\Rightarrow \; 2\,\Im m\, T = |T|^2, \end{aligned}$$

and for our matrix element $\mathcal{M}$ we can write

$$\begin{aligned} &(2\pi)^4\,\delta^{(4)}\left(\sum p_a - \sum p_b\right)\, 2\,\Im m\,\mathcal{M}(a \to b) = (2\pi)^4\,\delta^{(4)}\left(\sum p_a - \sum p_b\right) \times \\ &\sum_f \left(\prod_{i=1}^{n} \int \frac{d^3 p_i}{(2\pi)^3\, 2E_i}\right) \mathcal{M}^*(b \to f)\,\mathcal{M}(a \to f)\,(2\pi)^4 \delta^{(4)}\left(\sum p_a - \sum p_i\right) \end{aligned}$$

where $|f\rangle$ is a state consisting of n particles of momenta p_i, and we sum over all such possible states $|f\rangle$.

In the special case of the forward amplitude where $|a\rangle = |b\rangle$, this gives a convenient way of computing the integral of $|\mathcal{M}(a \to f)|^2$ over all final states $|f\rangle$, in terms of the imaginary part of the related matrix element $\mathcal{M}(a \to a)$. This is the optical theorem: the total cross section for the scattering of an incoming two-particle state $|a\rangle$ can be computed from the forward *amplitude*:

$$\sigma_{tot}(a \to \textit{anything}) = \frac{2\,\Im m\,\mathcal{M}(a \to a)}{F},$$

where for negligible incoming masses and virtualities, the flux factor $F = 2s$. Characterising a $2 \to 2$ scattering by the Mandelstam variables s, t, the forward amplitude corresponds to $\mathcal{M}(s,t) = \mathcal{M}(s,0)$, and we can treat s as a complex variable for mathematical manipulation. The S-matrix must be an analytic function of the Lorentz invariants s, t, ... , and this has various consequences (see [29]). Among them is the fact that the

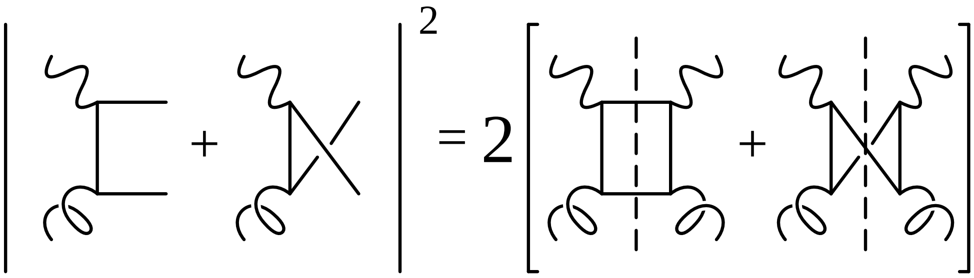

Figure B.3: Schematic depiction of working with squared diagrams via the optical theorem ("cut" propagators are on-shell).

imaginary part of an amplitude may be computed as the s-channel discontinuity

$$
\begin{aligned}
2\,\Im m\,\mathcal{M}(s,t) &= -i\,\mathrm{Disc}\,\mathcal{M}(s,t) \\
&\equiv -i\lim_{\epsilon\to 0}\left(\mathcal{M}(s+i\epsilon,t)-\mathcal{M}(s-i\epsilon,t)\right).
\end{aligned}
$$

We want to compute perturbative approximations to the cross section in terms of Feynman diagrams, which give real matrix elements except when internal virtual particles go on-shell (when the $+i\epsilon$ in the propagator is relevant). The discontinuity corresponds to a branch cut along the real s-axis, starting at some threshold $s = s_0$ (e.g. $(2m_b)^2$) above which it is possible to produce an n-particle state. Cutkosky [73] showed that we can compute the discontinuity of individual Feynman diagrams by "cutting" them (in all permutations) so that two or more propagators go simultaneously on-shell. The cuts are indicated by dashed vertical lines in Fig. B.3. In evaluating such a diagram, the $1/(p^2 - m^2 + i\epsilon)$ of each cut propagator is replaced by $-2\pi i\delta(p^2 - m^2)$, and these delta functions restrict the loop integrations $\int d^4\kappa/(2\pi)^4$.

As an illustration we consider again the $\gamma^* g^* \to b\bar{b}$ process[4], from the point of view

[4] We can either regard this as $b\bar{b}$ production, or sum over outgoing quark flavours and construct the structure functions for the DIS cross section.

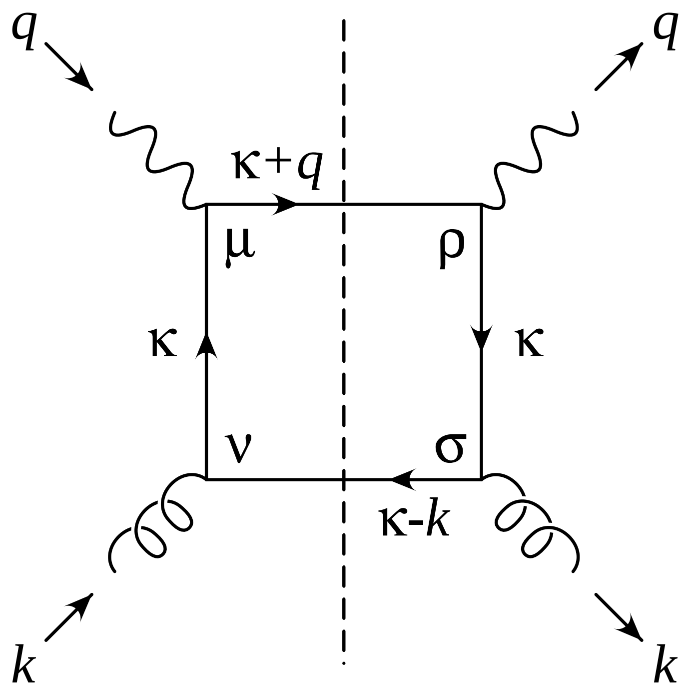

Figure B.4: The “box” diagram with momenta shown.

of squared, loop diagrams, with cuts on the b and $\bar{b}$ lines which are assumed on-shell outgoing particles. From Fig. B.3 we see we have two different loop diagrams to compute, the “box” and “crossed box”, in Figs. B.4 and B.5 respectively.

Using the momenta labelled in Fig. B.4, we write down the expression for the cut box diagram as

$$\begin{aligned} \mathrm{Disc}\, \mathcal{M}_{box} = - & \\ & \frac{(4\pi)^2 \alpha_s \alpha_{em} e_q^2}{(\kappa^2 - m^2)(\kappa^2 - m^2)} \int \frac{d^4\kappa}{(2\pi)^4} (2\pi)^2\, \delta\left((\kappa+q)^2 - m^2\right)\, \delta\left((\kappa-k)^2 - m^2\right) \\ & \quad \mathrm{Tr}\, \left((\not{\kappa} + m)\gamma^\nu (\not{\kappa} - \not{k} + m)\gamma^\sigma (\not{\kappa} + m)\gamma^\rho (\not{\kappa} + \not{q} + m)\gamma^\mu\right). \end{aligned} \tag{B.34}$$

Note that we have *not* multiplied by polarisation vectors to absorb the Lorentz indices μ, ν, ρ, σ — instead we will take appropriate projections to distinguish the contributions to the deep inelastic cross section from transverse and longitudinal photons. For the

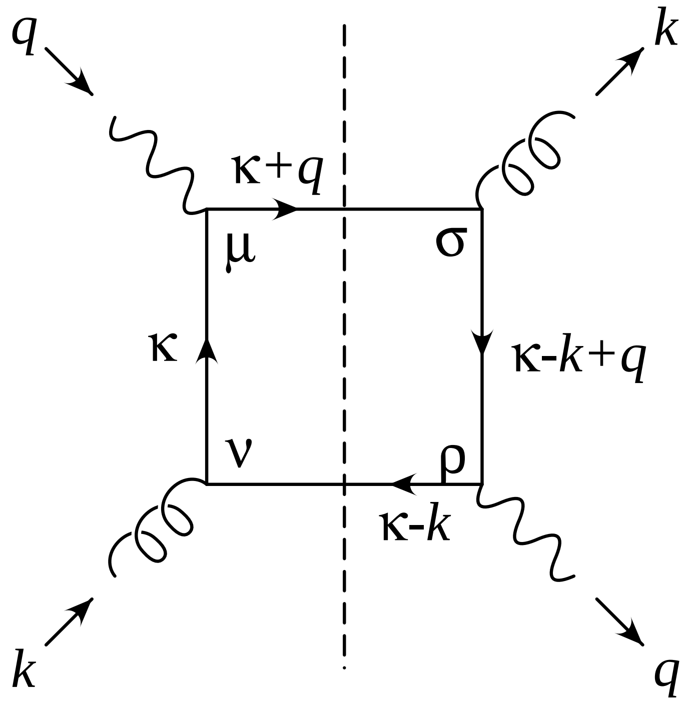

Figure B.5: The "crossed box" diagram (the outgoing photon and gluon have been swapped over, relative to Fig. B.4).

crossed box,

$$
\begin{aligned}
\mathrm{Disc}\,\mathcal{M}_{crossed} = - \\
&\frac{(4\pi)^2 \alpha_s \alpha_{em} e_q^2}{(\kappa^2 - m^2)((\kappa - k + q)^2 - m^2)} \int \frac{d^4\kappa}{(2\pi)^4} (2\pi)^2\, \delta\left((\kappa+q)^2 - m^2\right)\, \delta\left((\kappa-k)^2 - m^2\right) \\
&\mathrm{Tr}\ ((\not\kappa + m)\gamma^\nu (\not\kappa - \not k + m)\gamma^\rho (\not\kappa - \not k + \not q + m)\gamma^\sigma (\not\kappa + \not q + m)\gamma^\mu)\,. \qquad \text{(B.35)}
\end{aligned}
$$

The denominator factors (from the propagators which are *not* cut) can be evaluated in terms of the Sudakov parameters of Chapter 3, with

$$
\begin{aligned}
k &= ap - bq' + k_t \\
\kappa &= \alpha p - \beta q' + \kappa_t \\
q &= -xp + q'.
\end{aligned}
$$

(Some authors, including [29], use different notations.) Again, we set $b = 0$. Bearing in mind that α and a are determined by the mass-shell conditions (the delta functions in (B.34) and (B.35)), we find

$$\begin{aligned}
\frac{1}{(\kappa^2 - m^2)^2} &= \frac{(1-\beta)^2}{D_1^2}, \\
\frac{1}{(\kappa^2 - m^2)((\kappa - k + q)^2 - m^2)} &= \frac{\beta(1-\beta)}{D_1\, D_2},
\end{aligned}$$

with $D_1 = \kappa_t^2 + \beta(1-\beta)Q^2 + m^2$ and $D_2 = (\boldsymbol{\kappa_t} - \boldsymbol{k_t})^2 + \beta(1-\beta)Q^2 + m^2$, as in (3.14).

We could continue to compute (B.34) and (B.35) as they stand. However, to reproduce the result of [18], we make certain approximations, appropriate for the high energy limit, corresponding to fairly small values of x for the internal quark and the gluon. In the "eikonal approximation", we consider a gluon of comparatively low momentum k coupling to a quark, say[5], of much greater momentum p. Then we approximate $\bar{u}(p-k)\gamma^\nu u(p)$ to $\bar{u}(p)\gamma^\nu u(p)$, assuming that all components of k are small. This gives $\bar{u}(p-k)\gamma^\nu u(p) \simeq 2p^\nu$.

The consequence of the eikonal approximation for the calculation in this section is that we only need to consider certain projections of (B.34) and (B.35). Connecting the gluons in Figs. B.4 and B.5 to parent particles (in an evolution ladder), which have a much larger fraction of the proton's momentum p, effectively projects out the parts of (B.34) and (B.35) which remain after contraction with $p_\nu p_\sigma$. These are the terms proportional to $q'^\nu q'^\sigma$. We can rewrite the traces as

$$-\frac{4q'^\nu q'^\sigma}{(2p\cdot q')^2}\mathrm{Tr}\ ((\not{\kappa} + m)\not{p}(\not{\kappa} - \not{k} + m)\not{p}(\not{\kappa} + m)\gamma^\rho(\not{\kappa} + \not{q} + m)\gamma^\mu) \tag{B.36}$$

[5] In fact the eikonal approximation applies to other types of vertex too, not just the quark-gluon vertex discussed here.

and

$$-\frac{4q'^{\nu}q'^{\sigma}}{(2p\cdot q')^2}\mathrm{Tr}\ ((\not{\kappa}+m)\not{p}(\not{\kappa}-\not{k}+m)\gamma^{\rho}(\not{\kappa}-\not{k}+\not{q}+m)\not{p}(\not{\kappa}+\not{q}+m)\gamma^{\mu})\,, \qquad \text{(B.37)}$$

insofar as contracting with $p_\nu p_\sigma$ gives the same results.

Finally it remains to isolate the projections corresponding to interactions with longitudinally and transversely polarised photons. From (1.23) we see we can obtain

$$\begin{aligned} \frac{F_L\,(x,Q^2)}{x} &= \frac{Q^2}{(p\cdot q)^2}\,p_\mu p_\rho\,W^{\mu\rho} && \text{(B.38)} \\ \frac{F_T\,(x,Q^2)}{x} &= -\frac{g^{\perp}_{\mu\rho}}{2}\,W^{\mu\rho}, && \text{(B.39)} \end{aligned}$$

where $g^{\perp}_{\mu\rho}$ is the diagonal matrix with diagonal elements 0, -1, -1, 0. Our expressions are contributions to the hadronic tensor with some proportionality factor like α_{em}/Q^2. The longitudinal part is the easier: evaluating (B.38) for (B.36) gives (suppressing $q'^{\nu}q'^{\sigma}$, and evaluating all momenta in terms of the Sudakov parameters)

$$8\beta(1-\beta)\;.\;4Q^2\beta^2$$

and from (B.37) we have

$$-8\beta(1-\beta)\;.\;4Q^2\beta(1-\beta);$$

we then multiply by the appropriate denominator factors to get

$$F_L \sim 8\beta(1-\beta)\;.\;4Q^2\left[\beta^2(1-\beta)^2\right]\left(\frac{1}{D_1^2}-\frac{1}{D_1D_2}\right). \qquad \text{(B.40)}$$

For the transverse contributions we use (B.39) for (B.36) to obtain

$$8\beta(1-\beta)\;.\;\frac{(\kappa_t^2[\beta^2+(1-\beta)^2]+m^2)}{(1-\beta)^2}$$

and from (B.37)

$$-8\beta(1-\beta)\;.\;\frac{(\boldsymbol{\kappa_t}\cdot(\boldsymbol{\kappa_t}-\boldsymbol{k_t})[\beta^2+(1-\beta)^2]+m^2)}{\beta(1-\beta)},$$

giving

$$F_T \sim 8\beta(1-\beta)\;.\;\left\{\left[\beta^2+(1-\beta)^2\right]\left(\frac{\kappa_t^2}{D_1^2}-\frac{\boldsymbol{\kappa_t}\cdot(\boldsymbol{\kappa_t}-\boldsymbol{k_t})}{D_1D_2}\right)+m^2\left(\frac{1}{D_1^2}-\frac{1}{D_1D_2}\right)\right\}, \tag{B.41}$$

reproducing the structure of the integrands of (3.6) and (3.7) as in [18]. We rewrite the integration of the loop momentum κ in terms of the Sudakov parameters too, so $d^4\kappa \to p\cdot q\; d\alpha\, d\beta\, d^2\kappa_t$. Then the two delta functions in (B.34) and (B.35) can be recast as

$$\delta(\alpha-\cdots)\frac{x}{(1-\beta)Q^2}, \qquad \delta(z-\cdots)\frac{z^2}{\beta Q^2},$$

thus absorbing the extra factor of $\beta(1-\beta)$. We use the first delta function to remove the α integration. Finally, using the unintegrated gluon as a probability density, we insert

$$\int\frac{dz}{z}\int\frac{dk_t^2}{k_t^2}\,f_g\left(\frac{x}{z},k_t^2,\mu^2\right)$$

and immediately remove the z integration with the remaining delta function, leaving integrals over k_t^2, β and $\boldsymbol{\kappa_t}$ (the angle between $\boldsymbol{k_t}$ and $\boldsymbol{\kappa_t}$ is of course significant, see the discussion in Chapter 3).

In summary, the approaches of this section and the previous one are somewhat different on two counts. Firstly, here we use the squared matrix element approach (via the optical theorem), yielding directly expressions in terms of the internal quark momentum κ, rather than the outgoing momenta in Section B.2. The other difference is that not only do we project out transverse and longitudinal components with respect to the photon of DIS, we also employ the eikonal approximation, valid for reasonably small[6] values of x, whereby we only consider the longitudinal components with respect to the parton evolution ladder.

[6]We expect strong ordering in plus momenta to be a legitimate approximation in the gluon evolution ladder, and thus have small values of the splitting fraction z.

References

[1] M. A. Kimber, A. D. Martin and M. G. Ryskin, Eur. Phys. J. **C12** (2000) 655

[2] M. A. Kimber, J. Kwieciński, A. D. Martin and A. M. Stasto, Phys. Rev. **D62** (2000) 094006

[3] M. A. Kimber, J. Kwieciński and A. D. Martin, Phys. Lett. **B508** (2001) 58

[4] M. A. Kimber, A. D. Martin and M. G. Ryskin, Phys. Rev. **D63** (2001) 114027

[5] G. Altarelli and G. Parisi, Nucl. Phys. **B126** (1977) 298

[6] G. Marchesini and B. R. Webber, Nucl. Phys. **B310** (1988) 461

[7] S. Catani, M. Ciafaloni and F. Hautmann, Phys. Lett. **B242** (1990) 97; Nucl. Phys. **B366** (1991) 135; J. C. Collins and R. K. Ellis, Nucl. Phys. **B360** (1991) 3; E. M. Levin, M. G. Ryskin, Yu. M. Shabelski and A. G. Shuvaev, Sov. J. Nucl. Phys. **54** (1991) 867

[8] J. Kwiecinski, A. D. Martin and P. J. Sutton, Phys. Rev. **D52** (1995) 1445; G. Bottazzi, G. Marchesini, G. P. Salam and M. Scorletti, Nucl. Phys. **B505** (1997) 366; JHEP 9812 (1998) 011

[9] M. Ciafaloni, Nucl. Phys. **B296** (1988) 49; S. Catani, F. Fiorani and G. Marchesini, Phys. Lett. **B234** (1990) 339; Nucl. Phys. **B336** (1990) 18; G. Marchesini, in

Proceedings of the Workshop "QCD at 200 TeV", Erice, Italy, 1990, edited by L. Cifarelli and Yu. L. Dokshitzer (Plenum, New York, 1992), p.183

[10] G. Marchesini and B. Webber, Nucl. Phys. **B349** (1991) 617; **B386** (1992) 215; H. Jung, Nucl. Phys. Proc. Suppl. **79** (1999) 429; H. Jung and G. P. Salam, `hep-ph/0012143`; H. Kharraziha and L. Lönnblad, JHEP 98003 (1998) 006

[11] E. A. Kuraev, L. N. Lipatov and V. S. Fadin, Sov. Phys. JETP **44** (1976) 443; ibid. **45** (1977) 199; I. I. Balitskiĭ and L. N. Lipatov, Sov. J. Nucl. Phys. **28** (1978) 822

[12] Yu. L. Dokshitzer, V. A. Khoze, S. I. Troyan and A. H. Mueller, Rev. Mod. Phys. **60** (1988) 373

[13] New Muon Collaboration: M. Arneodo et al., Nucl. Phys. **B483** (1997) 3; ZEUS Collaboration: M. Derrick et al., Zeit. Phys. **C72** (1996) 399; H1 Collaboration: C. Adloff et al., Eur. Phys. J. **C13** (2000) 609

[14] E665 Collaboration: M. R. Adams et al., Phys. Rev. **D54** (1996) 3006

[15] Yu. L. Dokshitzer, D. I. Dyakanov, S. I. Troyan, Phys. Rep. **58** (1980) 269

[16] J. Kwieciński, A. D. Martin and P. J. Sutton, Phys. Rev. **D46** (1992) 921

[17] J. Kwieciński, A. D. Martin and P. J. Sutton, Z. Phys. **C71** (1996) 585

[18] A. J. Askew, J. Kwieciński, A. D. Martin and P. J. Sutton, Phys. Rev. **D47** (1993) 3775; Phys. Rev. **D49** (1994) 4402; A. J. Askew, thesis presented for the degree of Doctor of Philosophy, University of Durham, 1995

[19] J. Kwieciński, A. D. Martin and A. M. Staśto, Phys. Rev. **D56** (1997) 3991

[20] Anna Staśto, thesis presented for the degree of Doctor of Philosophy, H. Niewodniczański Institute of Nuclear Physics, Kraków, 1999

[21] S. Frixione, M. L. Mangano, P. Nason and G. Ridolfi, Phys. Lett. **B319** (1993) 339

[22] G. Heinrich, hep-ph/0105135

[23] Yu. M. Shabelski and A. G. Shuvaev, hep-ph/0107106

[24] P. Bussey, private communication, May 2000

[25] M. G. Ryskin, private communication, July 2000

[26] F. Halzen and A. D. Martin, *Quarks and Leptons: An Introductory Course in Modern Particle Physics*, Wiley (1984)

[27] R. D. Field, *Applications of Perturbative QCD*, Addison-Wesley (1989)

[28] R. K. Ellis, W. J. Stirling and B. R. Webber, *QCD and Collider Physics*, Cambridge University Press (1996)

[29] J. R. Forshaw and D. A. Ross, *Quantum Chromodynamics and the Pomeron*, Cambridge University Press (1997)

[30] I. S. Gradshteyn and I. M. Ryzhik, *Table of Integrals, Series, and Products*, corrected and enlarged edition, Academic Press (1980)

[31] W. H. Press et al., *Numerical Recipes in C: The Art of Scientific Computing*, Cambridge University Press (1993)

[32] A. D. Martin, R. G. Roberts, W. J. Stirling and R. S. Thorne, Eur. Phys. J. **C4** (1998) 463; Eur. Phys. J. **C14** (2000) 133; see HEPDATA website at `http://www-spires.dur.ac.uk/hepdata/mrs.html` for code

[33] J. Huston et al., Phys. Rev. **D51** (1995) 6139

[34] L. Apanasevich et al., Phys. Rev. **D59** (1999) 074007

[35] P. Aurenche, M. Fontannaz, J. Ph. Guillet, B. Kniehl, E. Pilon, M. Werlen, Eur. Phys. J. **C9** (1999) 107; P. Aurenche, M. Fontannaz, J. Ph. Guillet, B. Kniehl, M. Werlen, Eur. Phys. J. **C13** (2000) 347

[36] H.-L. Lai and H.-n. Li, Phys. Rev. **D58** (1998) 114020; H.-n. Li, Phys. Lett. B454 (1999) 328

[37] S. Catani, M. Mangano, P. Nason, C. Oleari, W. Vogelsang, JHEP 9903:025 (1999)

[38] E. Laenan, G. Sterman and W. Vogelsang, Phys. Rev. Lett. **84** (2000) 4296; Phys. Rev. **D63** (2001) 114018

[39] UA6 collaboration, G. Ballocchi et al., Phys. Lett. **B436** (1998) 222

[40] E706 collaboration, L. Apanasevich et al., Phys. Rev. Lett. **81** (1998) 2642

[41] CDF collaboration, F. Abe et al., Phys. Rev. Lett. **73** (1994) 2662

[42] ZEUS collaboration, J. Breitweg et al., Eur. Phys. J. **C6** (1999) 67; Eur. Phys. J. **C12** (2000) 1; Eur. Phys. J. **C18** (2001) 625

[43] H1 collaboration, C. Adloff et al., Phys. Lett. **B467** (1999) 156; hep-ex/0011034, proceedings of ICHEP 2000 conference, Osaka, July 2000

[44] H1 collaboration, H1prelim-01-072 (2001)

[45] P. Nason, S. Dawson and R. K. Ellis, Nucl. Phys. **B303** (1988) 607; W. Beenakker et al., Nucl. Phys. **B351** (1991) 507; M. L. Mangano, P. Nason and G. Ridolfi, Nucl. Phys. **B373** (1992) 295; R. Bonciani, S. Catani, M. L. Mangano and P. Nason, Nucl. Phys. **B529** (1998) 424; R. Ball and R. K. Ellis, JHEP 0105 (2001) 053

[46] M. G. Ryskin, Yu. M. Shabelski and A. G. Shuvaev, Lecture given at XXXIV PNPI Winter School, St. Petersburg, 2000, hep-ph/0011111

[47] Ph. Hagler et al., Phys. Rev. **D62** (2000) 071502

[48] L. V. Gribov, E. M. Levin and M. G. Ryskin, Phys. Rep. **100** (1983) 1

[49] A. H. Mueller and J. Qiu, Nucl. Phys. **B268** (1986) 427

[50] J. Kwieciński, Introductory talk presented at 30th International Symposium on Multiparticle Dynamics (ISMD 2000), Hungary, October 2000, hep-ph/0102018

[51] A. D. Martin, Summary of talk at DIS 2001, hep-ph/0106285

[52] N. N. Nikolaev and B. G. Zakharov, Z. Phys. **C49** (1991) 607; Z. Phys **C53** (1992) 331; Z. Phys. **C64** (1994) 651; JETP **78** (1994) 598

[53] A. H. Mueller, Nucl. Phys. **B415** (1994) 373; A. H. Mueller and B. Patel, Nucl. Phys. **B425** (1994) 471; A. H. Mueller, Nucl. Phys. **B437** (1995) 107

[54] A. H. Mueller, Nucl. Phys. **B335** (1990) 115; Yu. A. Kovchegov, A. H. Mueller and S. Wallon, Nucl. Phys. **B507** (1997) 367 ; A. H. Mueller, Eur. Phys. J. **A1** (1998) 19; Nucl.Phys. **A654** (1999) 370; Nucl.Phys. **B558** (1999) 285

[55] J. C. Collins and J. Kwieciński, Nucl. Phys. **B335** (1990) 89

[56] J. Bartels, G. A. Schuler and J. Blümlein, Z. Phys. **C50** (1991) 91; Nucl. Phys. Proc. Suppl. **18 C** (1991) 147; J. Bartels, Phys. Lett. **B298** (1993) 204; Z. Phys. **C60** (1993) 471; Z. Phys. **C62** (1994) 425; J. Bartels and M. Wüsthoff, Z. Phys. **C66** (1995) 157; J. Bartels and C. Ewerz, JHEP **9909** (1999) 026

[57] J. Bartels and E. M. Levin, Nucl. Phys. **B387** (1992) 617

[58] L. McLerran and R. Venugopalan, Phys. Rev. **D49** (1994) 2233, Phys. Rev. **D49** (1994) 3352, Phys. Rev. **D50** (1994) 2225; A. Kovner, L. McLerran and H. Weigert,

Phys.Rev. **D52** (1995) 6231, Phys. Rev. **D52** (1995) 3809; R. Venugopalan, Acta. Phys. Polon. **B30** (1999) 3731

[59] A. Białas and R. Peschanski, Phys. Lett. **B355** (1995) 301; Phys. Lett. **B378** (1996) 302; Phys. Lett. **B387** (1996) 405; A. Bialas Acta Phys. Polon. **B28** (1997) 1239; A. Bialas and W. Czyz, Acta Phys.Polon. **B29** (1998) 2095; A. Białas, H. Navelet and R. Peschanski, Phys. Rev. **D57** (1998) 6585; Phys. Lett. **B427** (1998) 147

[60] A. Białas, H. Navelet and R. Peschanski, Nucl. Phys. **B593** (2001) 438

[61] G. P. Salam, Nucl. Phys. **B449** (1995) 589; Nucl. Phys. **B461** (1996) 512; Comput. Phys. Commun. **105** (1997) 62; A. H. Mueller and G. P. Salam, Nucl. Phys. **B475** (1996) 293

[62] E. Gotsman, E. M. Levin and U. Maor, Nucl. Phys. **B464** (1996) 251; Nucl. Phys. **B493** (1997) 354; Phys. Lett. **B245** (1998) 369; Eur. Phys. J. **C5** (1998) 303; E. Gotsman, E. M. Levin, U. Maor and E. Naftali, Nucl. Phys. **B539** (1999) 535; A. L. Ayala Filho, M. B. Gay Ducati and E. M. Levin, Nucl.Phys. **B493** (1997) 305; Nucl. Phys. **B551** (1998) 355; Eur. Phys. J. **C8** (1999) 115; E. Levin and U. Maor, hep-ph/0009217

[63] Ia. Balitsky, Nucl. Phys. **B463** (1996) 99

[64] J. Jalilian-Marian, A. Kovner, L. McLerran and H. Weigert, Phys. Rev. **D55** (1997) 5414; J. Jalilian-Marian, A. Kovner and H. Weigert, Phys. Rev. **D59** (1999) 014014; Phys. Rev. **D59** (1999) 014015; Phys. Rev. **D59** (1999) 034007; Erratum-ibid. **D59** (1999) 099903; A. Kovner, J. Guilherme Milhano and H. Weigert, Phys. Rev. **D62** (2000) 114005; H. Weigert, NORDITA-2000-34-HE, hep-ph/0004044

[65] M. A. Braun, Eur. Phys. J. **C16** (2000) 337; hep-ph/0101070

[66] Y. V. Kovchegov, Phys. Rev. **D60** (1999) 034008; Phys. Rev. **D61** (2000) 074018

[67] E. M. Levin and K. Tuchin, Nucl. Phys. **B537** (2000) 833; hep-ph/0012167

[68] Y. V. Kovchegov and L. McLerran, Phys. Rev. **D60** (1999) 054025; Erratum-ibid. **D62** (2000) 019901; Y. V. Kovchegov and E. M. Levin, Nucl. Phys. **B577** (2000) 221

[69] K. Golec-Biernat, M. Wüsthoff, Phys. Rev. **D59** (1999) 014017; Phys. Rev. **D60** (1999) 114023

[70] Zhang Chen and A. H. Mueller, Nucl. Phys. **B451** (1995) 575

[71] A. De Roeck, Contribution to the First Workshop on Forward Physics at the LHC, Helsinki, November 2000

[72] J. A. M. Vermaseren, *Symbolic Manipulation with FORM*, Version 1, CAN, Amsterdam, 1989

[73] R. E. Cutkosky, J. Math. Phys. **1** (1960) 429